Rainy HW, Vermilion, and Rainy Lake Watershed HSPF model updates: Conversion to gridded weather data and extension through 2019

1 INTRODUCTION

This report documents the extension of the model time period for the Rainy River Headwaters (RRHW), Vermilion, and Rainy Lake Watershed linked HSPF models. The previous version of the models [Lupo, 2016] runs for the period 1995-2014 and is driven by weather data from individual weather stations within and near the watershed. For this update through the 2019, the models were adapted to use weather forcing input from several gridded meteorological products, including the North American Land Data Assimilation System (NLDAS), the Parameter-elevation Regressions on Independent Slopes Model (PRISM), and North American Regional Reanalysis (NARR). These datasets perform a more robust interpolation of weather data between observations than the previously-assumed uniform distribution of gauge data across the watershed and eliminate the need for time-consuming filling of data gaps. Point source, atmospheric nitrogen deposition, and reservoir outflow time series were also extended as part of this update.

Following the extension of the input time series, the hydrological and water quality calibration was revisited. Recently collected flow and water chemistry data were available to better constrain the model simulation. Additionally, independent estimates of evapotranspiration (ET) and snow cover were incorporated to constrain those components of the water balance and reduce uncertainty in the hydrological simulation.

The model's land cover dataset, which was developed from 2010 satellite imagery and lidar data [Olmanson and Bauer, 2017; Lupo, 2016], was maintained unchanged from the existing model, with one exception. Significant clearing of mature forest and conversion to pastureland occurred around the Blackduck River in the RRHW watershed since 2010. Because there is a sediment impairment and TMDL for the Blackduck River [MPCA, 2020a], it was a priority to represent the increased pasture area in the model. Newly cleared areas were delineated manually based on the most recent (2017) aerial imagery available for this location and land cover areas were updated accordingly in the model files.

Rainy Lake receives inflows from the Turtle River Watershed, which is to the north of the RRHW Watershed in Canada. That watershed is represented in a separate, linked HSPF model, which also had to be extended for the Rainy Lake model to run. However, because the focus of current MPCA work in the Rainy Lake Watershed is in tributaries to Rainy Lake rather than Rainy Lake itself (for example, the Blackduck River sediment TMDL and Rat Root River stressor identification work), the calibration of the extended Turtle River model was not checked or updated at this time.

2 TIME SERIES DEVELOPMENT

2.1 WEATHER FORCING DATA

HSPF requires seven hourly meteorological time series to model precipitation, ET, and snow accumulation and melt processes using the energy balance method applied in the Rainy River –Lake of the Woods basin models. These time series include precipitation, air temperature, wind speed, solar radiation, dewpoint temperature, cloud cover, and potential evapotranspiration (ET). Some of these variables are directly available from the gridded datasets described below, while others can be estimated from the variables provided.

The PRISM dataset includes daily precipitation, temperature, dewpoint temperature, and vapor pressure deficit at a 4 km grid resolution across the conterminous United States from 1981-present. The PRISM method, developed by the PRISM Climate Group at Oregon State University, is a statistical approach based on the strong control topography exerts on precipitation and temperature. Measured gauge station data are interpolated across cells of a digital elevation model based on a climate-elevation regression that also incorporates other physiographic information such as location, coastal proximity, topographic position and facet orientation, vertical atmospheric layer and orographic effectiveness of the terrain, as well as radar data [Daly et al., 2008; Daly, Neilson, & Phillips, 1994].

NARR is a regional reanalysis climate model covering North America from 1979-present, produced by NOAA's National Center for Environmental Analysis [Mesinger et al., 2006]. It assimilates a large amount of temperature, wind, moisture, pressure, and precipitation measurements to produce output for a wide variety of meteorological variables at a 32-km spatial resolution and 3 hour temporal frequency.

NLDAS [Mitchell et al., 2004; Xia et al., 2012] is produced by NASA's Earth Science Division and archived and distributed by the Goddard Earth Sciences (GES) Data and Information Services Center (DISC). It assimilates meteorological observation and model reanalysis data from a variety of sources to produce a dataset with 1/8th-degree (~14 km in Minnesota) grid spacing and hourly resolution across North America [Rui and Mocko, 2018]. NLDAS data are produced to drive several land-surface hydrological models, including the Variable Infiltration Capacity (VIC) and NOAA's Noah model, and include output to either directly or indirectly compute all HSPF required meteorological forcing input except for cloud cover. NLDAS precipitation data are based on daily rain gauge observations and spatially interpolated using the PRISM method. Data are distributed to an hourly time step using Doppler radar data when available, or else CMORPH satellite hourly precipitation analyses or NARR-simulated precipitation. All other NLDAS variables are derived from the NARR dataset and are spatially interpolated to the finer NLDAS grid and temporally disaggregated to an hourly frequency.

The PRISM, NLDAS, and NARR datasets were used together to take advantage of the strengths of each dataset. Following are details on the extraction of each HSPF time series from these datasets. All computations described below were done at the scale of each NLDAS grid cell. Non-NLDAS datasets were resampled and aligned to coincide with the NLDAS grid. Final computed values were averaged across each HSPF weather zone for input to the model. The weather zones were kept consistent with the existing model. Because the existing weather zones were developed based on the distribution of

weather stations in the basin [Kenner, 2014], the weather zones vary in size from about one NLDAS grid cell to 10 or more grid cells (Figure 1). To ensure consistency of the weather datasets over the model run, input time series were developed from the gridded datasets for the entire model period (1995-2019).

2.1.1 Air temperature and Solar Radiation

Values for these time series were obtained directly from NLDAS rasters. For each hour, an average value was computed for each weather zone using ArcGIS zonal statistics, and values were converted to the correct units required by HSPF.

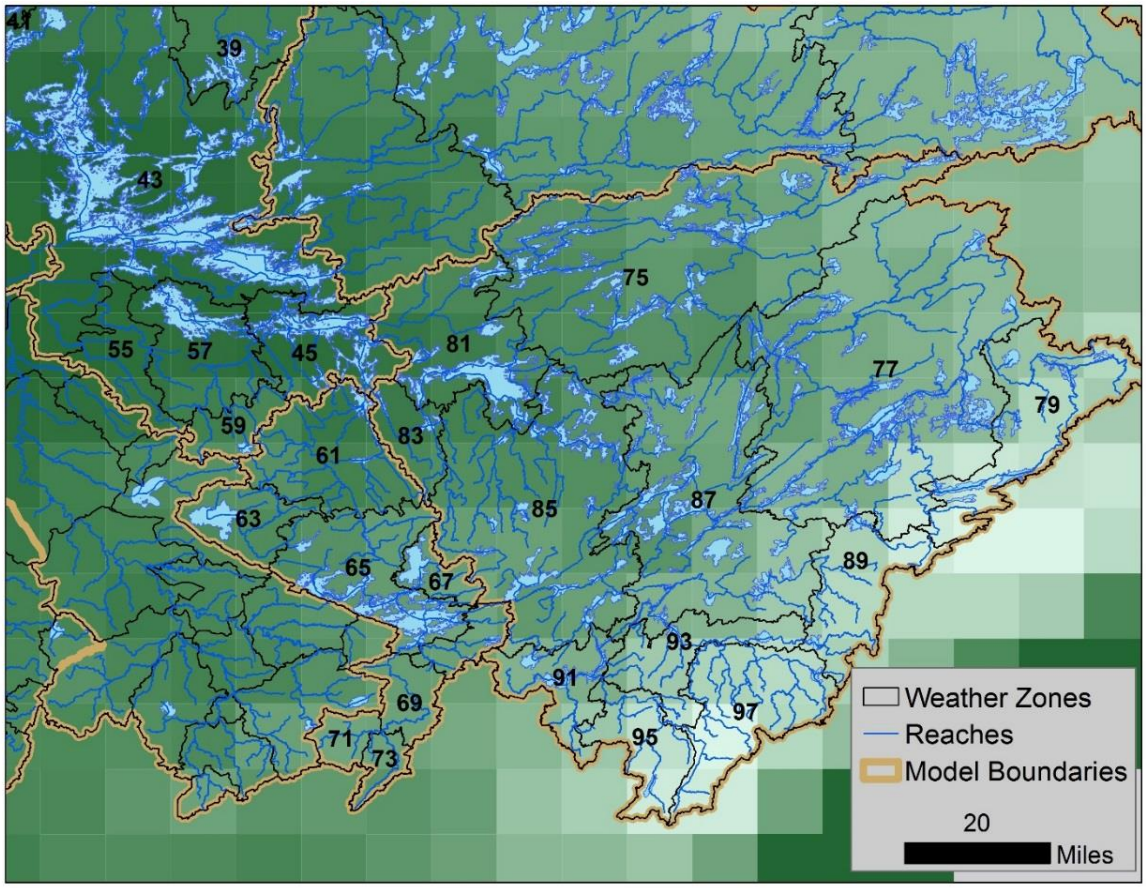

Figure 1. Weather zones used to average gridded weather dataset cells for input to HSPF. The green shaded grid is an example NLDAS dataset for reference.

2.1.2 Wind

Wind data are reported by NLDAS in separate north-south and east-west components and at 10m height. The magnitude of wind movement was computed from the two components, and estimated at 2m height (as expected by HSPF) assuming a logarithmic profile, following Snyder et. al. [2002].

2.1.3 Dewpoint Temperature

NLDAS does not directly report dewpoint temperature, but rather reports specific humidity as a measure of atmospheric water vapor content. Specific humidity, along with air pressure and temperature, was used to compute dewpoint temperature for input into HSPF. Computation, was done with a Python function developed by Tetra Tech [2019], which implements equations from Stull [2017].

2.1.4 Precipitation

Because precipitation can vary significantly in intensity over small spatial scales, the finer resolution of PRISM data compared with NLDAS (4km compared with~14km) is an advantage for accurately representing rainfall events. However, PRISM data are available only as daily totals, so the volume needs to be distributed throughout the hours of the day for application in HSPF. The hourly distribution of NLDAS precipitation values was used to disaggregate the daily PRISM precipitation volume, similar to the approach taken in other watershed modeling applications in MN [Tetra Tech, 2016b].

For each weather zone, an average value was extracted from each daily PRISM and hourly NLDAS precipitation grid over the model time period. On days when both PRISM and NLDAS reported precipitation, the PRISM precipitation volume was distributed based on the temporal distribution of NLDAS precipitation on that day. On some days, PRISM reported precipitation but NLDAS did not, preventing disaggregation directly from the NLDAS data. Precipitation on those days was disaggregated with the multiplicative cascade model implemented by the Python code "MELODIST" [Forster et. al, 2016]. Branching statistics for the model were estimated using the hourly NLDAS datasets for each weather zone, and the model values were applied on days when no precipitation was predicted by NLDAS.

2.1.5 Potential ET

Potential ET was derived on an hourly basis from meteorological variables available from NLDAS (air temperature and pressure, specific humidity, wind speed, and solar radiation) with the Penman-Monteith equation as described by Allen et al. [1998]. The computation was performed with Python code adapted from the GRASS GIS function "i.evapo.pm" [Cannata, 2006]. To compute the net shortwave radiation flux, albedo was estimated on a monthly basis from values reported for Minnesota by Baker and Ruschy [1987]. Vegetation canopy height for computing surface and aerodynamic resistance was estimated from a global, 1-km resolution raster developed by Simard et al. [2011], obtained from the Spatial Data Access Tool [ORNL DAAC, 2017]. That dataset represents a snapshot in time at 2005, not a seasonally or inter-annually variable value, although seasonal variation in vegetation height is likely to be less important in these primarily forested landscapes than it is in agricultural areas.

2.1.6 Cloud Cover

The cloud cover time series was developed using the NARR dataset. Because NARR is used to derive the non-precipitation land-surface forcing inputs for NLDAS [Rui and Mocko, 2018], the NARR cloud data are consistent with the NLDAS data used to generate the other HSPF weather time series. For each weather zone, an average value of the total percent cloud cover (TCDC variable in NARR) was computed. The temporal resolution of NARR is 3 hours, so values were linearly interpolated to obtain the hourly time step for HSPF.

2.2 POINT SOURCES

Multiple pollution point sources are present in the RRHW and Vermilion River watersheds. These sources include municipal wastewater treatment plants (both mechanical plants and controlled ponds) and mining operations. All permitted surface discharges (SD) of sufficient length (i.e., more than a few measurements) reported in MPCA's discharge monitoring database were represented explicitly in the models. Daily discharge monitoring report (DMR) data were used to develop flow and pollutant load time series for input to HSPF, where they are distributed to the model's hourly time step using the DIV command. Point source names, IDs, and additional monitoring and model information are presented in Table 1 (RRHW Watershed) and Table 2 (Vermilion River Watershed). The Rainy Lake Watershed contains no permitted point sources.

Table 1. Point sources represented in the RRHW HSPF model.

Point Source Name	Point Source ID	Discharge ID	HSPF reach	WDM ID[a]	Period of record	Measured Constituents	Discharge Type Assumption	Discharge Frequency
Ely WWTP	MN0020508	SD001	382	3821	1995-2019	Q, TSS, DO, BOD, TP, TAM, NO2+NO3, Temp	Class A municipal	Continuous
Winton WWTP	MNG580186	SD002	383	3871	1995-2019	Q, TSS, DO, BOD, TP, Temp	Class D municipal	Controlled
Cliffs - Dunka Mining Area	MN0042579	Multiple[b]	352	3521	1995-2014	Q, TSS	Other low volume	Continuous
		SD001	313	1361	2015-2019	Q, TSS	Other low volume	Continuous
		SD005	352	5211	2015-2019	Q, TSS	Other low volume	Continuous
		SD006	352	5221	2015-2019	Q, TSS	Other low volume	Continuous
		SD007	352	5231	2015-2019	Q, TSS	Other low volume	Continuous
		SD008	352	5241	2015-2019	Q, TSS	Other low volume	Continuous
		SD009	352	5251	2015-2019	Q, TSS	Other low volume	Continuous
Northshore Mining Co-Babbitt	MN0046981	Multiple[b]	313	3131	1995-2014	Q, TSS, TAM, Temp	Water treatment plant	Continuous
		SD001-203M	313	3141	1995-2009	Q, TSS, BOD,TP, Temp	Water treatment plant	Continuous
		SD001-301M	313	3151	1995-2010	Q, TSS, Temp	Water treatment plant	Continuous
		SD001-302M	313	3161	1995-2010	Q, TSS, TP, Temp	Water treatment plant	Continuous
		SD001-303M	313	3171	1995-2010	Q, TSS, Temp	Water treatment plant	Continuous
		SD001-304M	313	3181	1995-2010	Q, TSS, TP, Temp	Water treatment plant	Continuous
		SD002	313	1321	2015-2019	Q, TSS, TAM, Temp	Water treatment plant	Continuous
		SD004	311	1111	2015-2019	Q, TSS, TAM, Temp	Water treatment plant	Continuous
		SD005	311	1121	2015-2019	Q, TSS, TAM, Temp	Water treatment plant	Continuous
		SD017	311	1151	2015-2019	Q, TSS, BOD,TP	Water treatment plant	Continuous
		SD018	311	1161	2015-2016	Q, TSS	Water treatment plant	Intermittent
		SD019	311	1171	2015-2019	Q, TSS, BOD,TP	Water treatment plant	Continuous
		SD022	313	1341	2015-2019	Q	Water treatment plant	Continuous
		SD024	313	1351	2015-2019	Q, TSS, BOD,TP, DO	Water treatment plant	Intermittent

[a] This ID number is for the point source water discharge time series. Time series for different constituents (TSS, BOD, TP, etc.) from the same discharge are identical except for the last digit, which identifies each unique constituent.

[b] Multiple separate surface discharges from the same facility were combined into one time series in the previous model version. The existing time series of combined discharges was carried through in this update to represent the 1995-2014 period, but the separate discharges were represented independently for the 2015-2019 period.

Due to varied reporting requirements for different point sources, the discharge records have varying degrees of measurement frequency and number of monitored water quality constituents. Wastewater treatment plants generally measure the most constituents, often including nitrogen (nitrate and total ammonia) and total phosphorus data in addition to the TSS, BOD and water temperature commonly reported for most discharges. Water quality sampling frequency ranges from multiple times per week to every couple of months, depending on the point source and when they are discharging (for intermittent discharges and controlled ponds), with wastewater treatment plants measuring more frequently than mine tailings basins. Measured concentration values were interpolated to estimate water quality concentrations on days when no samples were taken, as long as the measurement gap was less than a month. For longer gaps, missing days were filled with the site's average value.

Table 2. Point sources represented in Vermilion River HSPF model.

Point Source Name	Point Source ID	Discharge ID	HSPF reach	WDM ID[a]	Period of record	Measured constituents	Discharge Type Assumption	Discharge Frequency
Crane Lake WWTP	MN0066371	SD001	420	4201	2005-2019	Q, TSS, BOD, DO, TP, Temp	Class C municipal	Continuous
Tower/Breitung WWTP	MNG580186	SD001	49	491	1995-2019	Q, TSS, BOD, DO, TP, Temp, TAM, NO3	Class B municipal	Controlled
Orr WWTP	MN0024422	SD001	220	2201	1995-2019	Q, TSS, BOD, DO, TP, NO3, Temp	Class B municipal	Continuous
ArcelorMittal Minorca Mine	MN0055964	SD001	7	91	1995-2019	Q, TSS, Temp	Water treatment plant	Intermittent
		SD002	7	81	1995-2019	Q, TSS, Temp	Water treatment plant	Intermittent
		SD003	7	71	1995-2019	Q, TSS, Temp	Water treatment plant	Intermittent
US Steel Corp - MN Ore Operations - Minntac Tailings Basin	MN0057207	SD002 and SD006	3	2151	1995-2010, 2019	Q, TSS, Temp	Water treatment plant	Continuous
MDNR Soudan State Park	MN0060151	SD001	80	801	1996-2019	Q, TSS, Temp	Water treatment plant	Controlled

[a] This ID number is for the point source water discharge time series. Time series for different constituents (TSS, BOD, TP, etc.) from the same discharge are identical except for the last digit, which identifies each unique constituent.

For constituents that were not monitored at a particular point source discharge, fixed surrogate concentrations were assumed based on point source class. These surrogate concentrations are summarized in Table 3, which was compiled by Tetra Tech (2018) based on data from Weiss (2012), Helgen (1992), and "Gary Rott's (April, 1990) summary of WWTF effluent data". Because water temperature has significant seasonal variation, a single representative value is not sufficient to estimate missing data. Gaps in temperature measurements were filled using monthly averages for that site.

Missing flow values were filled based on the point source type. Missing values for continuous dischargers were assumed to be erroneous and were filled by linear interpolation. Missing values for intermittent discharger flow time series were not filled. Controlled ponds often discharge for multiple days to weeks at a time. Often, flows are reported for every day during periods of discharge, but not always. To fill missing days during discharge periods, but avoid filling days between discharge periods that should have zero flow, flow values were linearly interpolated between reported values that were less than 15 days apart. Once daily flow and water quality concentration time series were filled appropriately, daily loads were computed by multiplying flow by concentration.

Table 3. Surrogate Nutrient Concentrations (mg/L) for Permitted Point Source Discharges

Discharge Type	NO_3-N	NH_4-N	Org-N	TN	CBOD5	Ortho P	Org P
Class A municipal - large mechanical	15	3	1	19	3	2.76	0.02
Class B municipal - medium mechanical	10	4	3	17	12	2.59	0.99
Class C municipal- small mechanical/pond mix	7	1	2	10	6	2.59	0.99
Class D municipal - mostly small ponds	3	1	2	6	6	1.6	1.1
Stabilization ponds, spring discharge	0.05	5.8	3.2	9.05	7.5	1.6	1.1
Stabilization ponds, fall discharge	0.008	0.07	4.43	4.508	4.5	0.66	0.13
Other low volume, peat mining, tile line to surface	7	2	1	10	0.5	0.1	0.02
Paper industry	7	2	1	10	0.5	0.1	0.02
Non-contact cooling	1	2	1	4	0.5	0.1	0.02
Power industry	1	2	1	4	0.5	0.1	0.02
Water treatment plant	3	1	0	4	0.5	0.1	0.02
Gravel mining wash water	1	1	0	2	0.5	0.1	0.02
Industrial facilities on ground water	0.25	0	0	0.25	0.5	0.02	0

Notes: WWTP classes were defined by average volume (X): Class A: 1 MGD < X; Class B: 0.1 MGD < X < 1.0 MGD; Class C: 0.01 MGD < X < 0.1 MGD; and Class D: X < 0.01 MGD

2.3 ADDITIONAL TIME SERIES

2.3.1 Atmospheric deposition

Consistent with the existing models, atmospheric deposition of NO3 and NH4 were estimated based on observed values from the nearest CASTNET (dry deposition) and NADP (wet deposition) network stations (Table 3). The nearest CASTNET station to all four of these models is at Voyageurs National Park (station VOY413), with data starting in June of 1996. Reported weekly flux data were disaggregated to a daily time series, assuming equal flux for every day within any given week. To cover the missing period January 1995 – May 1996, day-of-year average values calculated over the length of the dataset were used. Data were input to HSPF as daily pounds/acre NO3-N and NH4-N time series.

Wet deposition nitrogen concentration data were obtained from two separate NADP-NTN stations, based on proximity to each watershed (Table 4). Weekly reported concentration data were used to generate a daily time series, assuming each day had the same concentration as the weekly average. Data were input to HSPF as daily concentration (mg/L) NO3-N and NH4-N time series, which are applied to any precipitation within the model.

Atmospheric deposition of phosphorus is represented in the models, but due to limited availability of temporal data, it is not represented with daily time series. The model assumes a dry deposition load of 0.12 kilogram/hectare per year (kg/ha/yr) (0.00029 pound per acre per day [lbs/ac/day]) based on research by Barr Engineering [2007]. That load was distributed throughout the year with higher values in summer months and lower values in the winter [Ackerman, 2015]. These existing assumptions were maintained for this model update.

Table 4. Measurement sites used to estimate wet and dry atmospheric nitrogen deposition.

Model	Dry deposition CASTNET station	Wet deposition NADP-NTN station
RRHW	Voyageurs National Park (VOY413)	Fernberg Rd (MN18)
Vermilion	Voyageurs National Park (VOY413)	Fernberg Rd (MN18)
Rainy Lake	Voyageurs National Park (VOY413)	Voyageurs National Park-Sullivan Bay (MN32)
Turtle River	Voyageurs National Park (VOY413)	Fernberg Rd (MN18)

2.3.2 Reservoir outflow

A system of dams control water levels and flows at a number of locations in the Upper Rainy River basin. Because outflows from these controlled lakes are a function of dam operation rather than lake elevation, measured outflows from these lakes are input to the model as external time series. Reservoir flows represented in this way are listed in Table 5. Data were obtained from multiple sources, including MN Power, Lake of the Woods Control Board, the U.S. Geological Survey, and Environment Canada. Incomplete data records and gaps were filled using the standard depth-volume-discharge relationship (FTABLES) method in HSPF. Not all dam flows are represented explicitly. For example, the Kettle Falls Dam on Namakan Lake is not represented in the Rainy Lake watershed model because it controls flow between two segments of Namakan Lake. The HSPF model represents Namakan Lake as one entire basin, so the flow would be internal to the lake as represented.

Table 5. Locations of measured flows used as outflow demand time series from controlled lakes.

Model	Waterbody	Site Name	Period of measurement record	WDM ID	Data source
RRHW	Birch Lake (Kawishiwi River)	Birch Lake Reservoir total flow	2003-2019	4352	MN Power
	Garden Lake (Kawishiwi River)	Winton total station flow (Kawishiwi Falls)	1995-2019	4368	MN Power
	Lac La Croix	Namakan River at Outlet of Lac La Croix (05PA006) [ON)	1995-2019	4720	Environment Canada
Rainy Lake	Kabetogama Lake	Gold Portage Outlet from Kabetogama Lk nr Ray, MN	1995-2019	4108	U.S. Geological Survey
	Rainy Lake	Total Fort Frances/International Falls dam outflow	1995-2019	4380	Lake of the Woods Control Board
Turtle River	Seine River	Sturgeon Falls Dam	1995-2019	4350	H20 Power

3 CALIBRATION

The extension of the model time period through 2019 allowed for validation of the existing model parameterization against observed flow and water quality data collected since the model was originally developed, including at sites that were previously unmonitored. This validation exercise revealed that recalibration of the model parameterization would improve the model representation of hydrology and water quality. Therefore, the more recent monitoring data were used to guide an update of the model parameters. Parameters were updated independently for each of the three models, but an effort was made to maintain relative consistency between models to reflect the broad similarity of the landscapes, geology, and hydrology of these watersheds within the upper Rainy River Basin. For all models, the first year of the model run was omitted from the calibration and validation, as that year is considered a "spin-up" period for the model to equilibrate from uncertain initial conditions.

The upper Rainy Lake watershed is dominated by forest and wetland land cover, so the model is most sensitive to changes in parameters relating to those classes. Therefore, calibration was focused principally on those dominant land classes, and parameters for the remaining land classes were adjusted to preserve their relative values in relation to the dominant land classes. That approach should ensure a reasonable hydrologic behavior of those less dominant land classes in a relative sense, but there is lower confidence in the ability of the model to accurately represent them in detail. That reality is important to consider in using the models to explore water quality responses to land use change scenarios.

3.1 HYDROLOGY CALIBRATION

Independently estimated or measured values were used to calibrate the model representation of as many components of the hydrological cycle as possible, including snow accumulation and melt, ET, and surface runoff. Snow Data Assimilation System (SNODAS) data [SNODAS National Operational Hydrologic Remote Sensing Center, 2004] helped constrain the snow simulation. Subsequently, model outputs were compared simultaneously to total actual ET predicted independently using remote sensing data by MODIS (MOD16) [Mu et al., 2007] and to available measured stream discharge data.

3.1.1 Snow

Snow accumulation and melt are a major control on the annual hydrological cycle in Minnesota watersheds. Accurate simulation of these processes is critical to predict the magnitude, timing, and duration spring runoff. To ensure a reasonable snow simulation, HSPF simulated snow water equivalent (SWE) was compared to SNODAS. SNODAS integrates snowcover and snowfall data from satellite, airborne, and ground station sources into a physically based, energy- and mass- balance model to produce a gridded SWE dataset at 1 km spatial resolution and daily temporal resolution [SNODAS National Operational Hydrologic Remote Sensing Center, 2004]. SNODAS data are available for the study area from 2010 through present.

HSPF simulates snow cover separately for each individual land class within each distinct weather zone. However, the SNODAS grid size is too large to compare with individual land cover grid cells used in developing the HSPF model (any one SNODAS grid cell can contain many different land cover types). Therefore, a weighted average SWE value for each HSPF weather zone, computed based on the relative

areas of the land cover classes in the model, was compared that to the average SNODAS SWE value within that weather region. Representative time series plots for weather regions encompassing the primary flow calibration gages for the RRHW, Vermilion, and Rainy Lake models, are shown in Figures 2, 3, and 4, respectively. A comparison of time-averaged values over the entire model period for each weather zone is shown in Table 6. These statistics are presented only to give a general sense of the agreement between simulated and observed snow and as a check for systematic bias toward over- or under-predicting snow amounts. Because SWE is a cumulative property, the daily data exhibit strong serial correlation. Errors carry forward throughout a winter season, such that statistics computed daily over the course of the winter may be artificially biased by errors early in the season. Therefore, model calibration was primarily informed by graphical comparisons like Figures 2-4.

The timing of the beginning of snow accumulation and of spring melt are generally well captured by HSPF (Figures 2-4). HSPF SWE is generally in good agreement with SNODAS, although in some winters (e.g. 2010-2011) SWE is consistently under-predicted across all weather zones, whereas other years (e.g. 2016-2017) SWE is consistently over-predicted. The degree to which HSPF agrees with SNODAS varies inter-annually within a weather zone (Figures 2-4) and between weather zones (Table 6). However, no systematic bias toward over- or under-prediction is apparent.

Table 6. Average yearly snowpack SWE simulated by HSPF and SNODAS for each of the weather regions comprising the Rainy Lake watershed model.

Model	Weather Region	SNODAS Avg Snowpack water equivalent (in)	HSPF Avg Snowpack water equivalent (in)	Percent Bias	R^2
Rainy Lake	39	1.74	1.38	-20.2	0.76
	41	1.42	1.18	-17.2	0.82
	43	1.35	1.12	-17.6	0.84
	45	1.36	1.24	-8.6	0.85
	55	1.17	1.23	5.1	0.87
	57	1.25	1.26	0.7	0.85
	59	1.17	1.24	5.6	0.80
Vermilion	61	1.31	1.18	-9.87	0.85
	63	1.03	1.21	16.55	0.84
	65	1.15	1.25	9.04	0.86
	67	1.14	1.25	9.00	0.88
	69	0.98	1.17	19.38	0.88
	71	0.96	1.16	21.39	0.89
	73	1.00	1.21	21.31	0.87
Rainy Headwaters	75	1.83	1.13	-38.24	0.77
	77	1.70	1.37	-18.96	0.75
	79	1.88	1.47	-21.83	0.79
	81	1.53	1.38	-10.08	0.83
	83	1.44	1.25	-13.19	0.84
	85	1.39	1.24	-10.41	0.80
	87	1.57	1.49	-5.04	0.71
	89	1.76	1.28	-27.28	0.82
	91	1.18	1.31	11.28	0.83
	93	1.52	1.30	-14.53	0.84
	95	1.45	1.20	-16.69	0.88
	97	1.73	1.39	-19.82	0.87

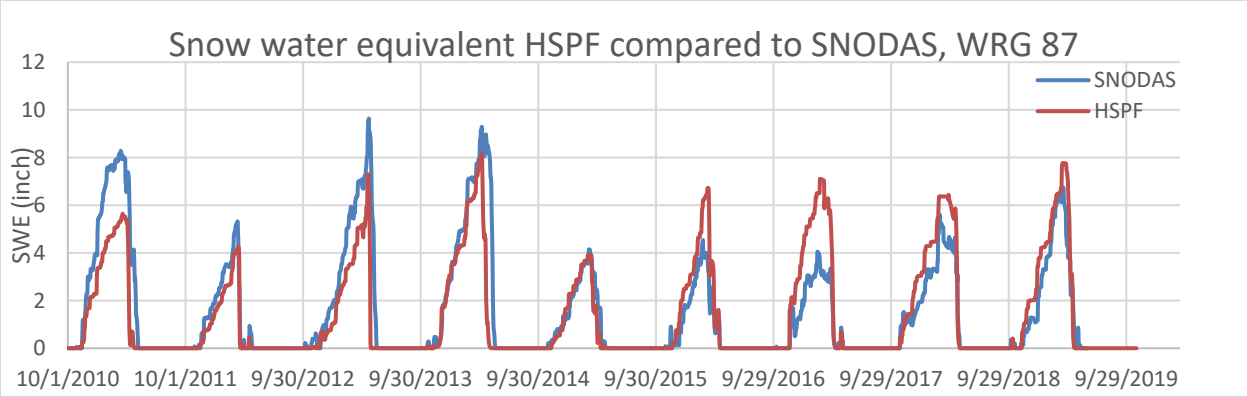

Figure 2. Daily comparison of HSPF modeled SWE to SNODAS SWE for weather region 87, in the RRHW model. This weather region contains the Kawishiwi River near Ely calibration gage, 05124480.

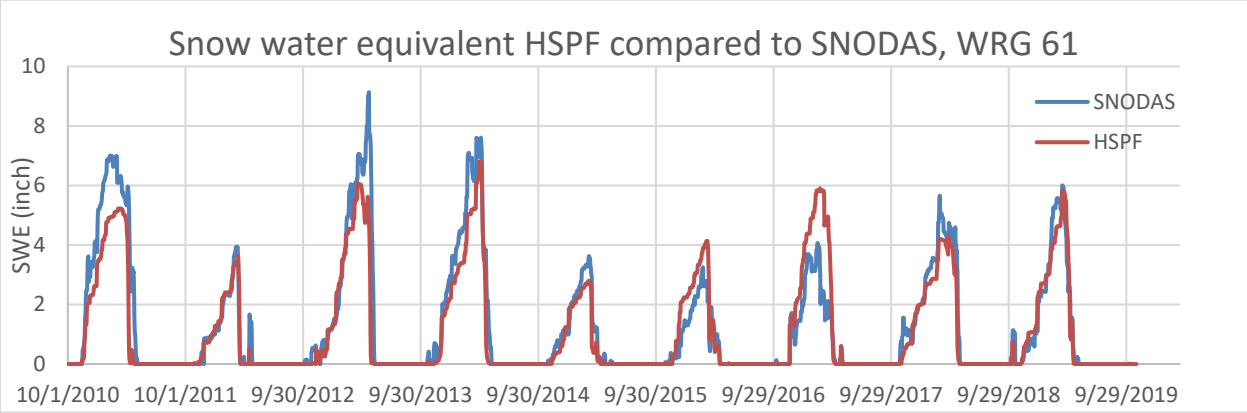

Figure 3. Daily comparison of HSPF modeled SWE to SNODAS SWE for weather region 61, in the Vermilion River model. This weather region contains the Vermilion River near Crane Lake calibration gage, 05129115.

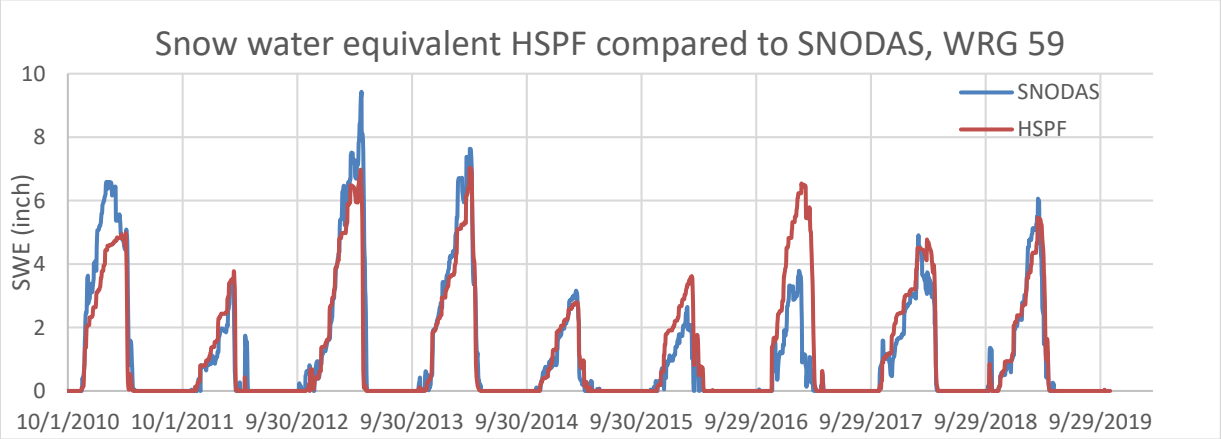

Figure 4. Daily comparison of HSPF modeled SWE to SNODAS SWE for weather region 59, in the Rainy Lake model. This weather region contains the Blackduck River near Ash Lake calibration gage, H74018008.

3.1.2 Evapotranspiration

ET represents the single largest outgoing water flux from northern Minnesota watersheds. For example, Nichols and Verry [2001] found that about 65% of precipitation was returned to the atmosphere via ET from several forested watersheds in the Marcell experimental forest. By removing water from soil storage, ET impacts antecedent soil moisture conditions and thereby surface runoff generated by storm events. Therefore, accurate representation of ET is crucial for reasonably apportioning the components of the water balance and simulating surface runoff.

MOD16 [Mu et al., 2007] presents an independent estimate of actual ET to which to compare HSPF results. The MOD16 algorithm uses satellite imagery to estimate a leaf-area index, which is used in conjunction with meteorological data to compute ET using the Penman-Monteith equation [Mu et al., 2007]. MOD16 data are available from 2000-2014. HSPF computes ET separately for each individual land class within each distinct weather zone. However, as with SNODAS, the MODIS grid size is too large to compare with individual land cover grid cells used in developing the HSPF model. Therefore, a weighted average actual ET value for each HSPF weather zone, computed based on the relative areas of the land cover classes in the model was compared that to the average MODIS estimate within that weather zone. A representative time series plot is shown in Figure 5 and a comparison of time-averaged values over the entire model period is shown in Table 7.

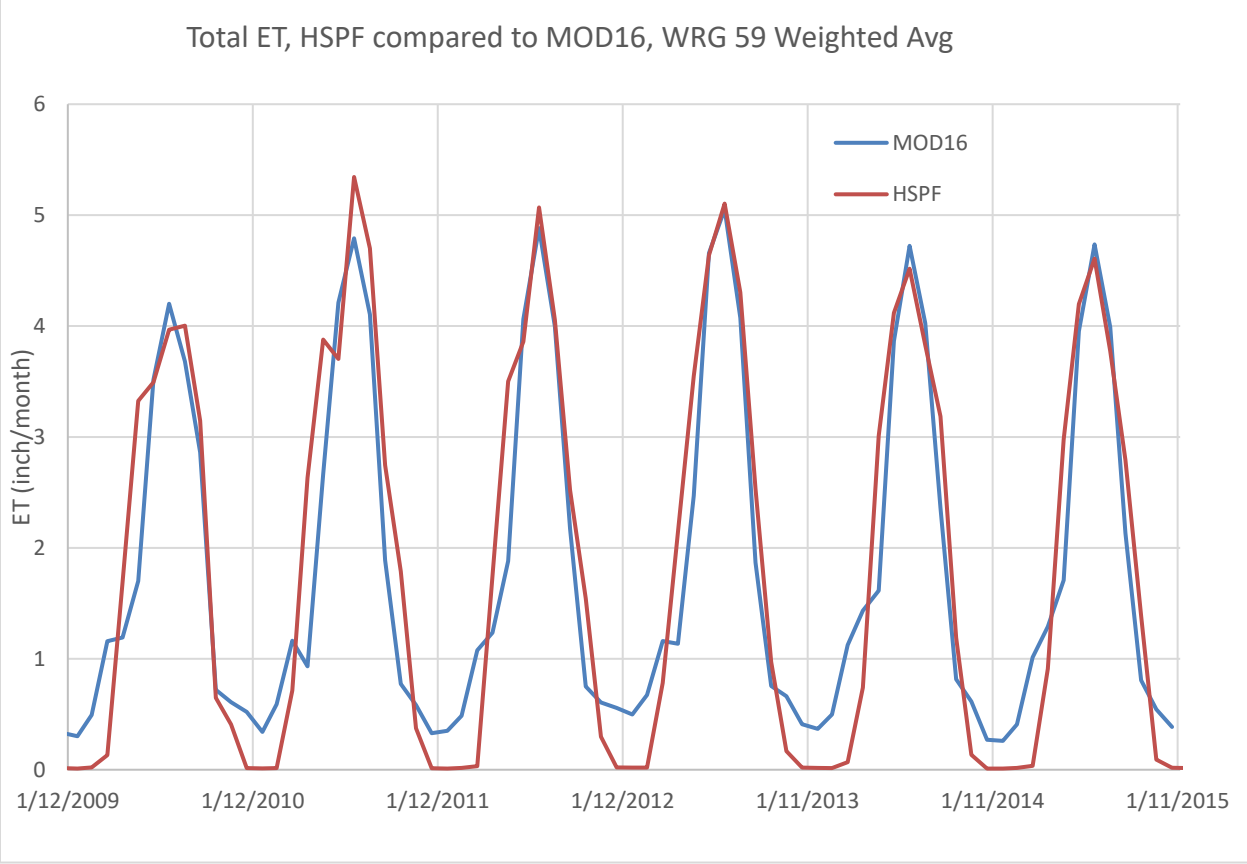

Figure 5. Comparison of monthly average HSPF modeled total actual ET to MODIS estimated total ET for weather region 59.

Table 7. Average yearly total ET modeled by HSPF and estimated by MODIS for each of the weather regions comprising the Rainy Lake watershed model.

Model	Weather Region	MODIS Avg ET (in/yr)	HSPF Avg ET (in/yr)	Percent Bias
Rainy Lake	39	19.0	20.7	9.2
	41	19.6	20.3	3.5
	43	19.8	20.5	3.7
	45	19.9	22.2	11.9
	55	21.5	22.0	2.2
	57	21.1	22.2	5.2
	59	21.7	22.3	2.6
Vermilion	61	21.2	20.6	-2.6
	63	21.4	20.5	-4.2
	65	20.4	20.6	1.2
	67	20.4	20.5	0.8
	69	21.4	20.2	-5.8
	71	20.9	20.4	-2.5
	73	21.3	20.5	-3.8
Rainy Headwaters	75	19.3	18.9	-1.8
	77	19.1	19.7	3.1
	79	19.4	19.5	0.7
	81	19.8	20.7	4.1
	83	20.2	20.7	2.4
	85	19.9	20.6	3.4
	87	19.2	20.4	5.9
	89	19.8	20.2	1.9
	91	20.1	19.8	-1.6
	93	19.8	20.3	2.6
	95	20.5	20.1	-1.9
	97	20.2	20.3	0.2

The HSPF simulated ET generally agrees well with the MODIS estimates; the seasonal pattern and magnitudes are similar (Fig. 5). HSPF consistently under-predicts MODIS ET during the winter months and ramps up ET slightly earlier in the spring. However, it is not clear whether the MODIS or HSPF algorithm is more accurate in predicting wintertime sublimation from the snowpack. Increasing the parameter controlling snowpack evaporation in HSPF resulted in a better match with the MODIS ET estimates during the winter, but decreased the agreement beween HSPF and SNODAS snow water equivalent and of simulated spring melt streamflow with observations at stream gages. Therefore, that change was not adopted.

3.1.3 Stream flow

Due to the remote nature of these watersheds, stream flow data are relatively sparse. The RRHW and Vermilion watersheds each contain long-term USGS gages that were used for model calibration. Each gage has a period of record covering the entire, or nearly the entire model period. Due to the long periods of record at these gage, the data were split into separate calibration and validation sets. The most recent ten years of data (2010-2019) were used for calibration, while the preceding years

(1997-2009 for the Kawishiwi River and 1996-2009 for the Vermilion River) were reserved for validation. Two gages were available for calibrating the Rainy Lake model, both in the Ash-Blackduck system. Both gages had only three years of data, so the data were not split into separate calibration and validation sets. All gages used for calibrating the three models are shown in Figure 6 and Table 8. Calibration results are presented in the subsections below for the primary calibration gages for each model (italicized in Table 8). Validation results and results for secondary calibration gages at each gage are presented in the appendix.

Table 8. Stream gages used for calibration of model hydrology. Primary calibration gages for each model are italicized.

Model	Site Name	HSPF Reach	Period of measurement record	Monitoring Agency	Site ID
RRHW	*Kawishiwi River near Ely, MN*	244	1997-2019	USGS	05124480
	Stony River nr Babbitt, Tomahawk Rd	341	2014-2019	DNR/MPCA	H72045001
Rainy Lake	*Blackduck River nr Ash Lake, Sheep Ranch Rd*	81	2017-2019	MPCA	H74018008
	Ash River nr Ash Lake, FR961	81+87*	2017-2019	MPCA	H74009004
Vermilion River	*Vermilion River nr Crane Lake, MN*	370	1995-2019	USGS	05129115

*This gage is located near the upstream end of HSPF reach 101, just below the confluence of reaches 81 and 87. Therefore, observed flows were compared to the sum of those two reaches rather than the simulated flow at the outlet of reach 101.

A variety of graphical and numerical methods were used to evaluate hydrologic model performance. Graphical approaches included examining hydrographs, flow duration curves, and boxplots of daily flows grouped by month. Numerical error metrics included percent bias (PBIAS) of total flow volumes and on flow volumes stratified by season and flow condition, as well as the Nash-Sutcliffe Efficiency (NSE). The NSE [Nash and Sutcliffe, 1970] is a metric commonly used to evaluate hydrological models. It is a normalized metric that compares the relative magnitudes of the residual (simulated – observed) variance and the measured data (observed – mean of observed values) variance. It varies from $-\infty$ to 1, with 1 indicating perfect fit and anything less than 0 indicating the mean of observed values is a better predictor than the model [Moriasi et. al., 2007]. Because the calculation involves the sum of the squared differences, the statistic is sensitive to errors at high values and less sensitive to errors at low flows. Performance ratings proposed by Moriasi et. al. [2007] for evaluating hydrological models based on these error metrics are shown in Table 9.

Several hydrologic parameters were estimated and adjusted during calibration. The lower zone nominal storage parameter (LZSN) was estimated from available water storage values from the SSURGO soil dataset [Soil Survey Staff, 2020]. Average water storage values were computed for each land cover category. The raw SSURGO values resulted in excessive ET compared to MODIS and correspondingly low runoff for all models. Therefore, the LZSN values were reduced proportionally to achieve reasonable ET and runoff results. The lower zone evapotranspiration parameter (LZET) can be varied monthly and was

adjusted to replicate the monthly timing and magnitude of ET predicted by MODIS. The "INFILT" parameter, the index to mean infiltration rate, was estimated by soil hydrologic group, consistent with values suggested by EPA [2000], and then adjusted to better match storm hydrographs.

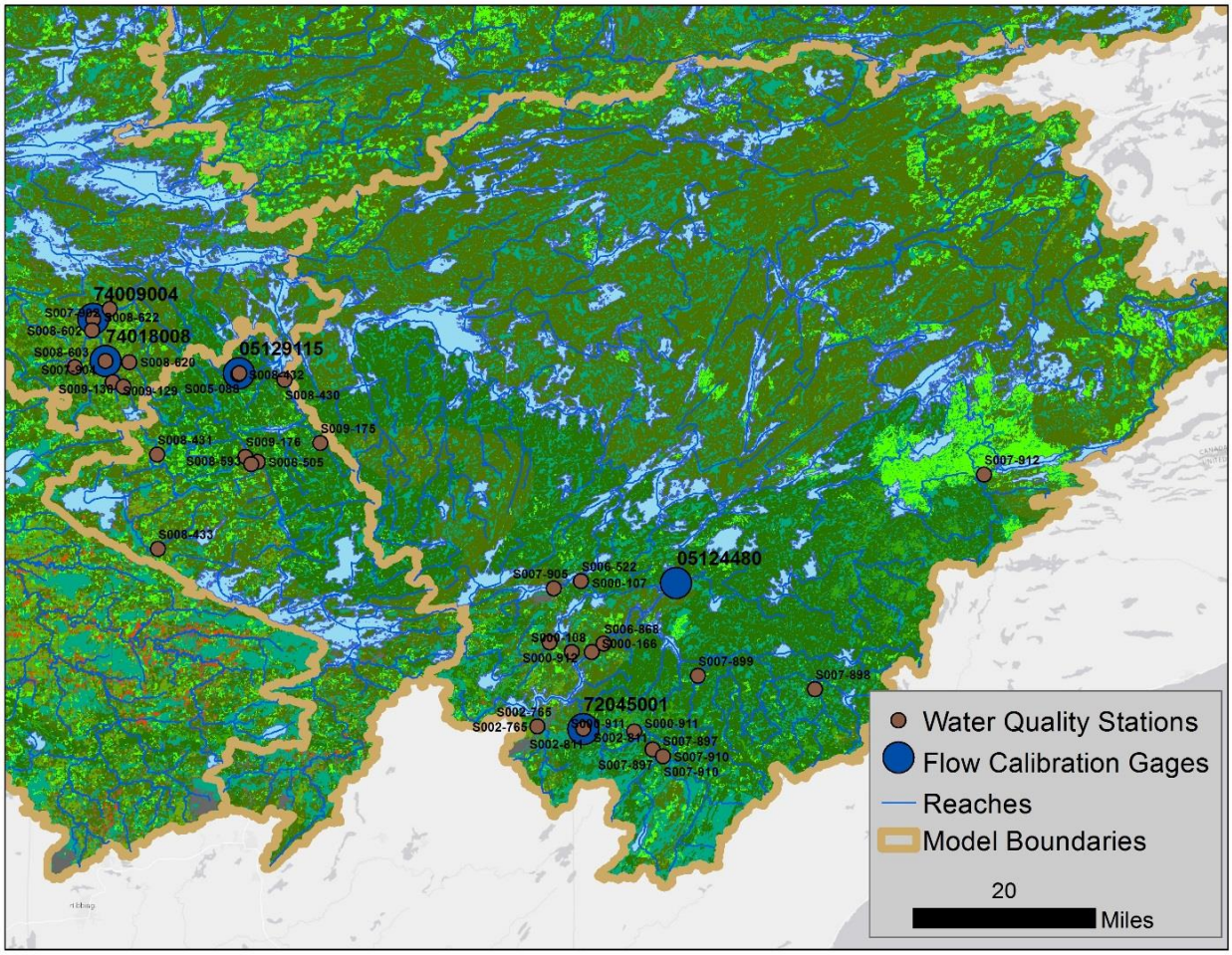

Figure 6. Stream gages and water quality stations used in model calibration/validation. Sites are labeled by site ID, with the larger labels corresponding to the flow gages.

Table 9. Hydrological model performance ratings for statistics computed at a monthly timestep. Adapted from Moriasi et al., 2007.

Performance Rating	NSE	PBIAS (%)
Very Good	0.75 < NSE < 1.00	PBIAS < ±10
Good	0.65 < NSE < 0.75	±10 < PBIAS < ±15
Satisfactory	0.50 < NSE < 0.65	±15 < PBIAS < ±25
Unsatisfactory	NSE < 0.50	PBIAS > ±25

3.1.3.1 Rainy River Headwaters Watershed

Calibration of the RRHW model was guided primarily by data from one gage on the Kawishiwi River (USGS 05124480, Kawishiwi River near Ely, MN). A gage located on the Basswood River (USGS 05127500) was not usable for calibration; the HSPF model does not simulate the different bays of Basswood Lake independently, so flow through the Basswood River is not simulated explicitly. A gage with a shorter term record (2014-present) is operated on the Stony River near Babbitt. The data are listed mostly as poor or provisional quality, however, so the gage was not used for primary calibration purposes. The calibration results at that gage are presented in the appendix.

Additionally, two other gages are located on the south branch of the Kawishiwi River (USGS gages 05125000 and 05126210). However, as originally configured, the model did not represent the branching of the river and routed all flow down the southern branch. Therefore, calibrating to the gages on the south branch would have resulted in over-prediction of flow in the rest of the model. Tributaries representing significant drainage area enter the south branch of the Kawishiwi between the split of flow and the downstream gages, so constraining the distribution of flow at the split based on data from the south branch gages was not attempted. However, during summer of 2020, after model calibration was completed, concurrent flow measurements were conducted on the north and south branches just below the split [J. D. Larson, personal communication, June 5, 2020]. These new data allowed for a reasonable preliminary estimation of the proportion of flow going to each branch, so the model was adjusted accordingly. At the time of writing, only one concurrent measurement was reported, so a constant proportional split was assumed across the entire range of flows. A total of five sets of measurements spanning a range of flow conditions over the summer was planned. Future updates to the model should incorporate those additional measurements to better represent the hydrology of the Kawishiwi River system.

Simulated flows match observed flows at the Kawishiwi River near Ely, MN gage well. Total flow volume over the calibration period is within 5 percent of the observed volume, as is flow volume in the highest 10th percentile of flows (Table 10, PBIAS). The NSE is 0.82 for monthly values and 0.72 for daily values. Both the PBIAS and NSE values achieve the “very good” performance rating following the criteria of Moriasi et. al. [2007]. Results for the validation period are similar, although surprisingly the model performs slightly better during the validation period than during the calibration period, with a PBIAS of -1.0 percent, monthly NSE 0.84 and daily NSE 0.76 (Table A.1. and Figures A.1-A.3).

The highest peak flows (~2-3 percentile), occurring during spring runoff, are occasionally over-predicted (Figures 7-8), particularly 2013-14 and 2018-19. Somewhat surprisingly, the over-prediction of spring runoff does not appear to be driven by an excess of snow, as SWE during the winters of those years is either predicted very close to SNODAS values or even slightly under-predicted (Figure 2). Whereas the highest flows are somewhat over-predicted by the model, low flows are underpredicted. The flow duration curves (Figure 8) show that flows above the 60th percentile are modelled well, but that below the 60th percentile flows, the curves diverge somewhat, with the model underpredicting these low flows. The underprediction occurs during summer (primarily June and July) and winter (December-February) (Table 10 and Figure 8).

The simulated hydrology at the Stony River gage displays similar patterns to the Kawishiwi River gage, although the model performance is somewhat worse. Calibration results are shown in the

appendix. Simulated peak flows during spring runoff are similarly biased high some years (Fig. A.4 and Table A.2), whereas lower flows the rest of the year (summer through winter) are biased low (Table A.2). The flow duration curve (Fig. A.5) shows that flows are biased low across most of the range of flows, below about the 10th percentile flow, although similar to the Kawishiwi gage, the curves don't diverge significantly until below about the 60th percentile flow. Because this gage drains a smaller drainage area than the Kawishiwi River gage, it is liable to be more impacted by uncertainties associated with simulating convective storms that may drop large amounts of rainfall on relatively small areas of a watershed. Therefore, it is not surprising that the simulation performs less well at this gage than at the Kawishiwi gage. Despite these errors, the calibration at this gage still achieves a "good" to "'very good" rating based on the criteria of Moriasi et. al. [2007], with PBIAS for total flow volume of -11.4%, monthly NSE of 0.80 and daily NSE of 0.61.

A possible explanation for the over-prediction of spring runoff some years and the under-prediction of flows later in the year is the limitations of HSPF's representation of wetland hydrology. Wetlands represent about 20 percent of this watershed, so their impact on hydrology is significant. Water generally cannot leave soil storage in HSPF except by ET. Whereas some wetlands may be disconnected from the stream network and store water only to lost by ET (i.e., behave similarly to the HSPF representation), other wetlands may be connected hydrologically to the stream network and function to attenuate peak flows and supply baseflow to streams through either surface or subsurface pathways [e.g. Erickson et. al., 2010]. In the latter case, the HSPF representation will struggle to capture wetland's impact on watershed hydrology. If storage is parameterized large enough to attenuate peak flows to the degree observed in gage data, that stored water will be lost to ET rather than released slowly as baseflow, and baseflow will be under-predicted. Conversely, if wetland storage is parameterized smaller to reduce ET and better simulate baseflow, there may not be enough storage capacity to accurately attenuate peak flows. The parameterization of the model is a compromise between these two extremes.

A possible mechanism for allowing wetlands to contribute to baseflow is the use of a monthly-variable upper zone nominal storage (UZSN). The UZSN can be set higher in the spring to store water and then reduced over the course of the year to force water out of soil storage and into interflow that then contributes to streamflow. A variable UZSN was applied to wetlands in the RRHW model (as well as the other two models described in this report). This approach improved the hydrological calibration, although the model was not as sensitive to this parameter as expected. However, an exhaustive exploration of possible values for this time-varied parameter was not possible due to time constraints, so further work could potentially lead to better representation of wetland hydrology in the future.

Table 10. Hydrology calibration statistics at Kawishiwi River near Ely, MN gage (USGS 05124480). Statistics are computed for modeled and observed datasets using only days with observed data, during the calibration period 2010-2019.

	HSPF Simulated Flow	Observed Flow	PBIAS (%)/NSE
Total in-stream flow volume (Acre-ft/month)	11245	11789	-4.6
Total of highest 10% flows (Acre-ft)	4507	4353	3.5
Total of lowest 50% flows (Acre-ft)	1326	1554	-14.7
Total summer flow volume (Acre-ft/month)	10847	11684	-7.1
Total fall flow volume (Acre-ft/month)	7096	6096	16.4
Total winter flow volume (Acre-ft/month)	2363	4204	-43.8
Total spring flow volume (Acre-ft/month)	24829	25386	-2.2
Daily NSE	-	-	0.72
Monthly NSE	-	-	0.82

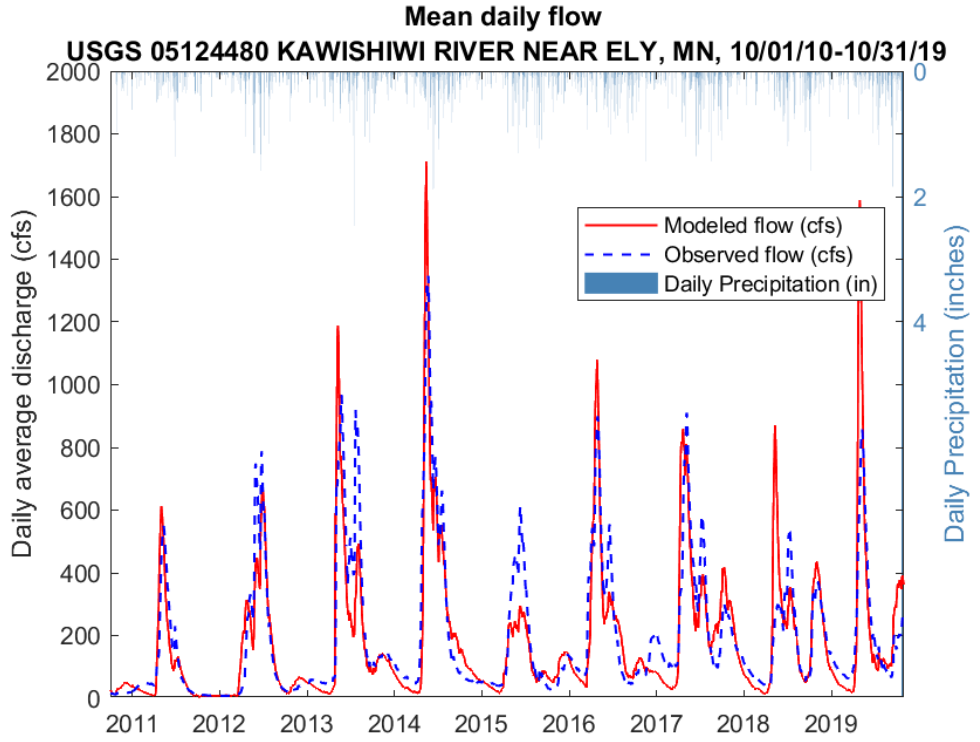

Figure 7. Hydrograph comparison of observed and simulated daily average values at USGS 05124480, Kawishiwi River near Ely, MN (RRHW model reach 244) during the calibration period.

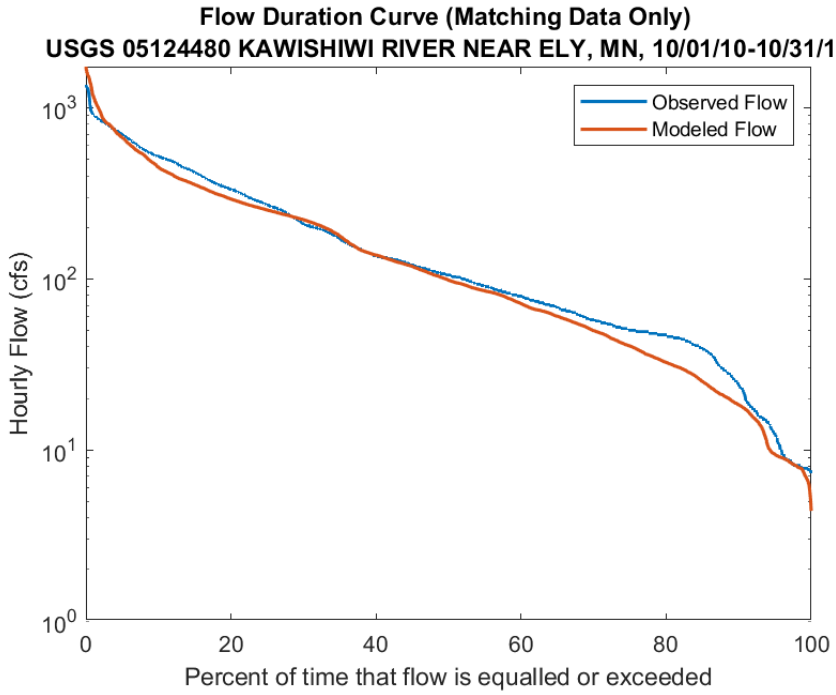

Figure 8. Flow duration curves for simulated and observed data at USGS 05124480, Kawishiwi River near Ely, MN (RRHW model reach 244) during the calibration period.

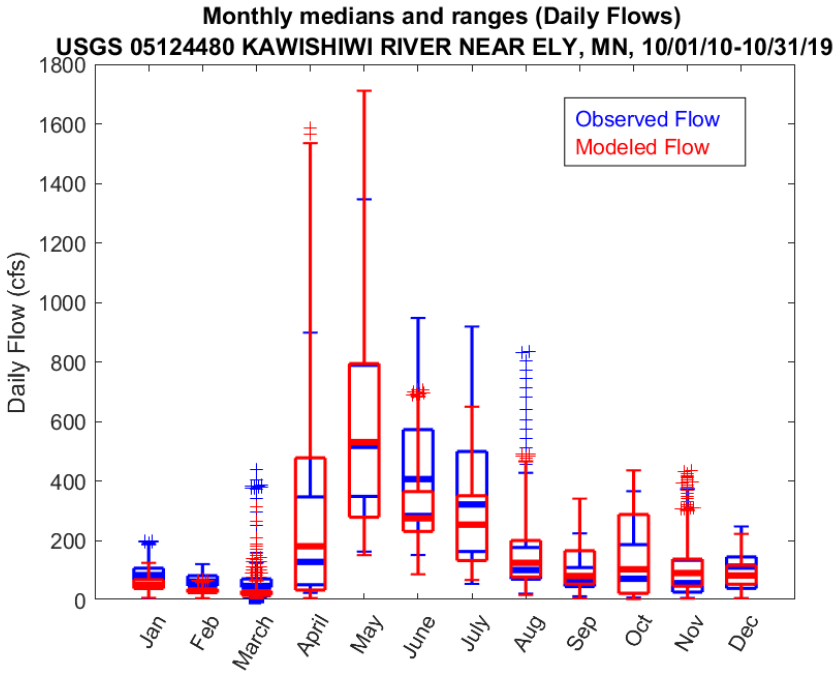

Figure 9. Boxplots comparing simulated with observed flow by month (daily average flows) at USGS 05124480, Kawishiwi River near Ely, MN (RRHW model reach 244) during the calibration period.

3.1.3.2 Vermilion River Watershed

The Vermilion River gage near Crane Lake is located near the outlet of the Vermilion River HUC8 watershed. Therefore, calibrating to this gage ensures a good representation of flow volumes leaving the watershed. Because of the large drainage area upstream of the gage, it is less sensitive to uncertainties in exact timing and spatial coverage of rainfall events than gages draining smaller areas, such as the Stony River gage described above and Ash and Blackduck Rivers described below. However, because the calibration at this gage is less sensitive to those processes important at smaller spatial scales, simulated flows in lower-order streams may have more uncertainty associated with them.

The calibration at this gage achieves a "'very good" rating based on the criteria of Moriasi et. al. [2007], for the calibration period (PBIAS for total flow volume = -9.8%, monthly NSE = 0.87 and daily NSE = 0.81; Table 11) and "good" to "very good" rating for the validation period (PBIAS for total flow volume = -11.3%, monthly NSE = 0.83 and daily NSE = 0.78; Table A.3). The timing and magnitude of flows are matched well throughout the calibration period (Fig. 10). The flow duration curves are comparable across most of the range of flows (Fig. 11). The model slightly under-simulates moderate flows and overestimates low flows below about the 70% exceedance flow value. Under-simulation of moderate flows occurs primarily during May-July and November-December (Fig. 12) and appears to be a result of a failure to register a streamflow response to some summer/fall rainstorms, for example during 2015 and 2016 (Fig. 10). As with the RRHW model, the Vermilion model somewhat under-predicts total flow volume (Table 11). Unlike the Rainy Headwaters model, the 10th percentile high flows are also under-predicted (Table 11), but the highest spring runoff flows are slightly over-predicted (Fig. 10-11).

Table 11. Hydrology calibration statistics at Vermilion River near Crane Lake gage (USGS 05129115). Statistics are computed for modeled and observed datasets using only days with observed data, during the calibration period 2010-2019.

	HSPF Simulated Flow	Observed Flow	PBIAS (%)/NSE
Total in-stream flow volume (Acre-ft/month)	33529	37175	-9.8
Total of highest 10% flows (Acre-ft)	11287	12237	-7.8
Total of lowest 50% flows (Acre-ft)	6095	6038	1.0
Total summer flow volume (Acre-ft/month)	33298	33959	-1.9
Total fall flow volume (Acre-ft/month)	21044	23360	-9.9
Total winter flow volume (Acre-ft/month)	14529	16855	-13.8
Total spring flow volume (Acre-ft/month)	64413	73607	-12.5
Daily NSE	-	-	0.81
Monthly NSE	-	-	0.87

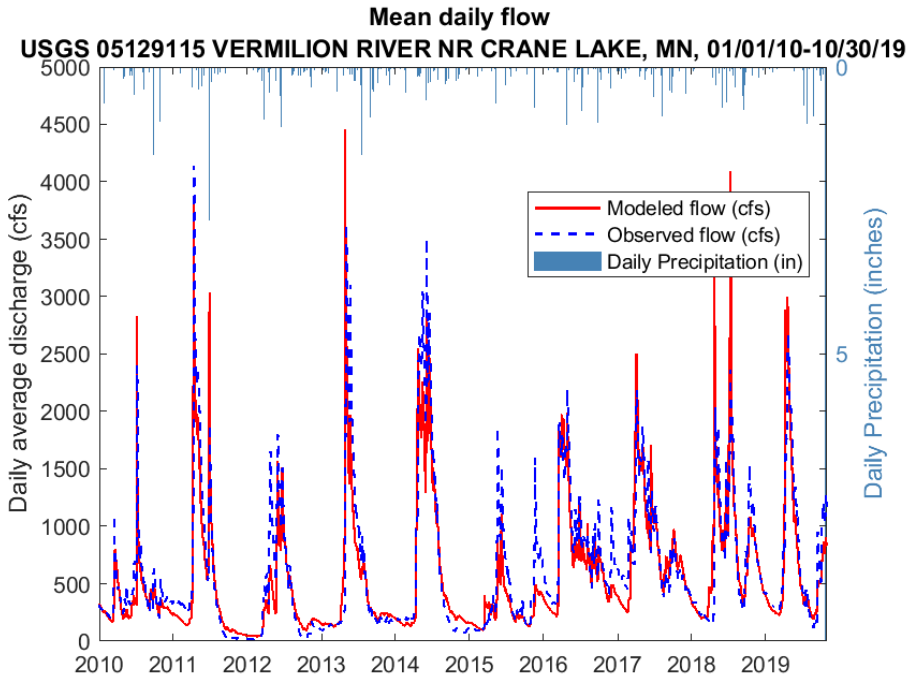

Figure 10. Hydrograph comparison of observed and simulated daily average values at Vermilion River near Crane Lake gage (USGS 05129115) (Vermilion River model reach 370) during the calibration period.

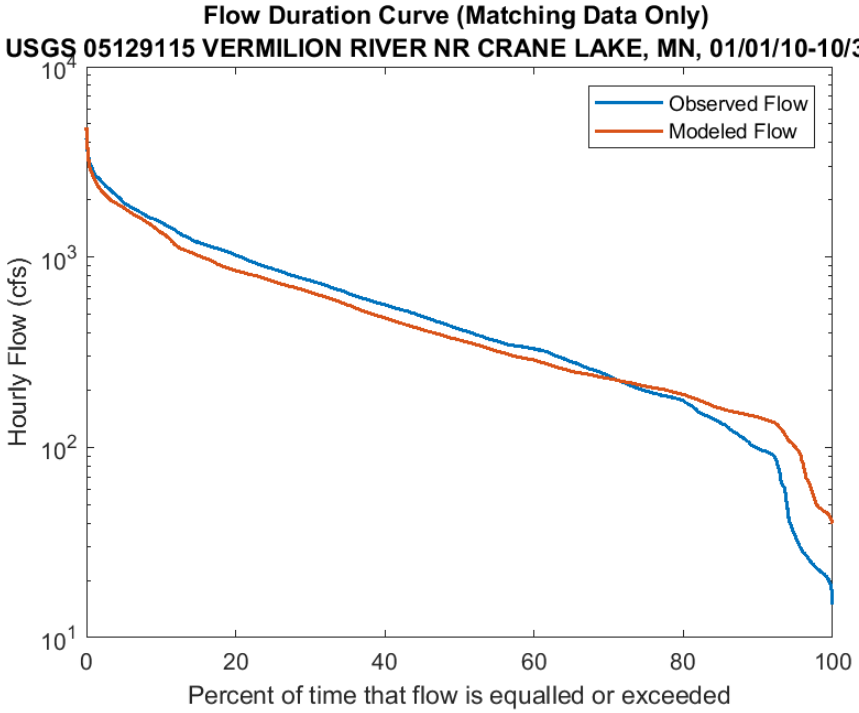

Figure 11. Flow duration curves for simulated and observed data at Vermilion River near Crane Lake gage (USGS 05129115) (Vermilion River model reach 370) during the calibration period.

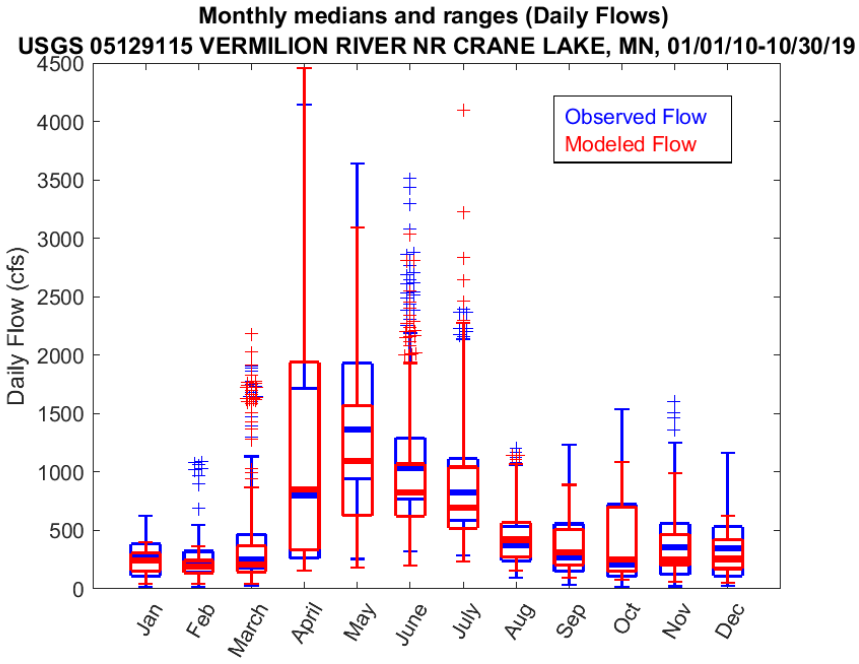

Figure 12. Boxplots comparing simulated with observed flow by month (daily average flows) at Vermilion River near Crane Lake gage (USGS 05129115) (Vermilion River model reach 370) during the calibration period.

3.1.3.3 Rainy Lake Watershed

Two gages were available for calibrating the hydrological simulation in the Rainy Lake Watershed model, on the Blackduck River and Ash River, both with three years of data from 2017-2019. Because of the intended use of the model to provide simulated flows for a sediment TMDL on the Blackduck River reach containing the stream gage, the Blackduck River gage was selected as the primary calibration target. Ash River gage data were used as a secondary calibration/validation target and results are shown in the Appendix (Table A.4 and Fig. A.10-A.12). The two gages have similar flow records, since the Blackduck River is a tributary of the Ash River about 10 miles upstream of the Ash River gage.

The PBIAS of total flow volume is excellent for the Blackduck gage, at 1.3 percent easily meeting the threshold for the "very good" rating [Moriasi et. al., 2007]. The monthly NSE of 0.44 falls below the "satisfactory" threshold, but the daily NSE of 0.62 meets the satisfactory criterion (for monthly NSE values). Daily NSE values are usually lower than monthly values. However, because of the short period of record at this gage, and the strong over-prediction of flows during one month (July 2018; Fig. 13), the monthly NSE is biased low.

Examination of the hydrograph (Fig. 13) suggests that with the exception of several rain events, simulated flows replicate the observed flow record well. The flow duration curves (Fig. 14) corroborate that observation, as the curves lie almost on top of each other except at the low end of the flow spectrum; flows smaller than approximately the 70th percentile flow are over-predicted. Several summer/fall storm peaks are significantly under-predicted by the model, whereas one peak in July 2018 is strongly over-predicted in magnitude and total volume (Fig. 13). The model's flow simulation of these

particular events was relatively insensitive to changes in hydrologic parameters such as infiltration and soil water storage. Given the small drainage area of the watershed draining to this gage, it is therefore likely that the poor simulation of these events is due to the inability of the precipitation input dataset to capture small-scale variations in rain intensity and duration that occur in reality, rather than an issue with the parameterization.

Table 12. Hydrology calibration statistics at Blackduck River near Ash Lake gage (H74018008). Statistics are computed for modeled and observed datasets using only days with observed data. This gage is operated seasonally, so no winter data are available.

	HSPF Simulated Flow	Observed Flow	PBIAS (%)/NSE
Total in-stream flow volume (Acre-ft/month)	2209	2181	1.3
Total of highest 10% flows (Acre-ft)	920	906	1.6
Total of lowest 50% flows (Acre-ft)	282	287	-1.9
Total summer flow volume (Acre-ft/month)	1581	1104	43.2
Total fall flow volume (Acre-ft/month)	2238	2089	7.1
Total winter flow volume (Acre-ft/month)	-	-	-
Total spring flow volume (Acre-ft/month)	2821	3308	-14.7
Daily NSE	-	-	0.62
Monthly NSE	-	-	0.44

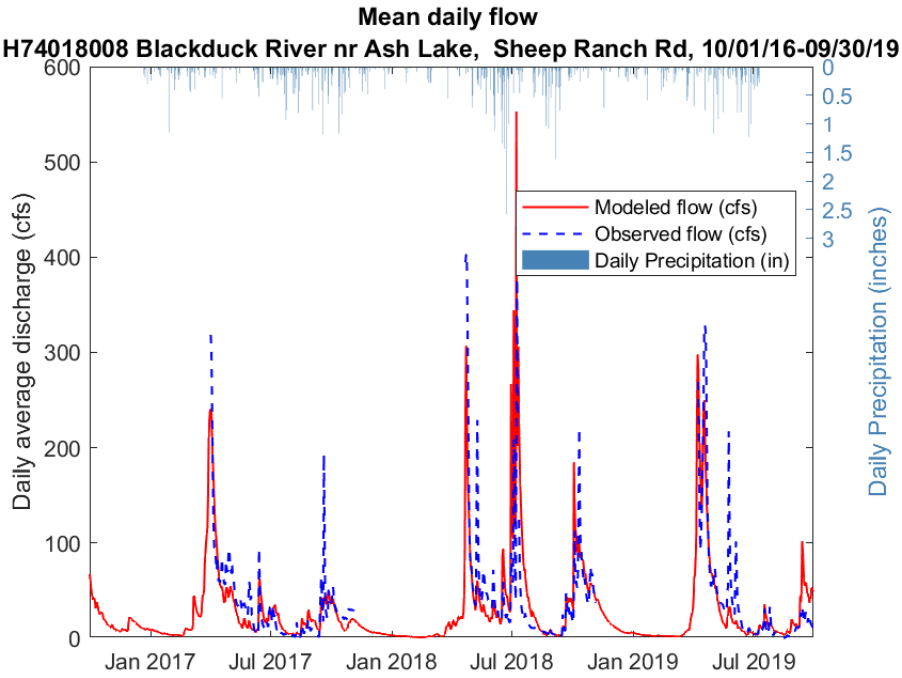

Figure 13. Hydrograph comparison of observed and simulated daily average values at Blackduck River near Ash Lake gage, H74018008.

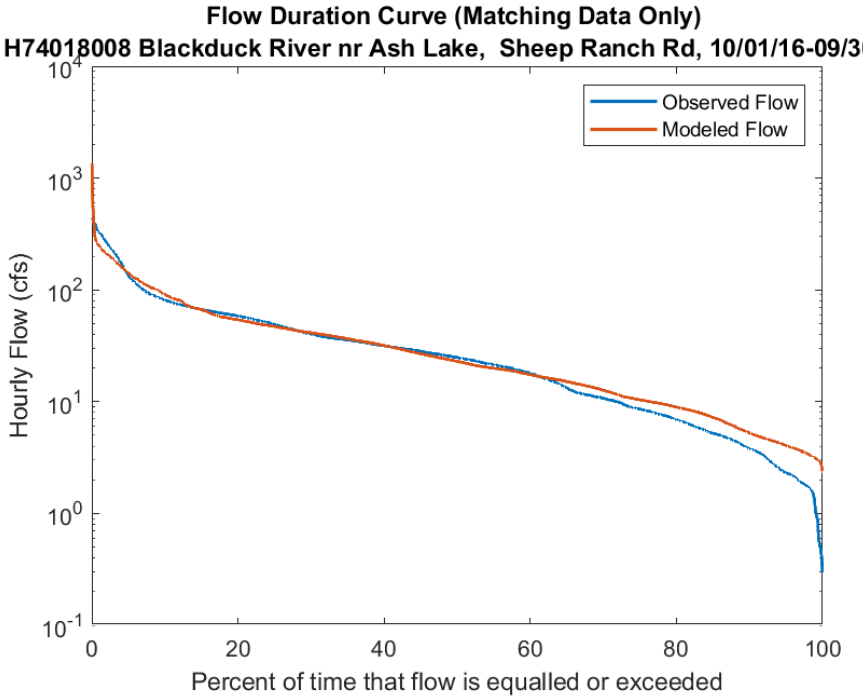

Figure 14. Flow duration curve for Blackduck River near Ash Lake gage, H74018008. Data are from 2016-2019 and include only days where observed flow was measured.

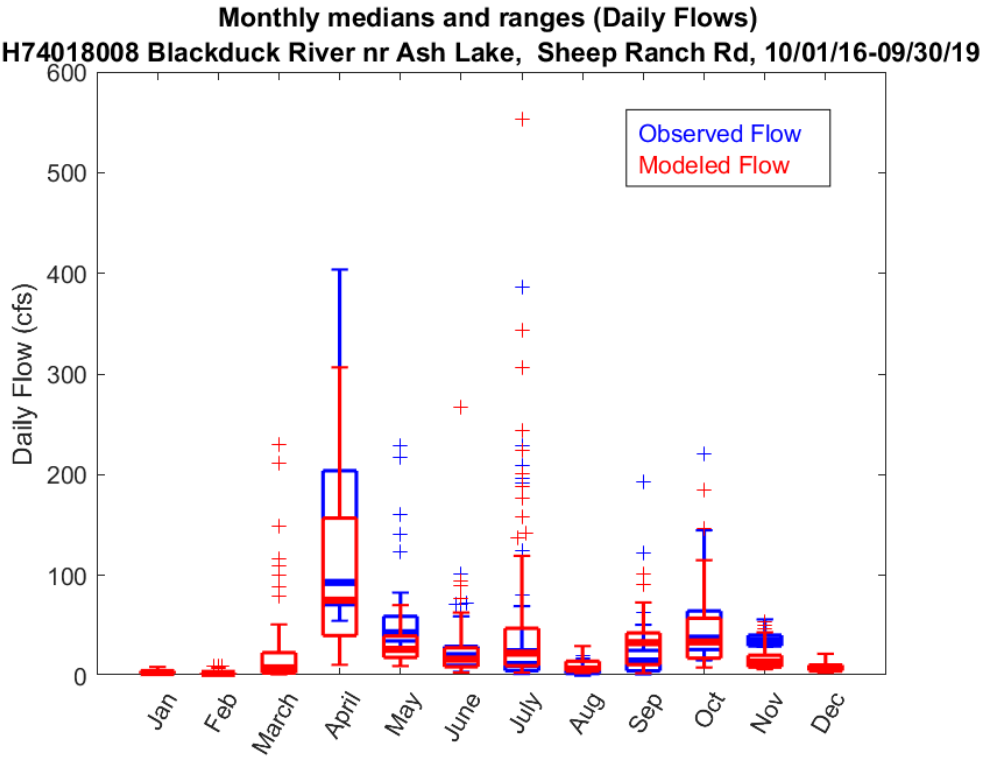

Figure 15. Boxplots comparing simulated with observed flow by month (daily average flows).

3.2 WATER QUALITY CALIBRATION

Water quality parameters modeled by HSPF include fine sediment (sand, silt and clay), phosphorous and nitrogen in organic and inorganic forms, benthic algae and phytoplankton. Most of these parameters have multiple non-point sources, including upland sources and near-channel or internal lake loading sources. The absolute or relative contributions of each source are generally poorly constrained by independently measured data in these watersheds. In cases where such data were available, such as with internal loading of phosphorus in Myrtle Lake in the Vermilion River watershed, they were used to constrain the HSPF simulation. When such data were not available, achieving a realistic representation of water quality in the simulation involved an iterative process of adjusting parameters controlling non-point upland loading rates to reasonable levels and adjusting in-stream loading rates and parameters to achieve agreement between simulated in-stream concentrations and observed values.

Because few data for non-point loading rates exist for these specific watersheds, literature values compiled for Minnesota generally (Table 13) [Mishra and Donigian, 2015] were consulted as targets for non-point loading rates. Data and model results used to develop those targets were skewed toward southern Minnesota and agricultural watersheds, and Mishra and Donigian [2015] note that there is more uncertainty on the low end of the ranges than the upper end. Experience calibrating these models and other northern Minnesota models [MPCA, 2020] has suggested that loading rates, especially for forested landcovers, must be lower than the suggested range to match observed instream concentrations. Nevertheless, these ranges were used as a reference, especially to constrain relative magnitudes of loading rates between landcover types.

Table 13. Nonpoint loading rate target ranges for Minnesota from Mishra and Donigian [2015].

	Forest		Pasture*		Developed		Cropland		Impervious	
Constituent	Low	High	Low	High	Low	High	Low	High	Low	High
Sediment/TSS (tons/ac/yr)	0.05	0.15	0.2	1.0	0.15	0.5	0.1	1.5	0.05	0.5
BOD/Organics (lbs/ac/yr)	2	10	5	70	5	15	5	50	3	20
NO3-N (lbs/ac/yr)	1	5	1	15	3	10	10	30	2	5
NH3-N (lbs/ac/yr)	0.1	1.0	0.2	1.5	0.2	2.0	0.5	2.0	0.5	1.5
TN (lbs/ac/yr)	2	8	2	25	5	15	10	50	3	10
PO4-P (lbs/ac/yr)	0.02	0.10	0.2	2.0	0.1	1.0	0.3	2.0	0.2	0.7
TP (lbs/ac/yr)	0.05	0.50	0.5	2.5	0.2	1.5	0.5	3.0	0.3	1.0

*excludes pasture receiving manure/litter applications

Water quality calibration was accomplished using measured concentration data from 15 sites in the Rainy River Heawaters watershed, 10 sites in the Vermilion River watershed, and 8 sites in the Rainy Lake Watershed. Sites are listed in Tables 14-16, and mapped in Figure 6. Many gages, principally on low-order tributaries, had data for only 1 or 2 years, limiting their usefulness for model calibration. These gages were nevertheless useful to expand the geographic extent of the calibration network and ensure the model was producing reasonable results higher up in the watershed and not just at the mouth of the major watersheds.

Most gages had total suspended solids (TSS), total phosphorus (TP) and total ammonia (TAM) observations. A smaller number of gages had dissolved orthophosphate (PO_4), nitrate plus nitrite (NO_2 + NO_3) and chlorophyll *a* (chl-*a*) data. Dissolved oxygen (DO) data were available at most gages as well, but due to time limitations, the models were not calibrated intensively for DO.

Table 14. Water quality monitoring stations in RRHW watershed used for model calibration.

Site Information				# Observations							
Waterbody	***Site ID***	***HSPF Reach***	***Period of record***	***TSS***	***TP***	***PO_4***	***NO_2 + NO_3***	***TAM***	***BOD***	***DO***	***Chl-a***
Cross River	S007-912	37	2014-2015	17	17	-	-	17	-	24	-
Dumbbell River	S007-898	261	2014-2018	13	13	-	-	13	-	25	-
Little Isabella River	S007-899	289	2014	11	11	-	-	11	-	23	-
South Kawishiwi River	S000-166	303*	2006-2009	11	19	1	-	1	-	19	17
South Kawishiwi River	S006-868	303*	2011-2018	-	39	-	-	-	-	285	39
Dunka River	S002-765	313	2014-2015	36	36	-	-	36	-	50	-
Stony River	S007-910	323	2014-2015	24	24	-	-	24	-	40	-
Stony River	S000-911	341*	2006-2008	16	32	-	-	-	-	116	32
Stony River	S002-811	341*	2014-2019	282	292	176	-	34	-	278	-
Stony River	S007-897	341	2014	10	10	-	-	10	-	6	-
South Kawishiwi River	S000-108	353	1995-2018	82	155	73	-	95	16	127	32
Bear Island River	S000-912	361	2014-2015	28	37	-	-	17	-	82	19
Kawishiwi River	S000-107	369*	2006-2008	11	20	-	-	-	-	20	19
Kawishiwi River	S006-522	369*	2008-2019	248	214	237	-	11	-	206	1
Shagawa River	S007-905	383	2014-2015	17	17	-	-	18	-	33	-

*When multiple sites were located on the same HSPF reach, data from all sites were aggregated for calibration.

Table 15. Water quality monitoring stations in Vermilion River watershed used for model calibration.

Site Information				# Observations							
Waterbody	***Site ID***	***HSPF Reach***	***Period of record***	***TSS***	***TP***	***PO_4***	***NO_2 + NO_3***	***TAM***	***BOD***	***DO***	***Chl-a***
Unnamed creek	S008-593	123	2015-2016	-	9	-	-	-	-	25	-
Unnamed creek	S009-176	125	2016	-	8	-	-	-	-	21	-
Vermilion River	S006-505	130	2014-2019	155	127	81	156	11	-	143	-
Elbow River	S008-433	227	2015-2016	11	11	-	11	11	-	19	-
Pelican River	S008-431	270	2015-2017	18	26	-	14	11	-	46	-
Vermilion River	S005-088	370*	2008	269	206	210	268	11	-	220	2
Vermilion River	S008-432	370*	2015-2016	11	17	-	17	11	-	19	14
Hunting Shack River	S009-175	413	2016	-	9	-	-	-	-	21	-
Echo River	S008-430	415	2015	11	11	-	11	11	-	19	-
Myrtle Lake	?	241	2018	-	14	-	-	-	-	-	14

*When multiple sites were located on the same HSPF reach, data from all sites were aggregated for calibration.

Table 16. Water quality monitoring stations in Rainy Lake watershed used for model calibration.

Site Information				# Observations							
Waterbody	***Site ID***	***HSPF Reach***	***Period of record***	***TSS***	***TP***	***PO_4***	***NO_2 + NO_3***	***TAM***	***BOD***	***DO***	***Chl-a***
Blackduck River	S009-130	73	2016-2017	9	8	-	-	-	-	14	-
Ninemile Creek	S008-620	75	2015-2016	12	13	-	-	-	-	27	-
Fawn Creek	S009-129	77	2016	12	12	-	-	-	-	19	-
Blackduck River	S007-904	81	2014-2017	51	43	-	-	17	-	82	-
Ash River	S008-603	83	2015-2017	15	13	-	-	-	-	36	-
Ash River	S008-602	87	2015-2017	19	14	-	-	-	-	33	-
Ash River	S007-902	101*	2014-2018	32	31	-	-	17	-	47	2
Ash River	S008-622	101*	2015-2017	41	37	16	-	-	-	47	-

*When multiple sites were located on the same HSPF reach, data from all sites were aggregated for calibration.

Table 17. Model performance ratings for water quality constituent load error statistics. Adapted from Moriasi et al., 2007.

Performance Rating	Sediment PBIAS (%)	N,P PBIAS (%)
Very Good	PBIAS < ±15	PBIAS < ±25
Good	±15 < PBIAS < ±30	±25 < PBIAS < ±40
Satisfactory	±30 < PBIAS < ±55	±40 < PBIAS < ±70
Unsatisfactory	PBIAS > ±55	PBIAS > ±70

3.2.1 Sediment

HSPF simulates upland soil detachment and wash-off, as well as in-channel erosion, transport, and deposition. Detailed sediment budgeting or sediment fingerprinting data were not available in any of these watersheds to constrain the relative contributions of upland and in-channel sediment sources. Therefore, there is inherent uncertainty in the model's predictions of the distribution of sediment between source areas. However, geomorphic information was available in the Ash and Blackduck River watershed [Jasperson, 2019] to inform the parameterization of upland and near-channel sediment loading in the Rainy Lake watershed model. The upland sediment parameterization for that model was used as a reference point for the other two models.

Although no long term sediment data records exist in the Ash/Blackduck system, observations spanning 2-4 years (2014-2017) were collected at numerous locations throughout the watershed in different geomorphic settings. Sediment transport dynamics varied significantly between geomorphic settings in the watershed, which allowed for an estimation of contributions from upland and near-channel sources. Sediment concentrations upstream of Blackduck River site S007-904 are consistently below 10 mg/L (e.g., Fig. 16), whereas concentrations at that site are as high as 70 mg/L and are strongly correlated with streamflow (Fig. 17). A field-based geomorphic assessment of channel and bank conditions throughout the watershed indicated that there is minimal bank erosion in the Blackduck River and its tributaries upstream of HSPF reach 81 [Jasperson, 2019]. However, much higher bank erosion rates were estimated within reach 81, likely due to historical channelization at the head of reach 81 that reduced the natural channel length and dramatically increased the slope of this reach [Jasperson, 2019]. To reflect these findings in the model's sediment simulation, the critical shear stress parameters controlling in-stream sediment dynamics in the tributaries upstream of reach 81 on the Blackduck River were adjusted to allow transport of sediment supplied to the stream, but very little scour. Then the parameters controlling upland sediment loading were adjusted to reproduce observed in-stream concentrations in those reaches.

Upland soil erosion is governed by two processes, sediment detachment by rainfall, and subsequent washoff of detached sediment by overland flow. Each process is represented in the model by a power function equation. According to EPA [2006], the coefficient in the detachment equation (KRER) is proportional to the K-factor parameter in the Universal Soil Loss Equation. K-factor values were obtained from the SSURGO soil dataset [Soil Survey Staff, 2020] and an average value was computed for each pervious land segment (PERLND). The KRER values were adjusted (using multiplication factors to maintain their proportionality) in tandem with values for KSER, the coefficient in the soil washoff

equation, to achieve reasonable relative unit area loading rates compared to literature values (Table 13) and replicate observed in-stream TSS concentrations (i.e., Fig. 16-19).

The model exhibits a pattern of under-predicting low and moderate concentrations and over-predicting many high-concentration events across most sites (Fig. 16-19). That bias appears to be driven by upland sediment erosion and washoff in the model, as it is apparent even in stream reaches with little modeled in-stream erosion (i.e., Fig. 16). To address this issue, the exponent parameters in the sediment detachment and washoff equations (JRER and JSER, respectively) for most land cover types were reduced to the minimum values recommended for those parameters by EPA [2006]. Those changes improved the sediment calibration, but future investigation of reducing the exponent parameters below recommended values may be warranted.

The multiplication factors to convert raw K-factor values to KRER values were applied to the rest of the Rainy Lake Watershed model and the Vermilion and Rainy Headwaters models, as were the calibrated KSER, JSER, and JRER values. Then, the critical shear stress parameters controlling scour and deposition of sediment were adjusted to match the timing and magnitude of observed sediment concentrations. Where geomorphic information and TSS data were available, in the Blackduck-Ash system, to allow a more detailed calibration, the critical shear stress and channel erodibility parameters were calibrated independently for each reach. However, in the rest of the Rainy Lake model and the Vermilion and RRHW model, those parameters were adjusted uniformly by stream order, to avoid over-fitting the models.

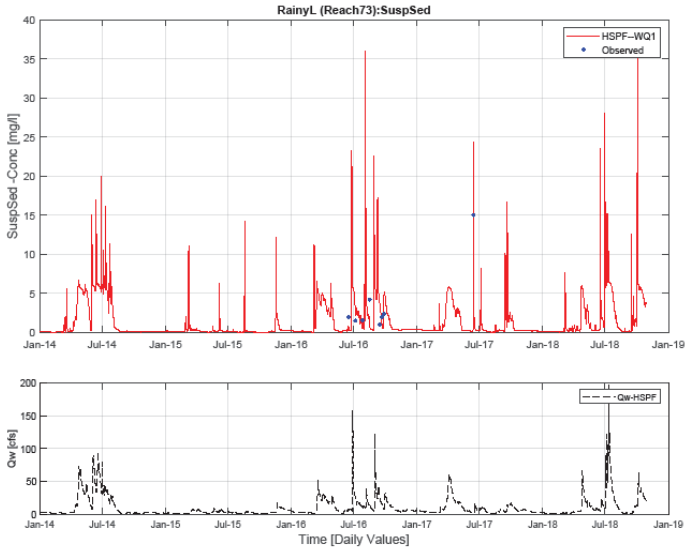

Figure 16. Time series of simulated and observed suspended sediment concentrations at S009-130, Blackduck River (Rainy Lake model reach 73).

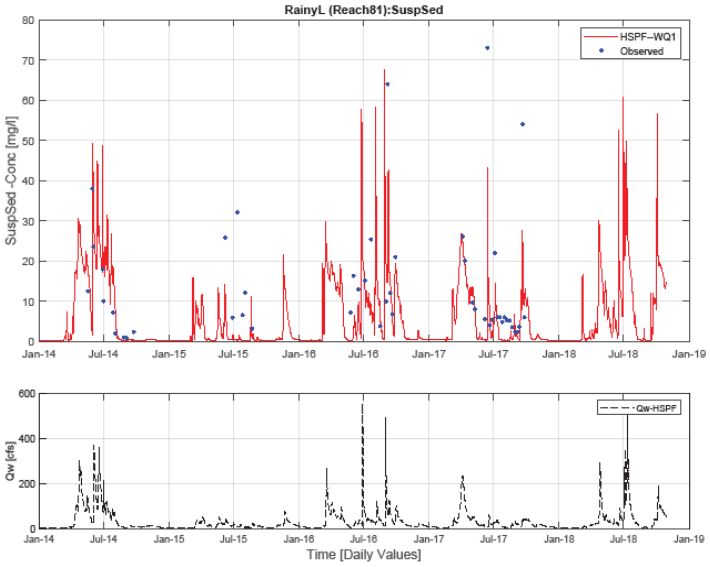

Figure 17. Time series of simulated and observed suspended sediment concentrations at S007-904, Blackduck River (Rainy Lake model reach 81).

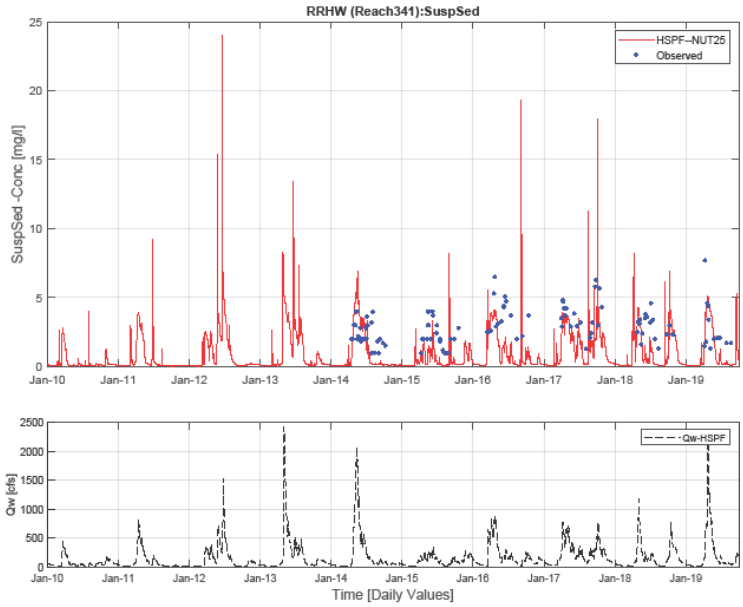

Figure 18. Time series of simulated and observed suspended sediment concentrations at S002-811, Stony River near Babbitt, Tomahawk Rd (RRHW Reach 341).

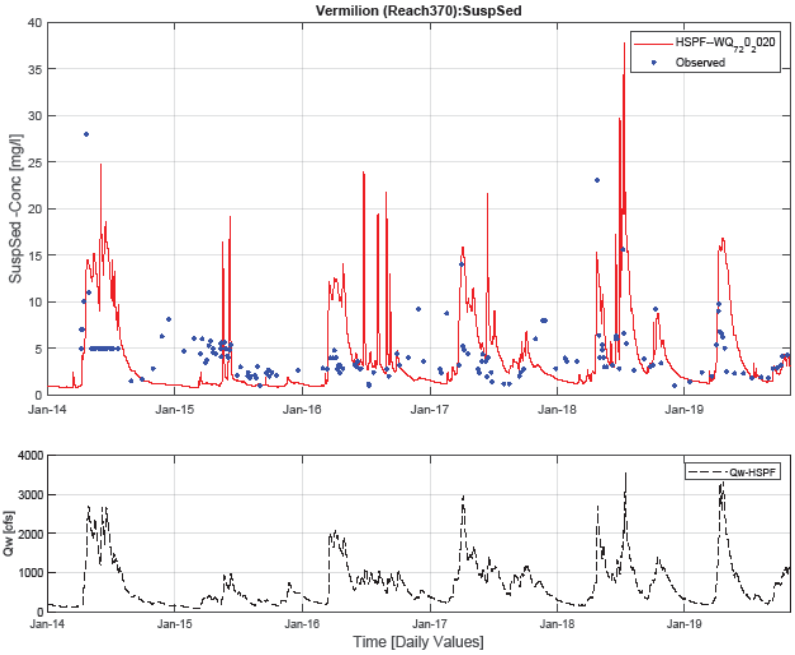

Figure 19. Time series of simulated and observed suspended sediment concentrations at S005-088, Vermillion River nr Crane Lake, MN (Vermilion River model reach 370).

Measured in-stream TSS concentrations were the primary calibration target to constrain sediment dynamics in the model. Calibration results from primary calibration sites for each model are presented in Fig. 16-19. Calibration plots for all sites are presented in Appendix 6.2. Additionally, several sites in these watersheds are part of the MPCA's Watershed Pollutant Load Monitoring Network (WPLMN) and have loads computed from measured concentration-discharge relationships. The WPLMN loads served as numerical targets for simulated sediment loads. Annual comparisons of sediment loads between HSPF and WPLMN are shown in Table 18.

Simulated sediment concentrations and loads match observed data relatively well. The timing and magnitude of TSS concentrations are generally well captured across the range of flows and concentrations, although, as described previously, low and moderate concentrations are somewhat under-predicted, whereas the highest concentrations are over-predicted across most sites (Figures 16-19). Percent bias values for sediment loads calculated over the entire time period covered by each WPLMN site all fall in the "very good" to "satisfactory" range suggested by Moriasi et al. [2007] (Tables 17-18). There is significant variability in percent bias values from year to year at all sites. Most sites have years where sediment load is under-predicted by HSPF and other years where sediment load is over-predicted (Table 18). The RRHW and Rainy Lake models show an overall bias toward under-prediction compared to the WPLMN sediment loads, whereas the Vermilion River model shows an overall over-prediction bias compared to WPLMN. It is important to keep in mind that with the low TSS

concentrations observed in these watersheds (generally below 10mg/L at most sites) relatively small absolute differences in TSS concentration and load can result in large percent bias values. Also important to keep in mind is that the WMPLN computed loads are also based on a model (statistical as opposed to physically-based) rather than continuous monitoring, and therefore also contain uncertainty.

Table 18. Annual TSS load comparison between HSPF and WPLMN.

Model	Site Name	HSPF Reach	Year	WPLMN Load (kg)	HSPF Load (kg)	PBIAS (%)
Rainy River HW	*Kawishiwi River nr Winton, CSAH18*	369	2009	1,148,293	1,220,624	6
			2010	399,040	84,982	-79
			2011	624,911	272,638	-56
			2012	1,283,733	1,145,442	-11
			2013	2,035,176	2,104,028	3
			2014	1,454,562	2,863,212	97
			2015	876,825	147,870	-83
			2016	1,856,944	1,132,533	-39
			2017	2,532,920	1,830,893	-28
			Mean	**1,356,934**	**1,200,247**	**-12**
	Stony River nr Babbitt, Tomahawk Rd	341	2014	373,216	622,186	67
			2015	236,304	52,674	-78
			2016	536,500	345,206	-36
			2018	333,903	269,891	-19
			Mean	**369,981**	**322,489**	**-13**
Vermilion River	*Vermilion River at Buyck, CSAH 24*	130	2015	524,508	141,025	-73
			2016	1,002,937	1,528,991	52
			2017	1,153,251	1,800,896	56
			Mean	**893,565**	**1,156,970**	**29**
	Vermilion River nr Crane Lake, MN	370	2009	2,312,143	3,478,076	50
			2010	1,395,613	1,355,395	-3
			2011	2,108,725	4,180,959	98
			2012	1,456,602	1,309,774	-10
			2013	2,001,549	2,996,132	50
			2015	1,355,635	622,187	-54
			2016	2,452,102	4,239,240	73
			2017	2,841,032	4,795,837	69
			Mean	**1,944,465**	**2,785,646**	**43**
Rainy Lake	*Rat Root River nr International Falls, CR145*	170	2016	1,410,203	1,126,285.0	-20
			2017	1,074,945	573,210.0	-47
			Mean	**1,242,574**	**849,747.5**	**-32**

Annual average simulated sediment loading rates by land cover type for each model are shown in Table 19 and Fig. 20-22. Loading rates generally below the target rates recommended by Mishra and Donigian [2015] were necessary to produce in-stream TSS in agreement with observed concentrations (yellow-shaded cells in Table 19). This result was also observed in another forest- and wetland-

dominated watershed in northeastern Minnesota [MPCA, 2020b], suggesting that erosion rates and/or sediment delivery ratios in these forested northern watersheds may be lower than for forested areas in other parts of the state. Because forest and wetlands make up the vast majority of land cover in these watersheds, the model is predominantly sensitive to loading rates from those cover types and relatively insensitive to loading rates from less dominant cover types (e.g., agricultural and urban land). Parameters controlling loading rates were adjusted uniformly across cover types to maintain reasonable values in a relative sense, but the simulated loading rates from less dominant cover types have large uncertainty. This uncertainty must be kept in mind when evaluating land cover change scenarios using the models.

Calibrated sediment loading rates are higher across land cover types in the RRHW and Vermilion River watersheds than in the Rainy Lake watershed (Table 19). The difference may be a result of the influence of lakes along the channel network in both the Vermilion and Rainy Headwaters models. HSPF may be overestimating the trapping efficiency of these lakes, thereby requiring larger sediment inputs to replicate observed TSS concentrations downstream of these lakes.

Table 19. Annual average simulated sediment loading rates (tons/acre/yr) by land cover type. Cells are color coded based on their relation to the ranges proposed by Mishra and Donigian [2015]. Cells shaded green fall within the expected range, whereas cells shaded yellow fall below the expected range.

	Wetland	Urban	Mature Deciduous Forest	Young Forest	Mature Evergreen Forest	Agricultural	Grasslands	Feedlot	Urban Impervious
Rainy Lake Watershed	0	0.019	0.002	0.006	0.001	0.138	0.010	0.057	0.1
RRHW Watershed	0	0.037	0.003	0.016	0.001	N/A	0.021	N/A	0.117
Vermilion River Watershed	0	0.032	0.004	0.019	0.002	0.22	0.021	0.109	0.187

3.2.2 Nutrients and Algae

Phosphorus and nitrogen are simulated in both inorganic and organic forms, and each have multiple source pathways and sinks within the model. Simulated phosphorus species include inorganic orthophosphate (PO_4) in both particulate and dissolved phases, as well as organic phosphorus. Simulated nitrogen species include Nitrite (NO_2), Nitrate (NO_3), total ammonia (TAM), and organic nitrogen. Nutrient loading and cycling processes were calibrated jointly and iteratively along with algal processes, since they all influence and interact with one another. As with sediment, the primary calibration targets were observed concentrations and loads of organic and inorganic nutrient species, and chlorophyll, within the stream/lake network. Achieving non-point loading rates compatible with the targets in table 13 was also a consideration.

Simulated phosphorous sources include upland-derived orthophosphate (PO_4) through sediment-associated surface runoff and dissolved interflow and groundwater pathways, as well as a P component of washed-off organic matter (i.e., BOD). Additionally, sediment re-suspension within streams and lakes introduces sediment-bound PO_4 to the water column, and internal loading of

dissolved PO_4 and organic P (as a component of BOD) can occur in lakes and streams at specified aerobic and anaerobic rates of benthic release. The primary P sinks within the model are lakes along the channel network, where sediment and organic matter fall out of suspension and are deposited on the bed along with the P associated with them.

Each of those sources and sinks have calibration parameters associated with them. Interflow and groundwater originating from each land cover class have user-defined concentrations of dissolved PO_4. Measurements of groundwater PO_4 concentrations are sparse in northeastern MN, and concentrations measured from aquifers may not necessarily reflect the shallow, active groundwater represented in HSPF. Nevertheless, simulated concentrations were kept consistent with measured values from within the Minnesotan Northern Lakes and Forests/Wetlands ecoregion reported by MPCA [2013], and adjusted to reproduce observed in-stream dissolved PO_4 concentrations during baseflow conditions. Subsequently, interflow concentrations were adjusted based on observed in-stream concentrations during storm events.

Sourcing of sediment-bound $P0_4$ is governed by user-defined concentrations (mg-PO_4/kg sediment) for soil washed off the uplands and for bank/bed sediment eroded/suspended within the stream channel. Storage of sediment-bound P within the system is governed by parameters controlling sediment deposition, including the critical shear stress for deposition and settling rate. Critical shear stresses were adjusted during the sediment calibration, but not during the nutrient calibration. Observed in-stream PO_4 values generally include only the dissolved fraction, and so are not useful for calibrating the sediment-bound fraction. However, TP measurements do incorporate the particulate fraction, and were used to guide the parameterization of this component following the calibration of the dissolved component.

Internal diffusive loading of PO_4 from lake bed sediments has been shown to be a large source of P loading to some lakes in northern MN, particularly under anoxic hypolimnetic conditions [e.g., James, 2017; Edlund et al., 2017; Edlund et al., 2019]. Whether lake sediments act as a net source or sink depends on lake-specific limnological and geochemical conditions, land cover and disturbance histories [Holdren and Armstrong, 1980]. In HSPF, PO_4 loading rates can be specified uniquely for each explicitly modeled lake and stream reach, with separate rates provided for oxygenated and anoxic conditions. In practice, however, because lakes are modeled as fully mixed, homogenous bodies of water, thermal stratification is not modeled and anoxic conditions rarely occur in the simulation. Benthic release rates are applied uniformly per unit area of lakebed.

In the summer of 2018, multiple sediment cores were collected from Myrtle Lake in the Vermilion River Watershed and incubated to analyze diffusive P flux under oxic and anoxic conditions. Aerobic release rates varied from 0.14 to 0.35 mg P/m^2/d and anaerobic rates varied from 1.39 to 8.60 mg P/m^2/d [Edlund et al., 2019]. An aerobic rate at the upper end of the measured range was used for Myrtle Lake in HSPF, since the higher anaerobic rate is seldom achieved in the model, as described previously. Myrtle Lake is impaired for phosphorus and has higher average concentrations than other lakes in the area. Therefore, the internal loading rates measured from Myrtle sediments were not applied directly to other lakes in these watersheds. Smaller rates were assumed for several other relatively shallow lakes in the Vermilion watershed, including Pelican Lake. Many lakes in these watersheds are oligotrophic, so very small or zero internal loading was assumed for most.

Modeled inorganic nitrogen inputs from the uplands occur in the form of both nitrate (NO_3) and ammonia (TAM = NH_3 + NH_4). As with PO_4, both constituents occur in the dissolved phase in interflow and groundwater, at user-defined concentrations that vary by land cover and seasonally. Groundwater NO_3 concentrations were informed by shallow groundwater monitoring of gravel and sand aquifers conducted by MPCA [2013], which showed that statewide median NO_3 concentrations underlying undeveloped land were 0.05 mg/L, residential/commercial developed land ~2 mg/L, and agricultural land 8.75 mg/L. Simulated concentrations were reduced across the land cover classes from those median values to reproduce in-stream NO_3 concentrations measured in these Rainy River Basin watersheds.

Both inorganic nitrogen species are also simulated to accumulate on the land surface (for example by atmospheric deposition and decay of organic material), from where they are washed off by overland flow. Key parameters controlling this process are the maximum storage capacity of the constituent, the amount of surface runoff necessary to remove accumulated material, and the rate of accumulation beyond atmospheric deposition (which is supplied as an external time series based on monitored data, as described earlier in this report). These parameters were treated essentially as pure calibration parameters, and adjusted to match observed in-stream NO_3 and TAM concentrations at high flows, as well as the target upland loading rates (Table 13).

Inorganic nitrogen can also be sourced internally from the stream/lake network, in the form of benthic release of TAM. The previous versions of these models had large inputs of TAM from lake bed sediments. However, it was found that the TAM was quickly oxidizing to NO_2 and then NO_3 in the model, causing simulated NO_3 concentrations much higher than observed values. Adjusting parameters to slow the TAM oxidation resulted in more realistic NO_2 + NO_3 concentrations, but resulted in excessively high TAM concentrations. The decision was made, therefore, to remove the internal TAM loading. This led to under-prediction of observed Total Kjeldahl Nitrogen values, as described in further detail below. However, this result was deemed preferable to the alternatives.

Organic matter such as leaf litter is an important component of the TP and TN budgets in forested watersheds. Organic material is washed off in particulate form by surface flow, and leached and dissolved into groundwater and interflow. Such inputs are highest during leaf fall in the autumn and during snowmelt, when organic matter stored and leached over the winter runs off [Bratt et al., 2017]. Leaf fall is not represented explicitly in HSPF. However, the concentration of dissolved organic matter in interflow is allowed to change monthly, so concentrations were increased in the spring and fall relative to the rest of the year to account for the seasonal variation in loading.

Simulated TN and TP concentrations and loads were found to be extremely sensitive to parameters controlling organic matter decay, settling, and resuspension in lakes and streams. This sensitivity was especially pronounced in the RRHW and Vermilion models, because of the predominance of lakes with large hydrological residence times, and thereby longer opportunity for those processes to occur. For example, small changes, on the order of several thousandths of a ft/hr in the settling rate of organic matter in lakes (KODSET), resulted in significant changes in simulated TP concentrations near the outlet of the Vermilion River Watershed (Fig. 20). The sensitivity of these in-stream parameters has implications for the amount of certainty one can attribute to the simulated non-point loading rates for N and P. In this example, one might achieve similar simulated in-stream TP concentrations under two

different parameter sets: one with greater non-point P loading and higher BOD settling rate, or a lower non-point loading rate with a lower BOD settling rate. It is difficult to ascertain without other supporting evidence which set of parameters better reflects reality.

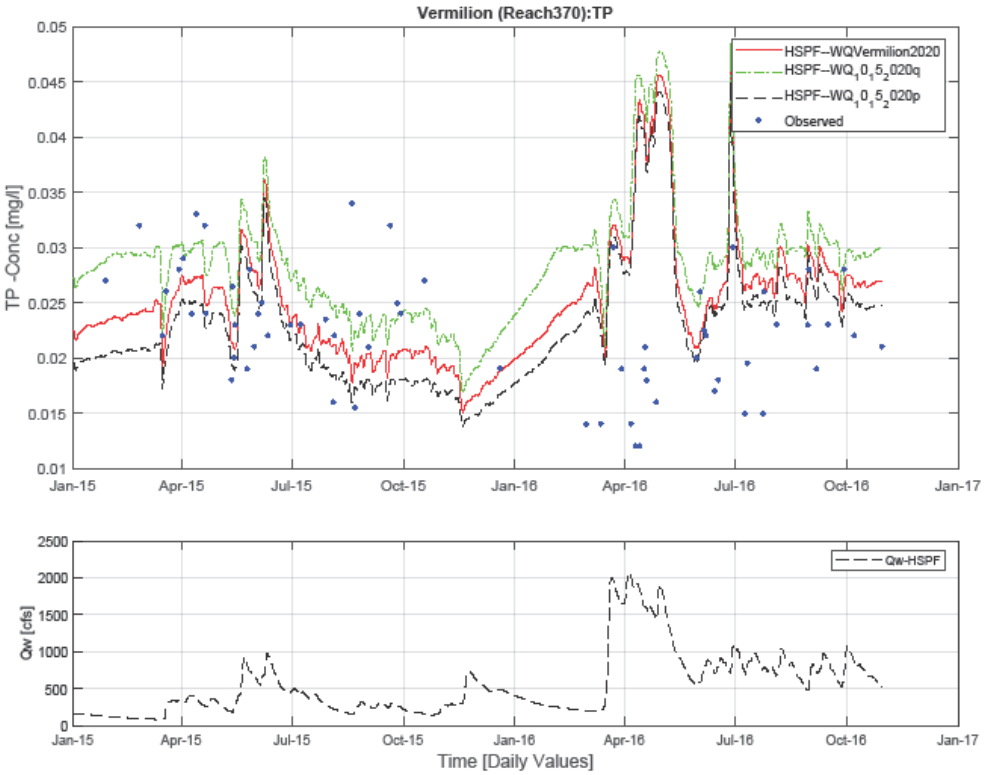

Figure 20. Sensitivity analysis showing impact of the organic matter settling rate (KODSET) parameter on TP concentrations at a representative stream reach in the Vermilion River model. Blue dots are observed TP concentrations. Solid lines are simulated TP concentrations resulting from a range of KODSET values, with all other parameters held constant: 0.003, 0.005 and 0.007 ft/hr for the green, red and black lines, respectively. The red line represents the final parameterization.

Nutrient cycling and export are integrally linked with algal dynamics, as algae take up dissolved NO_3 and PO_4 in their life cycles. Nutrient concentrations were therefore also found to be sensitive to model parameters governing algal growth in lakes, particularly the maximum concentration of benthic algae (MBAL) and maximum growth rate of phytoplankton (MALGR). Again, simulation results were most sensitive to these parameters in the RRHW and Vermilion River Watersheds, given the large volume and long residence times of water in lakes. The generally low nutrient and phytoplankton concentrations in these watersheds tended to made the algal simulation unstable and difficult to calibrate. Overly large algal growth rates would easily use up all available NO_3 and PO_4, causing the algal populations to crash and not easily recover. Chlorophyll-*a* data were used where available to constrain algal dynamics.

3.2.3 Phosphorus Results

All three models reproduce observed phosphorus loads and concentrations relatively accurately. Simulated TP loads compare favorably with measured loads at all WPLMN sites (Table 20). While there is significant inter-annual variability in model performance relative to measured loads, there is no persistent bias toward over- or under-prediction, and PBIAS values integrating data from all years with monitoring data fall within the "very good" range suggested by Moriasi et al. [2007]. WPLMN sites also report measured dissolved PO_4 loads for most of these sites. However, PO_4 concentrations at the sites in these watersheds are frequently at or below the reporting limit for the laboratory methods, which complicates the calculation of the load and reduces certainty in the accuracy. Therefore, load comparisons for dissolved PO_4 are not presented.

Table 20. Annual TP load comparison between HSPF and WPLMN.

Model	Site Name	HSPF Reach	Year	WPLMN Load (kg)	HSPF Load (kg)	PBIAS (%)
Rainy River HW	*Kawishiwi River nr Winton, CSAH18*	369	2009	12,349	16,077	30
			2010	4,137	5,299	28
			2011	6,737	7,203	7
			2014	18,749	21,032	12
			2015	13,445	8,676	-35
			2016	15,885	16,505	4
			2017	21,142	21,099	0
			Mean	**13,206**	**13,699**	**4**
	Stony River nr Babbitt, Tomahawk Rd	341	2014	3,320	3,742	13
			2015	2,073	1,000	-52
			2016	3,093	2,852	-8
			2018	2,318	2,907	25
			Mean	**2,701**	**2,625**	**-3**
Vermilion River	*Vermilion River at Buyck, CSAH 24*	130	2015	3,433	2,840	-17
			2016	6,783	7,892	16
			2017	8,862	8,372	-6
			Mean	**6,359**	**6,368**	**0**
	Vermilion River nr Crane Lake, MN	370	2009	15,745	12,078	-23
			2010	12,012	7,569	-37
			2011	13,407	10,109	-25
			2015	8,083	6,361	-21
			2016	14,336	14,462	1
			2017	17,045	15,702	-8
			Mean	**13,438**	**11,047**	**-18**
Rainy Lake	*Rat Root River nr International Falls, CR145*	170	2016	4,744	5,105.4	8
			2017	2,727	2,549.4	-7
			Mean	**3,736**	**3,827.4**	**2**

Plots comparing simulated to measured P concentrations are shown in Fig. 21-25. TP and dissolved PO_4 data are presented for one representative gage per watershed. The Rainy Lake watershed had no PO_4 data available, so only TP data are shown. Plots for all remaining gages are shown in Appendix 6.2. Measured dissolved PO_4 concentrations are consistently low in these watersheds, and are frequently at or below the reporting limit of 0.002 or 0.005 mg/L depending on the laboratory analysis (e.g., Fig. 23). Simulated concentrations match these low values well, although in cases where observed values are at the reporting limit, it is unclear how far below the reporting value the true concentration falls. Simulated dissolved PO_4 (and by extension, TP) concentrations occasionally peak significantly in the winter and early spring before falling dramatically during spring runoff, likely due to dilution (e.g., the year 2014 in Fig. 21 and 22). Measured data are generally not collected during the winter to verify whether the elevated simulated concentrations are realistic. However, that pattern is observed in the observed data to some degree in the Vermilion River near Crane Lake gage (Fig. 23), where the pattern is also present, but less pronounced, in the simulation.

Simulated TP values also generally replicate observed concentrations. TP concentrations respond more than dissolved PO_4 to storm events, since sediment-bound and organic P tend to be mobilized by high flows. The models mostly do a good job of matching the timing and magnitude of storm event- driven high TP values (e.g., during 2017 and 2018 at the Vermilion River near Crane Lake gage, Fig. 24). However, the models do miss some low-flow, elevated TP conditions, such as during 2015 at the Stony River gage (Fig. 22). Those conditions may reflect algae blooms that are not captured by the simulation in some cases, perhaps due to the model failing to represent anoxic conditions that could lead to high rates of diffusive PO_4 loading from bed sediments.

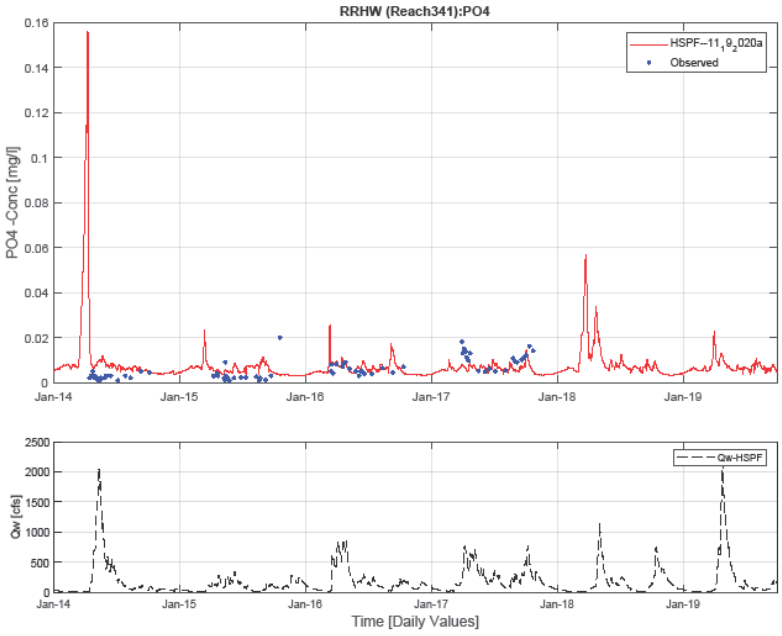

Figure 21. Time series of simulated and observed dissolved orthophosphate concentrations at S002-811, Stony River near Babbitt, Tomahawk Rd (RRHW Reach 341).

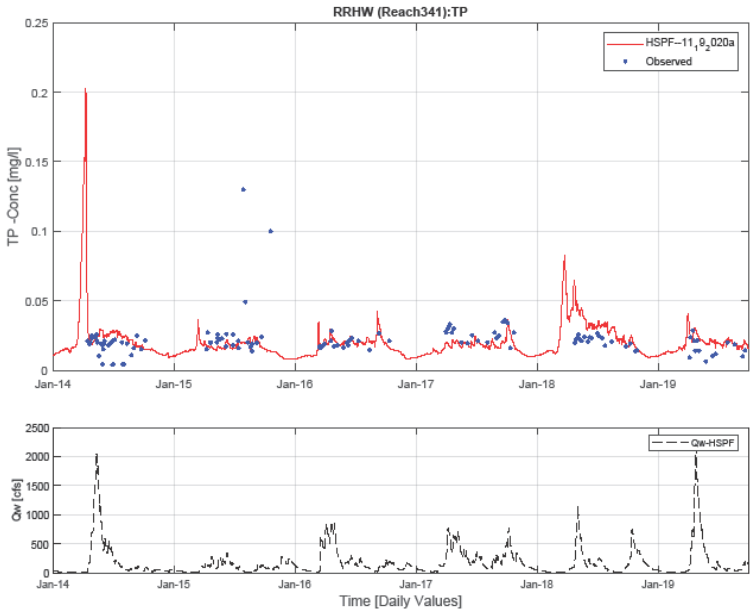

Figure 22. Time series of simulated and observed total phosphorus concentrations at RRHW S002-811, Stony River near Babbitt, Tomahawk Rd (Reach 341).

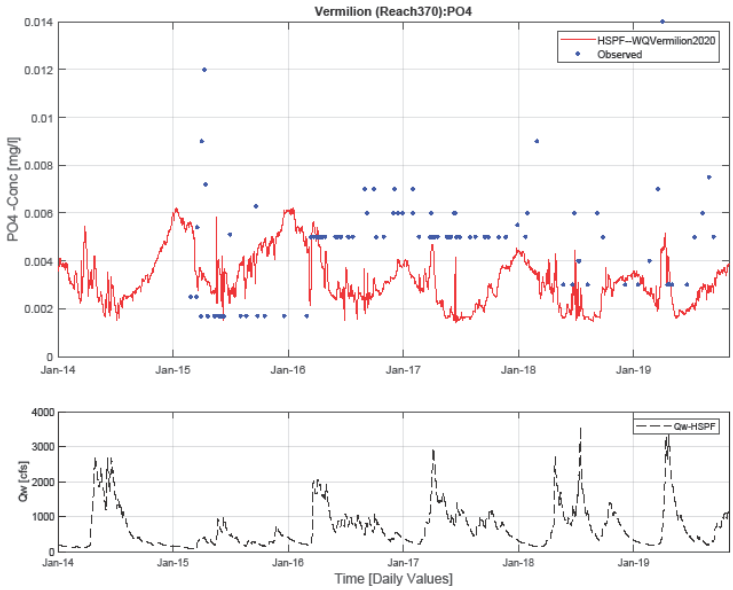

Figure 23. Time series of simulated and observed dissolved orthophosphate concentrations at S005-088, Vermillion River nr Crane Lake, MN (Vermilion River model reach 370).

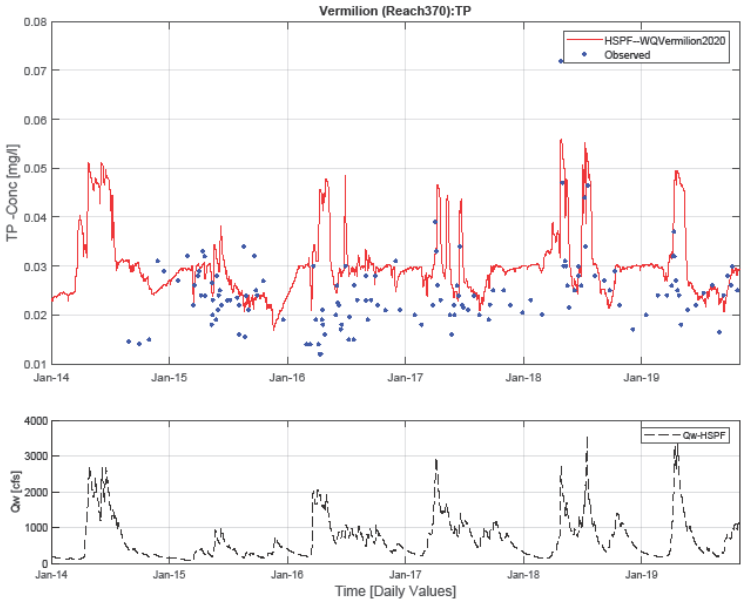

Figure 24. Time series of simulated and observed total phosphorus concentrations at S005-088, Vermillion River nr Crane Lake, MN (Vermilion River model reach 370).

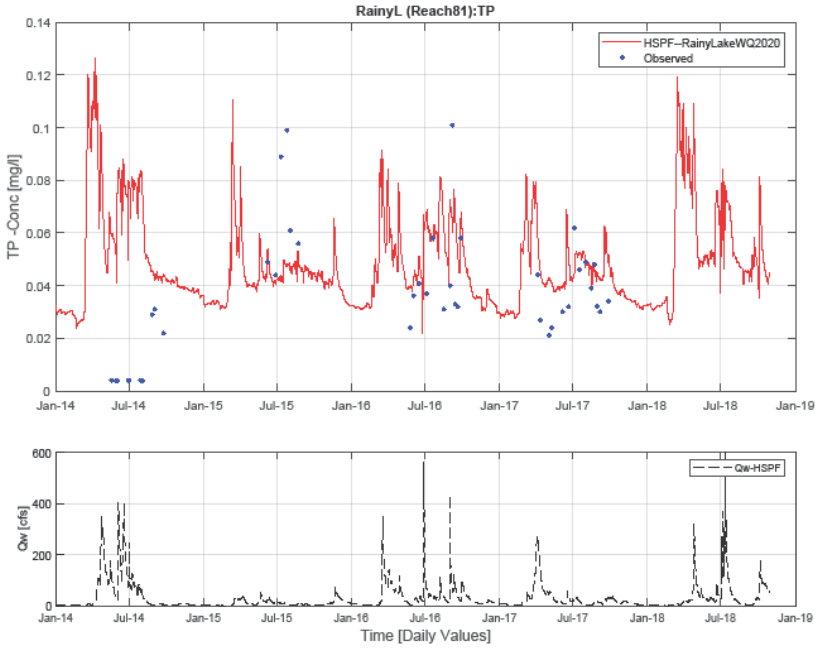

Figure 25. Time series of simulated and observed total phosphorus concentrations at S007-904, Blackduck River (Rainy Lake model reach 81).

Simulated non-point TP loading rates fall within the target ranges for most land cover types (Table 21; green shaded cells). All forest types fall within the expected range, except for mature evergreen forest in the Vermilion River model, where the loading rate is slightly below the expected range (shaded yellow). Wetland TP loading rates are lower than recommended by Mishra and Donigian [2015], but wetland P dynamics are complicated. Site-specific conditions determine whether wetlands are net sources or sinks for P, i.e., [e.g., Reddy et al., 1999]. HSPF does not represent wetland nutrient cycling in sufficient detail to distinguish such variable conditions, and treats all wetlands as potential sources. The loading rate for grasslands is below the target rate, but that target is specifically intended for pastureland. While the grassland category does encompass pastureland in these watersheds, it is defined more broadly and also includes grasslands not used for pasture that likely produce lower P loads. Pervious developed urban land loading rates fall within the target range for all models, although rates for impervious developed land are slightly above the target in the RRHW and Rainy Lake watersheds. Agricultural cropland is sparse in these watersheds, and nonexistent in the RRHW watershed. Therefore, the loading rate have very little impact on total P loads. The rate is within the target range in the Vermilion River Watershed, but lower than the target in the Rainy Lake Watershed.

Table 21. Annual average simulated TP loading rates (pounds/acre/yr) by land cover type. Cells are color coded based on their relation to the ranges proposed by Mishra and Donigian [2015]. Cells shaded green fall within the expected range, whereas cells shaded yellow fall below the expected range and cells shaded red fall above the expected range.

	Wetland	Urban	Mature Deciduous Forest	Young Forest	Mature Evergreen Forest	Agricultural	Grasslands	Feedlot	Urban Impervious
Rainy Lake Watershed	0.047	0.279	0.099	0.147	0.086	0.426	0.201	1.084	1.629
RRHW Watershed	0.039	0.437	0.062	0.078	0.054	N/A	0.098	N/A	1.739
Vermilion River Watershed	0.03	0.353	0.055	0.072	0.047	1.462	0.085	0.891	0.946

3.2.4 Nitrogen Results

As with inorganic P, inorganic N (NO_2 + NO_3 and TAM) concentrations are extremely low in these watersheds. Observed concentrations are frequently at the reporting limit, especially for TAM, making a precise calibration for these constituents difficult. However, for both inorganic N constituents, the models successfully capture both low-flow concentrations and the timing and magnitude of high-flow concentrations (with occasional over-prediction of the highest concentrations) (Fig. 26-30). However, TKN concentrations are systematically biased low in the RRHW and Vermilion Watersheds (Fig. 31 and 32). TKN measures the sum of TAM and organic N, and the bias could, therefore, come from inaccurate simulation of either of those components. Given the uncertainty associated with exact TAM values because most observations are at the reporting limit, it is possible TAM is under-predicted, contributing to the bias in TKN values to some degree. However, because observed TAM concentrations are so low, they make up only a small fraction of TKN and cannot account for the degree of under-prediction observed. Therefore, the bias must be explained in part by too-low simulated organic N loads. An attempt was made to increase organic N by increasing BOD loading rates and decreasing the BOD settling rate. These changes had the desired effect on TKN values, but simultaneously increased TP values excessively. Accurately predicting TP loads was considered to be a higher priority for these models, since they were used to develop a P TMDL for Myrtle Lake in the Vermilion watershed, and because P is a priority for research and conservation efforts downstream in Lake of the Woods. Therefore, the increased organic matter loading was not adopted in the final models.

The under-prediction of TKN is reflected in TN loads as well. Simulated and observed TN loads are compared in Table 22 for stream gages in the WPLMN network. Simulated loads are biased low by 55% - 68% across the gages in the RRHW and Vermilion River Watersheds. While these percent bias results fall within the “acceptable” range [Moriasi et al., 2007], there is clearly room for improvement in the N simulation. Interestingly TN loads in the Rainy Lake model match the magnitude of observed loads well (Table 22), as do TKN concentrations (Fig. 31).

One potential solution to resolve the unbalanced TN and TP loads would be to increase nonpoint BOD loading as described above -- which would increase both organic N and P -- while simultaneously decreasing particulate PO_4 loading to maintain TP concentration/loads at reasonable levels. Because observed particulate PO_4 concentrations are not available in this watershed, the relative contributions of organic P and particulate PO_4 to TP are poorly constrained. However, reducing particulate PO_4 inputs and increasing organic loads to better represent TN loads may be worth pursuing in future work with these models.

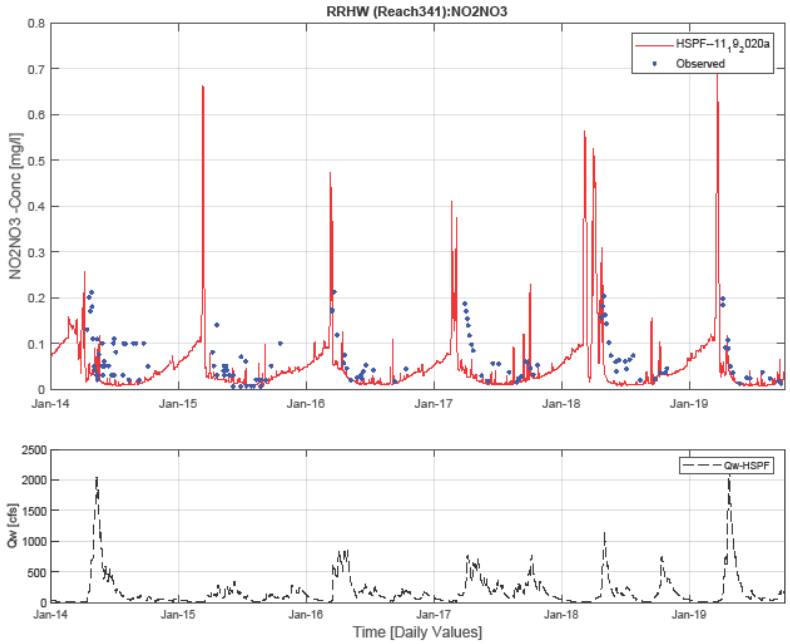

Figure 26. Time series of simulated and observed NO2+NO3 concentrations at RRHW S002-811, Stony River near Babbitt, Tomahawk Rd (Reach 341).

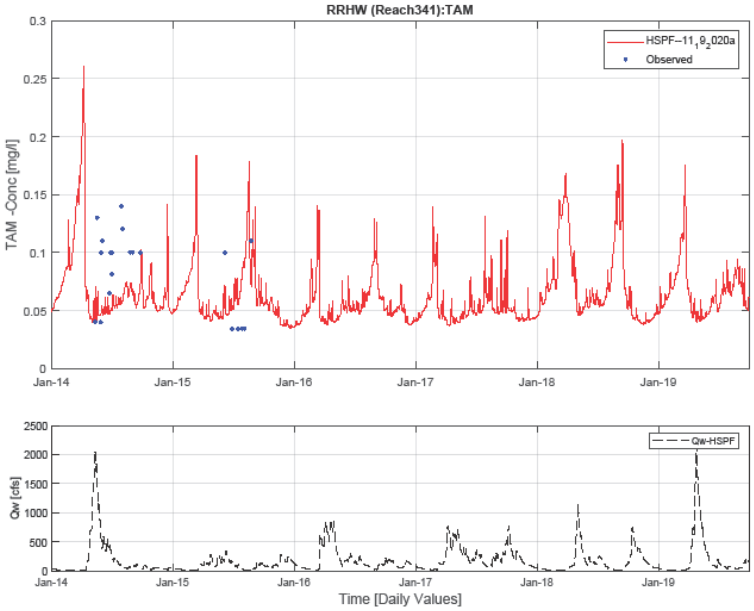

Figure 27. Time series of simulated and observed dissolved total ammonia concentrations at RRHW S002-811, Stony River near Babbitt, Tomahawk Rd (Reach 341).

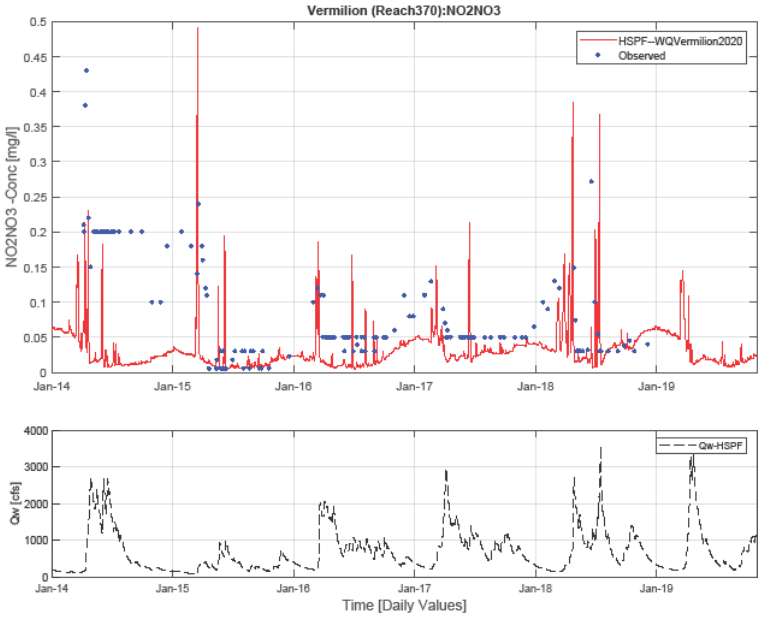

Figure 28. Time series of simulated and observed NO_2+NO_3 concentrations at S005-088, Vermillion River nr Crane Lake, MN (Vermilion River model reach 370).

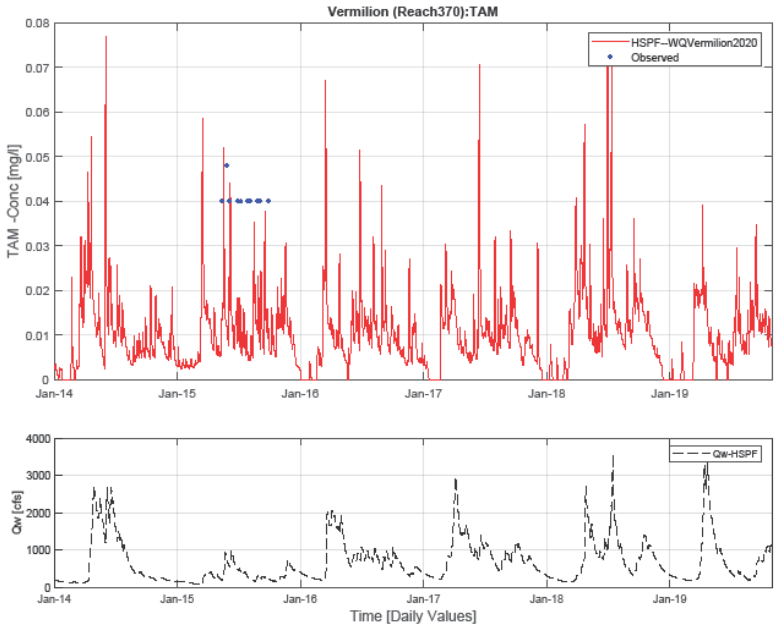

Figure 29. Time series of simulated and observed dissolved total ammonia concentrations at S005-088, Vermillion River nr Crane Lake, MN (Vermilion River model reach 370).

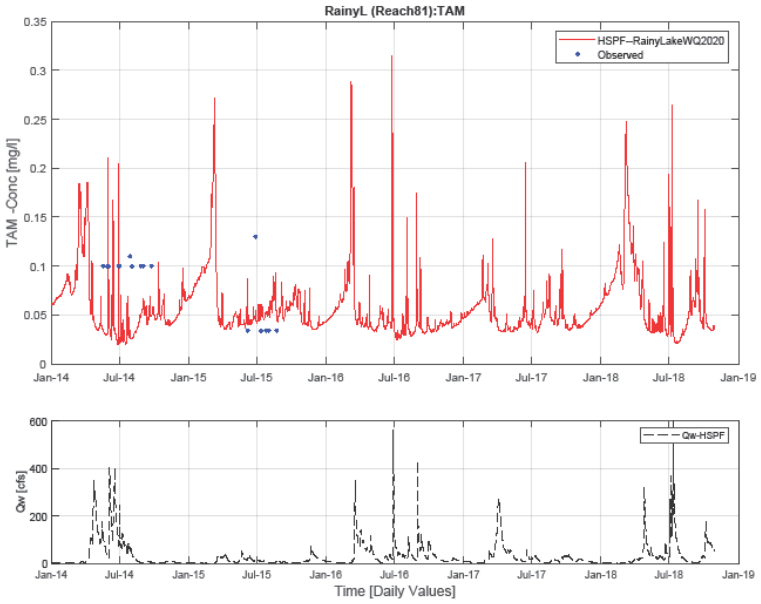

Figure 30. Time series of simulated and observed dissolved total ammonia concentrations at S007-904, Blackduck River (Rainy Lake model reach 81).

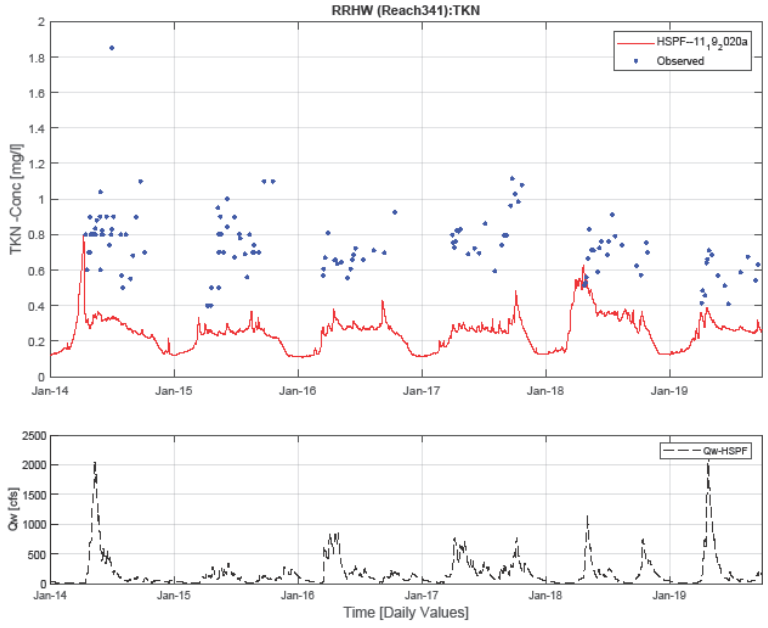

Figure 31. Time series of simulated and observed TKN concentrations at RRHW S002-811, Stony River near Babbitt, Tomahawk Rd (Reach 341).

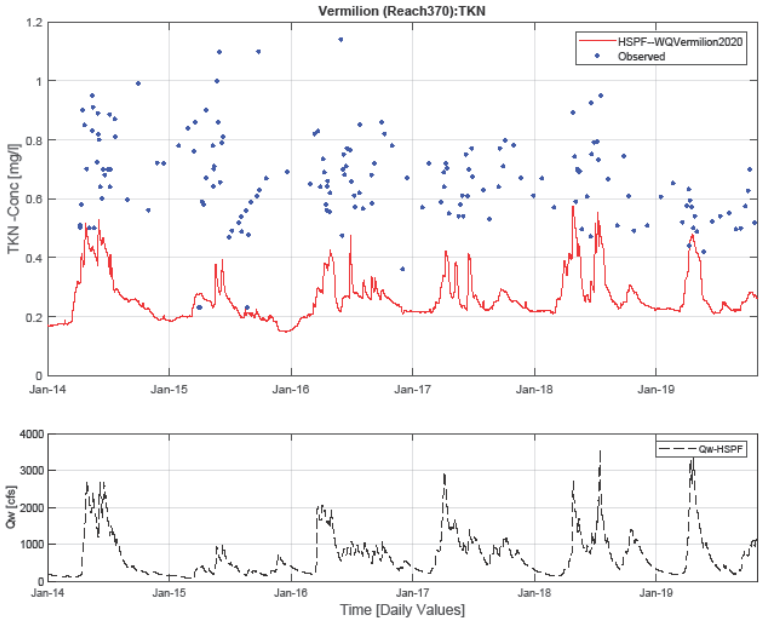

Figure 32. Time series of simulated and observed TKN concentrations at S005-088, Vermillion River nr Crane Lake, MN (Vermilion River model reach 370).

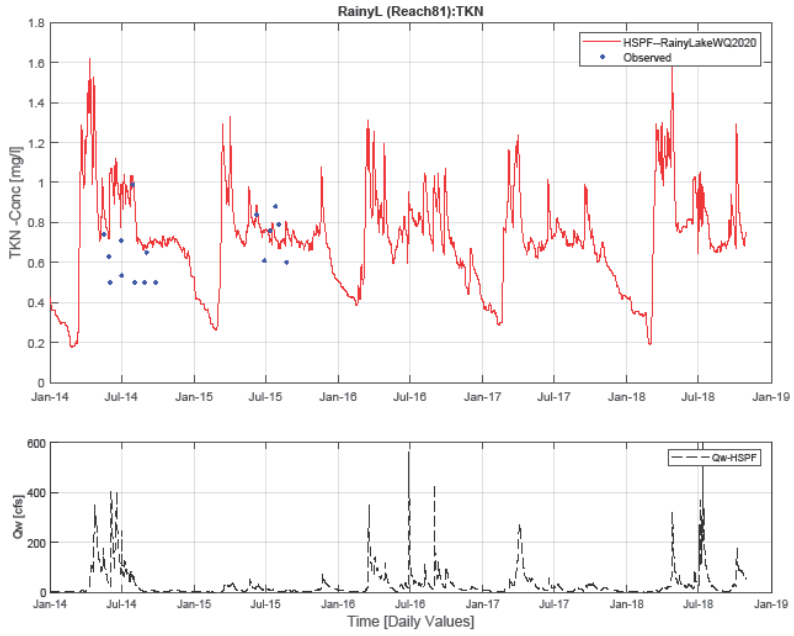

Figure 33. Time series of simulated and observed TKN concentrations at S007-904, Blackduck River (Rainy Lake model reach 81).

Table 22. Annual TN load comparison between HSPF and WPLMN.

Model	Site Name	HSPF Reach	Year	WPLMN Load (kg)	HSPF Load (kg)	PBIAS (%)
Rainy River HW	*Kawishiwi River nr Winton, CSAH18*	369	2009	418304	255328	-39
			2010	204429	67517	-67
			2011	292126	116101	-60
			2012	451916	175143	-61
			2013	676808	316101	-53
			2014	668176	293728	-56
			2015	397049	113303	-71
			2016	585909	299170	-49
			2017	696320	351130	-50
			Mean	**487893.0**	**220835.6**	**-55**
	Stony River nr Babbitt, Tomahawk Rd	341	2014	138,588	58,350	-58
			2015	79,990	16,617	-79
			2016	115,769	46,247	-60
			2018	85,795	43,594	-49
			Mean	**105,036**	**41,202**	**-61**
Vermilion River	*Vermilion River at Buyck, CSAH 24*	130	2015	97,381	26,576	-73
			2016	256,905	76,665	-70
			2017	239,877	93,849	-61
			Mean	**198,054**	**65,697**	**-67**
	Vermilion River nr Crane Lake, MN	370	2009	431,460	149,201	-65
			2010	357,853	105,067	-71
			2011	369,339	148,834	-60
			2012	309,769	94,826	-69
			2015	292,998	65,100	-78
			2016	555,544	155,611	-72
			2017	501,626	184,527	-63
			Mean	**402,656**	**129,024**	**-68**
Rainy Lake	*Rat Root River nr International Falls, CR145*	170	2016	85,466	81,514.3	**-5**
			2017	43,055	45,646.4	**6**
			Mean	**64,261**	**63,580**	**-1**

Non-point TN loading rates are somewhat lower than the target range for forest land cover (Table 23), although most are not much below the lower range of 2 pounds/acre/yr. As described above, the model simulates in-stream NO_2+NO_3 and TAM concentrations consistent with observed data, but appears to under-predict organic N concentrations. Therefore, these low non-point loading rates may represent insufficient loading of organic matter from the forested areas of the watersheds. TN loading rates for wetland and grasslands fall within expected ranges, except for the Vermilion model, in which they are slightly below the range. Urban pervious loading rates are slightly lower than the target range (5 mg/L at the low end), whereas urban impervious rates are either right at (Rainy Lake model) or slightly above (RRHW and Vermilion models) the upper end of the range (10 mg/L). The overall loading

rate from developed land should, therefore, be reasonably represented, although land cover change scenarios that involve more intense development (and therefore more impervious surface) may somewhat over-predict change in nitrogen loads, and vice versa for scenarios involving less intense development.

Table 23. Annual average simulated TN loading rates (pounds/acre/yr) by land cover type. Cells are color coded based on their relation to the ranges proposed by Mishra and Donigian [2015]. Cells shaded green fall within the expected range, whereas cells shaded yellow fall below the expected range and cells shaded red fall above the expected range.

	Wetland	Urban	Mature Deciduous Forest	Young Forest	Mature Evergreen Forest	Agricultural	Grasslands	Feedlot	Urban Impervious
Rainy Lake Watershed	0.979	4.35	1.866	2.476	1.632	4.86	3.254	10.942	10.00
RRHW Watershed	0.597	3.447	1.083	1.509	0.964	N/A	2.279	N/A	10.712
Vermilion River Watershed	0.483	3.163	1.063	1.409	0.939	6.87	1.76	10.841	11.046

3.2.5 Clorophyll-a Results

As discussed previously, the generally low concentrations of inorganic nutrients and algae made achieving a stable algal simulation difficult. Phytoplankton populations were extremely sensitive to parameters including the maximum grown rate (MALGR), the settling rate (PHYSET), and the maximum concentration of benthic algae (MBAL), which controlled nutrient availability for phytoplankton. However, stable simulations were achieved and simulated chlorophyll-*a* concentrations agreed fairly well with observed data. Concentrations in the South Kawishiwi River, in particular, captured the timing and magnitude of algal growth well (Fig. 34). Chlorophyll-*a* concentrations in the Vermilion River matched observed data well some years, but were somewhat over-predicted other years (Fig. 35).

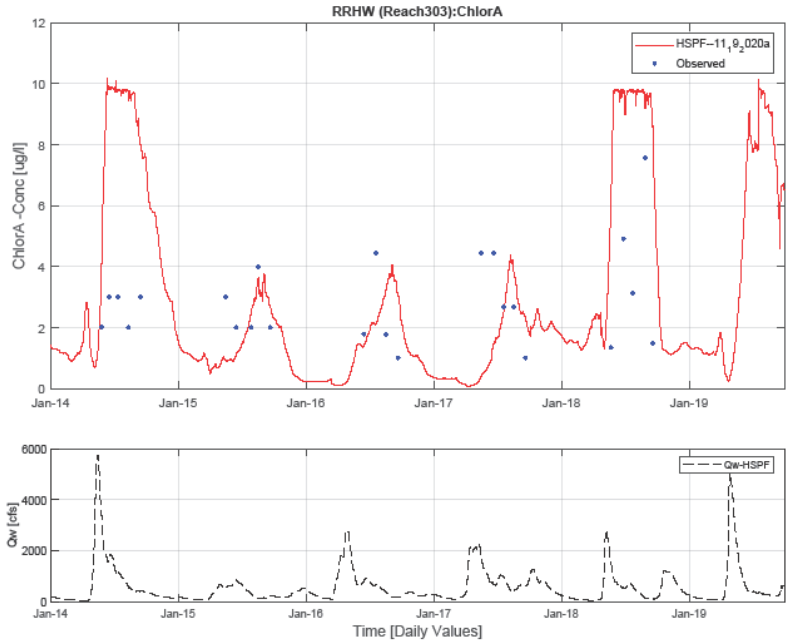

Figure 34. Time series of simulated and observed chlorophyll-a concentrations at RRHW S006-868, South Kawishiwi River (Reach 303).

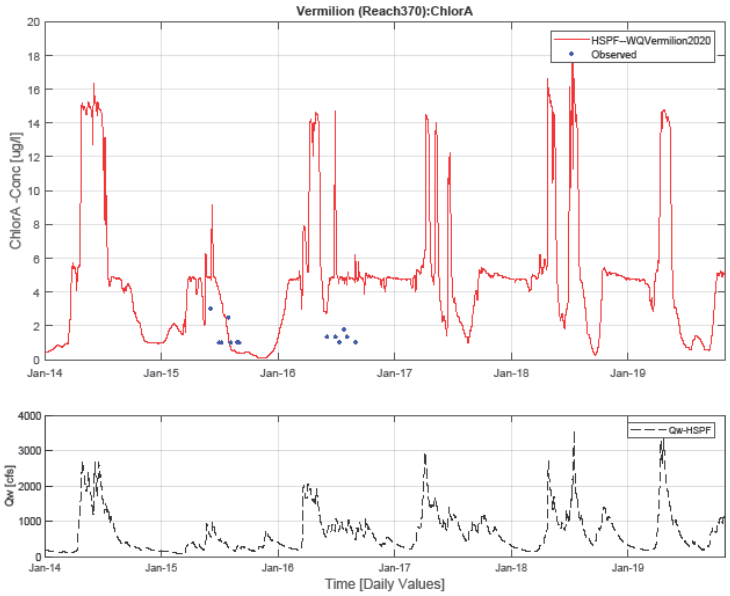

Figure 35. Time series of simulated and observed chlorophyll-a concentrations at S005-088, Vermillion River nr Crane Lake, MN (Vermilion River model reach 370).

4 SUMMARY

In this modeling effort, the three HSPF models comprising the upper portion of the Rainy River Basin were updated to run through 2019, using gridded meteorological data as forcing inputs. Point source and atmospheric deposition time series were also extended, and the model calibration was updated for hydrology, sediment, nutrients, and algae based on the most recent observed data in these watersheds. Simulated flows are generally consistent in magnitude and timing with observed flow records across flow regimes and at a range of spatial scales, although results from gages on small sub-watersheds such as the Blackduck River suggest that some rain events are missed at that smaller spatial scale, even when using gridded precipitation inputs. Sediment and phosphorus concentrations and loads are generally well captured also, although there is some variability in the quality of the simulation between events and from year to year. Simulated inorganic nitrogen loads are also consistent with measured values. Organic nitrogen concentrations/loads, however, are consistently biased low in the Vermilion and RRHW watersheds and warrant more investigation in the future.

The updated models were used to support ongoing watershed management activities in the RRHW and Vermilion River watersheds, including the Watershed Restoration and Protection Strategies (WRAPS) studies for each of those watersheds, as well as TMDLs in the Blackduck River and Myrtle Lake. This work therefore focused on tributaries to Rainy Lake. Future use of the models to investigate hydrology and water quality in Rainy Lake itself and the Rainy River downstream should include an examination of the calibration of the Canadian Turtle River Watershed model as well as the downstream linked models.

5 REFERENCES

Ackerman, D. C., 2015. Hydrologic and Water Quality Calibration for the Lake of the Woods, the Rainy River, and the Associated Watershed Drainage Areas in Both the United States and Corresponding Canadian Watersheds Draining Into the Lake of the Woods, RSI(RCO)-2153/2-15/37, prepared by RESPEC, Rapid City, SD, for Dr. C. Regan, Minnesota Pollution Control Agency, St. Paul, MN, February 27.

Allen, R.G., L.S.Pereira, D. Raes, and M. Smith. 1998. Crop evapotranspiration: guidelines for computing crop water requirements Food and Agriculture Organization of the United Nations, Rome.

Baker, Donald G. and D.L. Ruschy, 1987. Historical Albedo Values at St. Paul, Minnesota, 1969-85, *Journal of Applied Meteorology*, 27.

Barr Engineering, 2007. Detailed Assessment of Phosphorus Sources to Minnesota Watersheds– Atmospheric Deposition: 2007 Update, prepared by Barr Engineering, Minneapolis, MN, for Minnesota Pollution Control Agency, St. Paul, MN.

Bratt, A.R., Finlay, J.C., Hobbie, S.E., Janke, B.D, Worm, A.C., and Kemmitt, K.L., 2017. Contribution of Leaf Litter to Nutrient Export during Winter Months in an Urban Residential Watershed. *Environmental Science & Technology 51* (6), 3138-3147. DOI: 10.1021/acs.est.6b06299

Cannata M., 2006. GIS embedded approach for Free & Open Source Hydrological Modelling. PhD thesis, Department of Geodesy and Geomatics, Polytechnic of Milan, Italy.

Daly, C., Halbleib, M., Smith, J. I., Gibson, W. P., Doggett, M. K., Taylor, G. H., Pasteris, P. P., 2008. Physiographically sensitive mapping of climatological temperature and precipitation across the conterminous United States. *International Journal of Climatology*, 28(15), 2031–2064. https://doi.org/10.1002/joc

Daly, C., Neilson, R. P., & Phillips, D. L., 1994. A statistical-topographic model for mapping climatological precipitation over mountainous terrain. *Journal of Applied Meteorology*, 33(2), 140–158.

Edlund, M.B., Ramstack Hobbs, J.M., Burge, D.R.L. and Heathcote, A.J. 2019. A Paleolimnological Study of Myrtle Lake, St. Louis Co., Minnesota. Final Report to the Minnesota Pollution Control Agency. St. Croix Watershed Research Station, Science Museum of Minnesota, Marine on St. Croix, Minnesota, 38 pp.

Edlund MB, Schottler SP, Reavie ED, Engstrom DR, Baratono NG, Leavitt PR, Heathcote AJ, Wilson B, Paterson AM. 2017. Historical phosphorus dynamics in Lake of the Woods (USA–Canada) — does legacy phosphorus still affect the southern basin? *Lake and Reservoir Management* 33, 386–402.

Environmental Protection Agency (EPA) Office of Water, 2000. BASINS Technical Note 6: Estimating Hydrology and Hydraulic Parameters for HSPF. Doc#: EPA-823-R00-012.

Erickson, T.O., Herb, W.R., and Stefan, H.G., 2010. Streamflow Modeling of Miller Creek, Duluth, Minnesota. Project Report No. 536 prepared for Minnesota Pollution Control Agency, St. Paul, MN. 57 pp.

Förster, K., Hanzer, F., Winter, B., Marke, T., and Strasser, U.: An open-source MEteoroLOgical observation time series DISaggregation Tool (MELODIST v0.1.1), *Geosci. Model Dev*., 9, 2315-2333, https://doi.org/10.5194/gmd-9-2315-2016, 2016.

Helgen, J. C. 1992. Biology and Chemistry of Wastewater Stabilization Ponds in Minnesota. Minnesota Pollution Control Agency, St. Paul, MN. Report to the Legislative Committee for Minnesota Resources.

Holdren, G.C. and Armstrong, D.E., 1980. Factors affecting phosphorus release from intact lake sediment cores. *Environ. Sci. Technol*. 14, 1, 79–87, doi: https://doi.org/10.1021/es60161a014

James WF. 2017. Internal phosphorus loading contributions from deposited and resuspended sediment to the Lake of the Woods. *Lake and Reservoir Management* 33, 347–359.

Jasperson, J., 2019. Rainy River Headwaters Stressor Identification Report. Doc #: wq-ws5-09030001a, Minnesota Pollution Control Agency, St. Paul, MN. 81 pp.

Kenner, S. J., 2014. Model Development for the Lake of the Woods, the Rainy River, and the Associated Watershed Drainage Area in Both the United States and Corresponding Canadian Watersheds Draining Into the Lake of the Woods, RSI(RCO)-2156/1-14/22, prepared by RESPEC, Rapid City, SD, for N. Baratono, Minnesota Pollution Control Agency, St. Paul, MN, January 16.

Lupo, C., 2016. Model Land-Class Update and Recalibration for the Lake of the Woods, Rainy River, and Associated Drainage Areas in Both the United States and Corresponding Canadian Watersheds. Prepared by RESPEC, Rapid City, SD, for C. Regan, Minnesota Pollution Control Agency, St. Paul, MN, January 16.

Mesinger, F., G. DiMego, E. Kalnay, K. Mitchell, and Coauthors, 2006: North American Regional Reanalysis. *Bulletin of the American Meteorological Society*, 87, 343–360, doi:10.1175/BAMS-87-3-343.

Minnesota Pollution Control Agency (MPCA), 2013. The Condition of Minnesota's Groundwater, 2007 - 2011. Doc #: wq-am1-06, Minnesota Pollution Control Agency, St. Paul, MN. 65 pp.

Minnesota Pollution Control Agency (MPCA), 2020a. Draft Rainy River-Headwaters Watershed Total Maximum Daily Load: Blackduck River TMDL. Doc #:_____, Minnesota Pollution Control Agency, St. Paul, MN. 63 pp.

Minnesota Pollution Control Agency (MPCA), 2020b. Draft Cloquet River Watershed Restoration and Protection Strategy Report, Apendix B: HSPF Recalibration Methods and Results. Doc #: wq-ws4-72a, Minnesota Pollution Control Agency, St. Paul, MN. 26 pp.

Mishra, A., A.S. Donigian, Jr. 2015. NPS Target Loading Rates for Minnesota. Report prepared for Minnesota Pollution Control Agency.

Mitchell, K.E., D. Lohmann, P.R. Houser, E.F. Wood, J.C. Schaake, A. Robock, B.A. Cosgrove, J. Sheffield, Q. Duan, L. Luo, R.W. Higgins, R.T. Pinker, J.D. Tarpley, D.P. Lettenmaier, C.H. Marshall, J.K. Entin, M. Pan, W. Shi, V. Koren, J. Meng, B.H. Ramsay, and A.A. Bailey, 2004: The multi-institution North American Land Data Assimilation System (NLDAS): Utilizing multiple GCIP products and partners in a continental distributed hydrological modeling system, *J. Geophys. Res.*, 109, D07S90, doi:10.1029/2003JD003823.

Moriasi, D.N., J.G. Arnold, M.W. Van Liew, R.L. Bingner, R.D. Harmel, Veith, T.L., 2007. Model evaluation guidelines for systematic quantification of accuracy in watershed simulations. *Transactions of the ASABE, 50(3)*: 885-900.

Mu, Q., Heinsch, F. A., Zhao, M., and Running, S. W. 2007. Development of a global evapotranspiration algorithm based on MODIS and global meteorology data. *Remote Sensing of Environment*, *111*(4), 519-536.

Nash, J. E., and J. V. Sutcliffe, 1970. River flow forecasting through conceptual models: Part 1: A discussion of principles. *Journal of Hydrology, 10(3)*: 282-290.

National Operational Hydrologic Remote Sensing Center, 2004. *Snow Data Assimilation System (SNODAS) Data Products at NSIDC, Version 1*. Full unmasked version of snow water equivalent product. Boulder, Colorado USA. NSIDC: National Snow and Ice Data Center. doi: https://doi.org/10.7265/N5TB14TC. Accessed 1/29/2020.

Nichols, D.S. and Verry, E.S., 2001. Stream flow and ground water recharge from small forested watersheds in north central Minnesota. *Journal of Hydrology*, *245*(1-4), 89-103. doi: 10.1016/S0022-1694(01)00337-7.

Olmanson, L.G. and Bauer, M.E., 2017. Land cover classification of the Lake of the Woods/Rainy River Basin by object-based image analysis of Landsat and lidar data. *Lake and Reservoir Management, 33:4*, 335-346, DOI: 10.1080/10402381.2017.1373171

ORNL DAAC, 2017. Spatial Data Access Tool (SDAT). ORNL DAAC, Oak Ridge, Tennessee, USA. Accessed April 4, 2018. https://doi.org/10.3334/ORNLDAAC/1388

PRISM Climate Group, Oregon State University, http://prism.oregonstate.edu, created 2 Dec 2019.

Reddy, K. R., Kadlec, R. H., Flaig, E., and Gale, P. M., 1999. Phosphorus Retention in Streams and Wetlands: A Review, *Critical Reviews in Environmental Science and Technology, 29:1*, 83-146, DOI: 10.1080/10643389991259182

Rui, H., Mocko, D., 2018. README Document for North American Land Data Assimilation System Phase 2 (NLDAS-2) Products. Goddard Earth Sciences Data and Information Services Center.

Simard, M., Pinto, N., Fisher, J. B., and Baccini, A., 2011. Mapping forest canopy height globally with spaceborne lidar, *J. Geophys. Res.*, 116, G04021, doi:10.1029/2011JG001708.

Snyder, R. and Eching, S. 2002. Penman-Monteith (hourly) Reference Evapotranspiration Equations for Estimating ETos and ETrs with Hourly Weather Data.

Soil Survey Staff, Natural Resources Conservation Service, United States Department of Agriculture. Web Soil Survey. Available online at https://websoilsurvey.nrcs.usda.gov/. Accessed 02/1/2020.

Stull, R. 2017. Practical Meteorology: An Algebra-based Survey of Atmospheric Science -version 1.02b. Univ. of British Columbia. Equation 4.15a.

Tetra Tech, 2016a. St. Louis, Cloquet, and Nemadji River Basin Models, Volume 1: Hydrology and Sediment Model Calibration. Report prepared for Minnesota Pollution Control Agency.

Tetra Tech, 2016b. Lake Superior North and Lake Superior South Basins Watershed Model Development Report. Report prepared for Minnesota Pollution Control Agency.

Tetra Tech, 2018. Point Source Updates in the Minnesota River Basin. Memorandum prepared for Minnesota Pollution Control Agency.

Tetra Tech, 2019. Gridded Weather Data Processing (MET) Tool: User Guide for Hydrologic Simulation Program – FORTRAN (HSPF) Application. Report prepared for Minnesota Pollution Control Agency.

United States Environmental Protection Agency (USEPA), 2000. BASINS Technical Note 6: Estimating Hydrology and Hydraulic Parameters for HSPF. Doc#: EPA-823-R00-012

Weiss, S. 2012. Point Source Nitrogen Load Estimates for Minnesota. Minnesota Pollution Control Agency, St. Paul, MN.

Xia, Y., K. Mitchell, M. Ek, J. Sheffield, B. Cosgrove, E. Wood, L. Luo, C. Alonge, H. Wei, J. Meng, B. Livneh, D. Lettenmaier, V. Koren, Q. Duan, K. Mo, Y. Fan, and D. Mocko, 2012, Continental-scale water and energy flux analysis and validation for the North American Land Data Assimilation System project phase 2 (NLDAS-2): 1. Intercomparison and application of model products, *J. Geophys. Res*., 117, D03109, doi:10.1029/2011JD016048.

Xia, Y., K. Mitchell, M. Ek, J. Sheffield, B. Cosgrove, E. Wood, L.Luo, C. Alonge, H. Wei, J. Meng, B. Livneh, D. Lettenmaier, V. Koren, Q. Duan, K. Mo, Y. Fan, and D. Mocko, 2012, Continental-scale water and energy flux analysis and validation for North American Land Data Assimilation System project phase 2 (NLDAS-2): 2. Validation of model-simulated streamflow, *J. Geophys. Res*., 117, D03110, doi:10.1029/2011JD016051.

6 APPENDICES

6.1 ADDITIONAL FLOW CALIBRATION AND VALIDATION RESULTS

6.1.1 Flow Validation - Kawishiwi River near Ely, MN (USGS 05124480)

Table A.1. Hydrology validation statistics at Kawishiwi River near Ely, MN gage (USGS 05124480). Statistics are computed for modeled and observed datasets using only days with observed data, during the validation period 1997-2009.

	HSPF Simulated Flow	Observed Flow	PBIAS (%)/NSE
Total in-stream flow volume (Acre-ft/month)	9690	9784	-1.0
Total of highest 10% flows (Acre-ft)	3899	3811	2.3
Total of lowest 50% flows (Acre-ft)	1449	1539	-5.9
Total summer flow volume (Acre-ft/month)	8217	7636	7.6
Total fall flow volume (Acre-ft/month)	8331	7151	16.5
Total winter flow volume (Acre-ft/month)	2235	3892	-42.6
Total spring flow volume (Acre-ft/month)	20092	20677	-2.8
Daily NSE	--	--	0.76
Monthly NSE	--	--	0.84

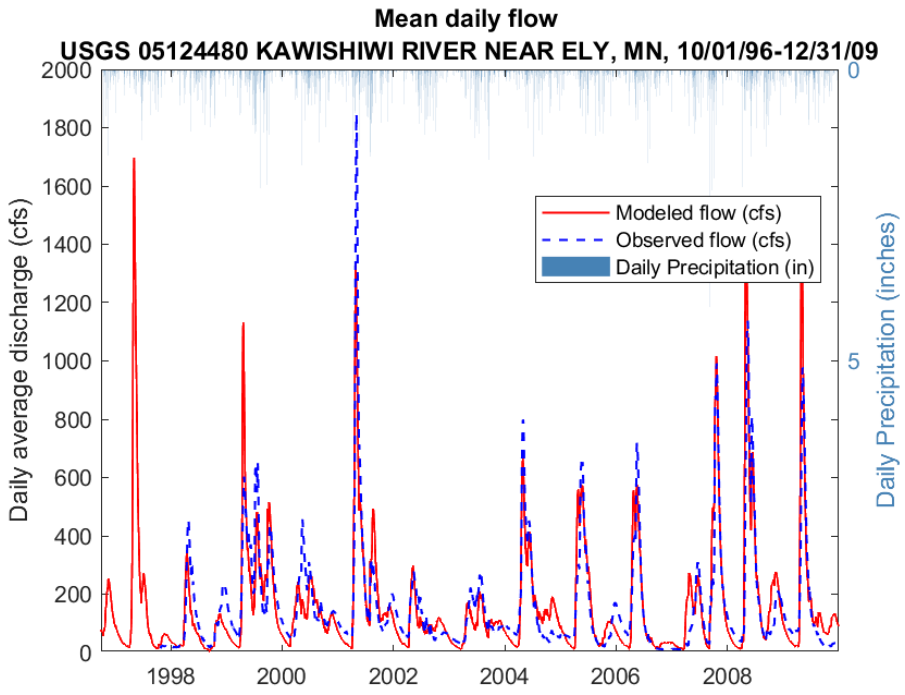

Figure A.1. Hydrograph comparison of observed and simulated daily average values at USGS 05124480, Kawishiwi River near Ely, MN (RRHW model reach 244) during the validation period.

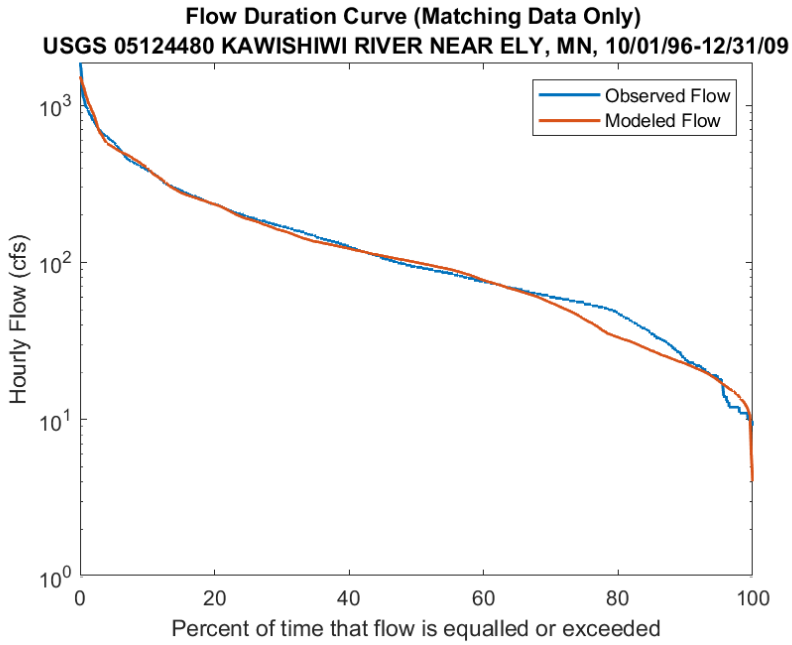

Figure A.2. Flow duration curves for simulated and observed data at USGS 05124480, Kawishiwi River near Ely, MN (RRHW model reach 244) during the validation period.

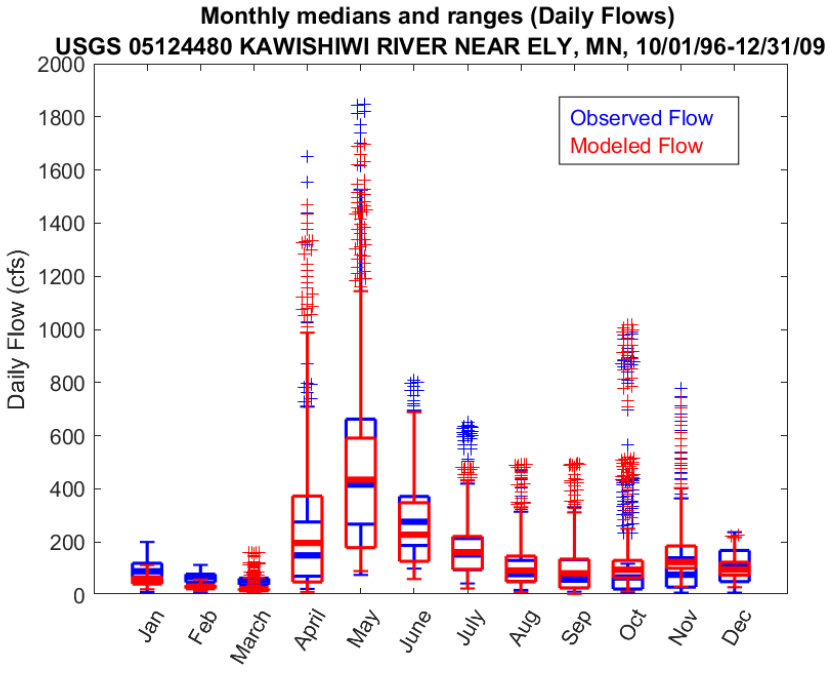

Figure A.3. Boxplots comparing simulated with observed flow by month (daily average flows) at USGS 05124480, Kawishiwi River near Ely, MN (RRHW model reach 244) during the validation period.

6.1.2 Secondary Calibration Gage - H72045001 Stony River nr Babbitt, Tomahawk Rd

Table A2. Hydrology calibration statistics at H72045001 Stony River nr Babbitt, Tomahawk Rd (RRHW model reach 341). Statistics are computed for modeled and observed datasets using only days with observed data. 2019 data were provisional and were omitted for the analysis.

	HSPF Simulated Flow	Observed Flow	PBIAS (%)/NSE
Total in-stream flow volume (Acre-ft/month)	5191	5860	-11.4
Total of highest 10% flows (Acre-ft)	1897	1800	5.4
Total of lowest 50% flows (Acre-ft)	743	1098	-32.3
Total summer flow volume (Acre-ft/month)	3544	4199	-15.6
Total fall flow volume (Acre-ft/month)	5266	6506	-19.1
Total winter flow volume (Acre-ft/month)	2181	4171	-47.7
Total spring flow volume (Acre-ft/month)	8176	7749	5.5
Daily NSE	-	-	0.61
Monthly NSE	-	-	0.80

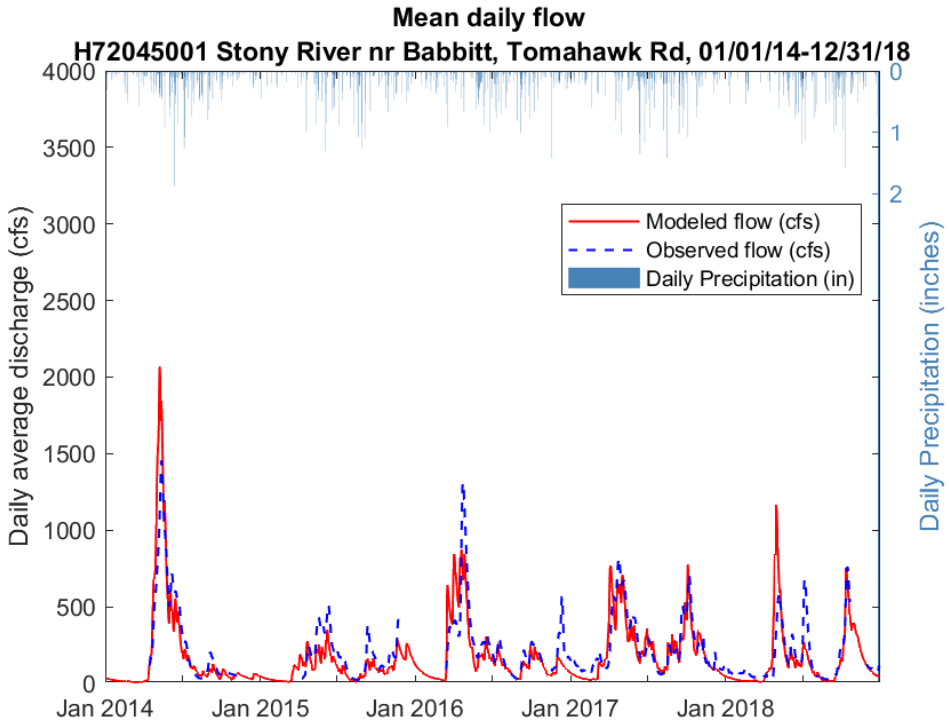

Figure A.4. Hydrograph comparison of observed and simulated daily average values at H72045001 Stony River nr Babbitt, Tomahawk Rd (RRHW model reach 341). 2019 data were provisional and were omitted for the analysis.

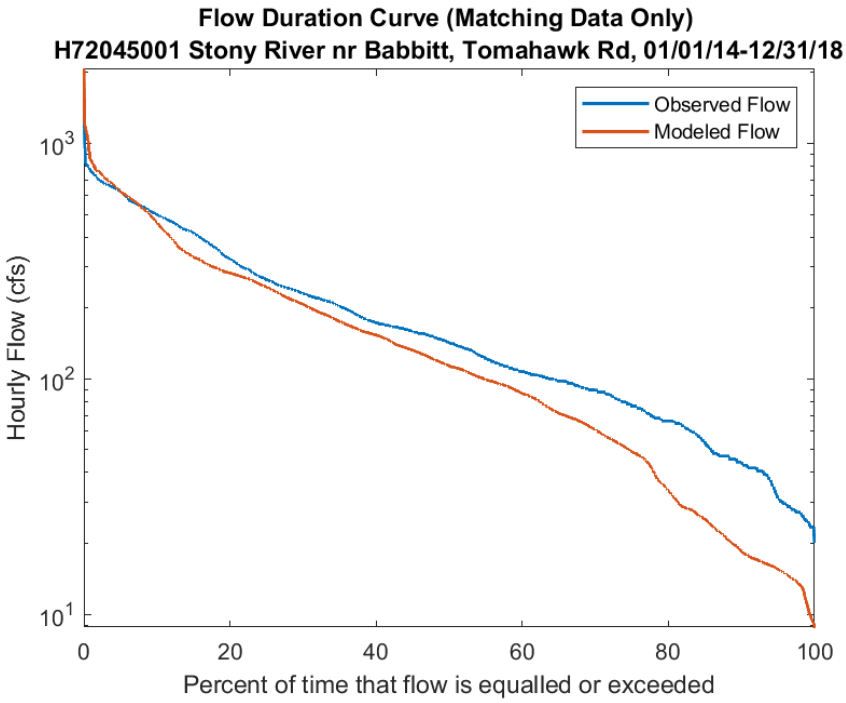

Figure A.5. Flow duration curves for simulated and observed data, H72045001 Stony River nr Babbitt, Tomahawk Rd (RRHW model reach 341).

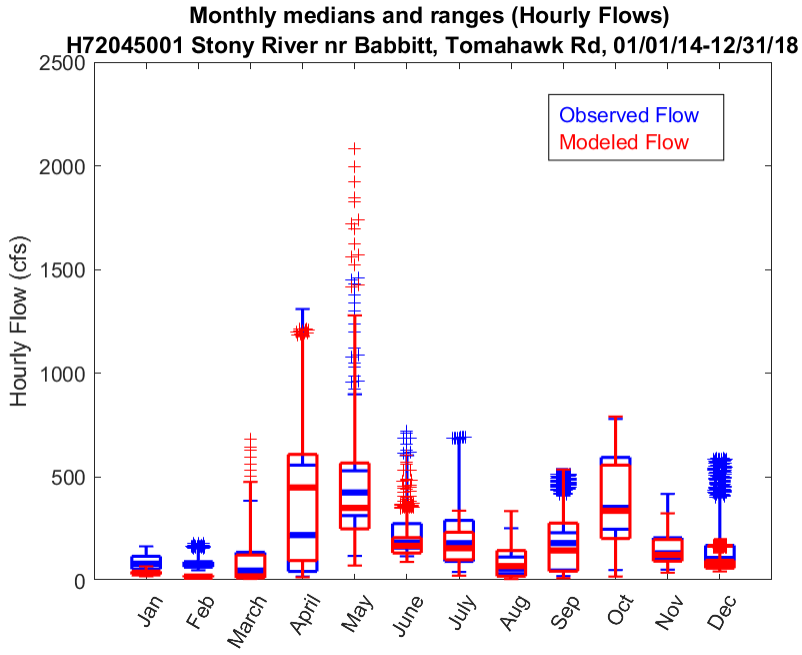

Figure A.6. Boxplots comparing simulated with observed flow by month (daily average flows) for H72045001 Stony River nr Babbitt, Tomahawk Rd (RRHW model reach 341).

6.1.3 Flow Validation - Vermilion River near Crane Lake (USGS 05129115)

Table A.3. Hydrology validation statistics at Vermilion River near Crane Lake gage (USGS 05129115) (Vermilion River model reach 370). Statistics are computed for modeled and observed datasets using only days with observed data, during the validation period 1996-2009.

	HSPF Simulated Flow	Observed Flow	PBIAS (%)/NSE
Total in-stream flow volume (Acre-ft/month)	30392	34257	-11.3
Total of highest 10% flows (Acre-ft)	10455	12510	-16.4
Total of lowest 50% flows (Acre-ft)	6281	5694	10.3
Total summer flow volume (Acre-ft/month)	27570	25033	10.1
Total fall flow volume (Acre-ft/month)	20364	22858	-10.9
Total winter flow volume (Acre-ft/month)	10851	13351	-18.7
Total spring flow volume (Acre-ft/month)	60685	73523	-17.5
Daily NSE	-	-	0.78
Monthly NSE	-	-	0.83

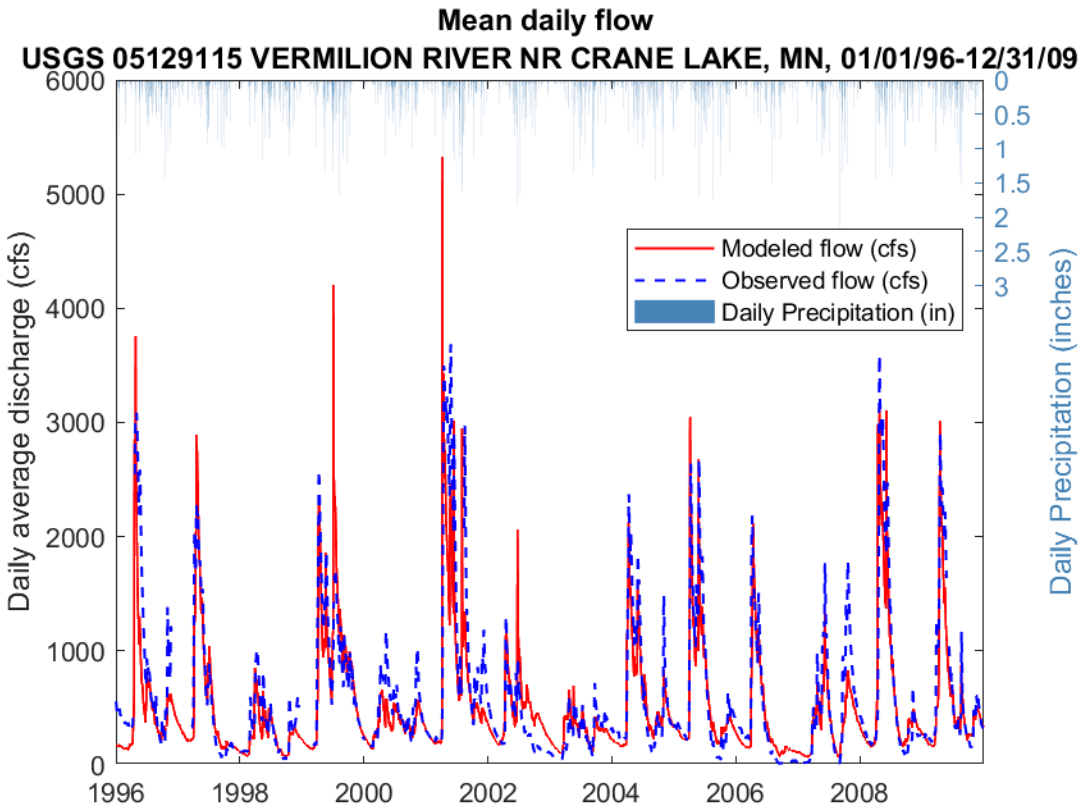

Figure A.7. Hydrograph comparison of observed and simulated daily average values at Vermilion River near Crane Lake gage (USGS 05129115) (Vermilion River model reach 370) during the validation period.

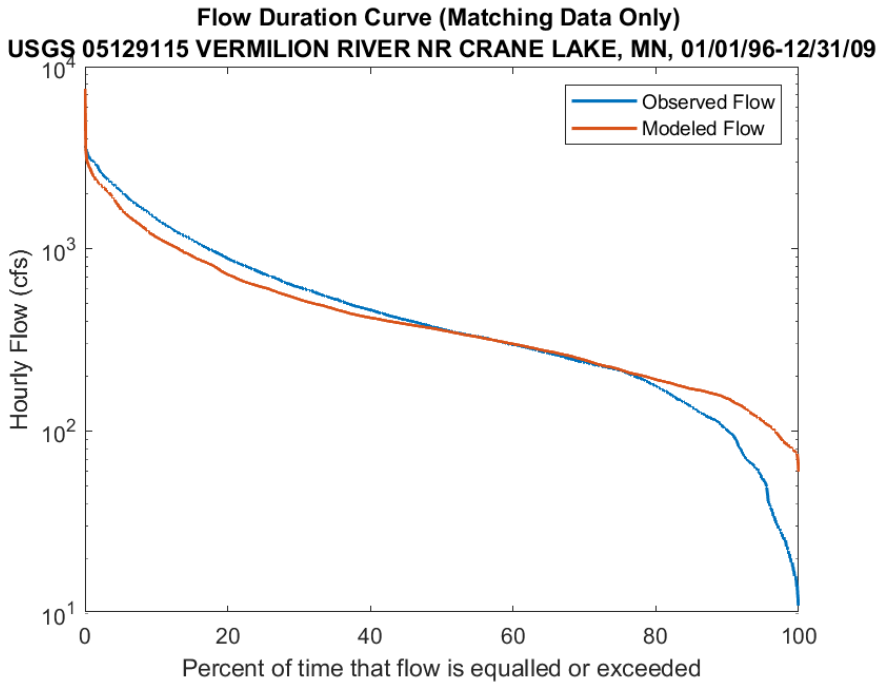

Figure A.8. Flow duration curves for simulated and observed data at Vermilion River near Crane Lake gage (USGS 05129115) (Vermilion River model reach 370) during the validation period.

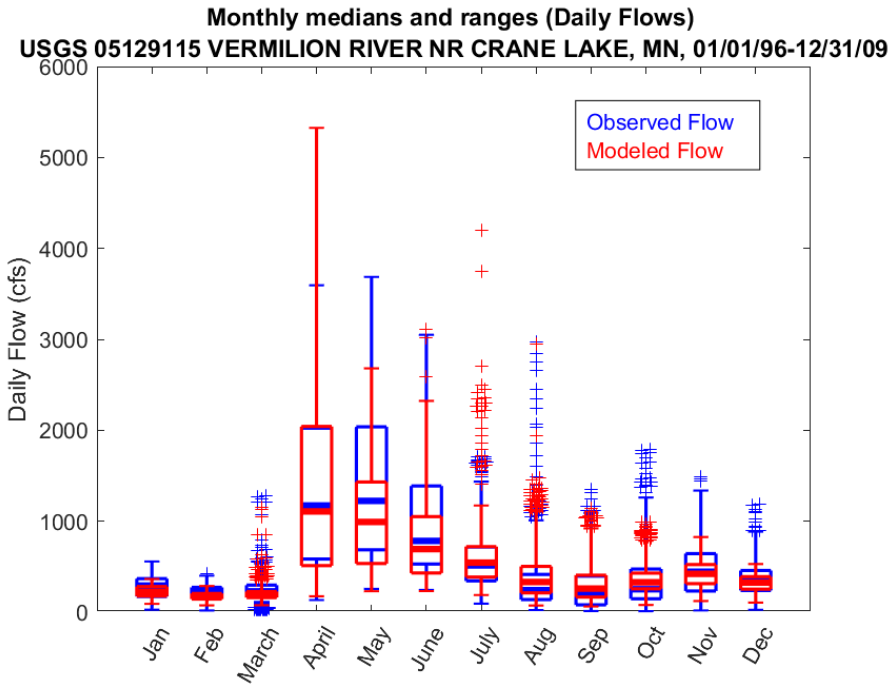

Figure A.9. Boxplots comparing simulated with observed flow by month (daily average flows) at Vermilion River near Crane Lake gage (USGS 05129115) (Vermilion River model reach 370) during the validation period.

6.1.4 Secondary Calibration Gage - H74009004, Ash River near Ash Lake, FR961

Table A.4. Hydrology calibration statistics at Ash River near Ash Lake, FR961 (Rainy Lake model reach 101). Statistics are computed for modeled and observed datasets using only days with observed data. This gage is seasonal, so no winter flow data are available.

	HSPF Simulated Flow	Observed Flow	PBIAS (%)/NSE
Total in-stream flow volume (Acre-ft/month)	4963	6267	-20.8
Total of highest 10% flows (Acre-ft)	2164	2495	-13.3
Total of lowest 50% flows (Acre-ft)	602	719	-16.3
Total summer flow volume (Acre-ft/month)	3430	3128	9.7
Total fall flow volume (Acre-ft/month)	4718	6309	-25.2
Total winter flow volume (Acre-ft/month)	-	-	-
Total spring flow volume (Acre-ft/month)	6633	9383	-29.3
Daily NSE	-	-	0.63
Monthly NSE	-	-	0.53

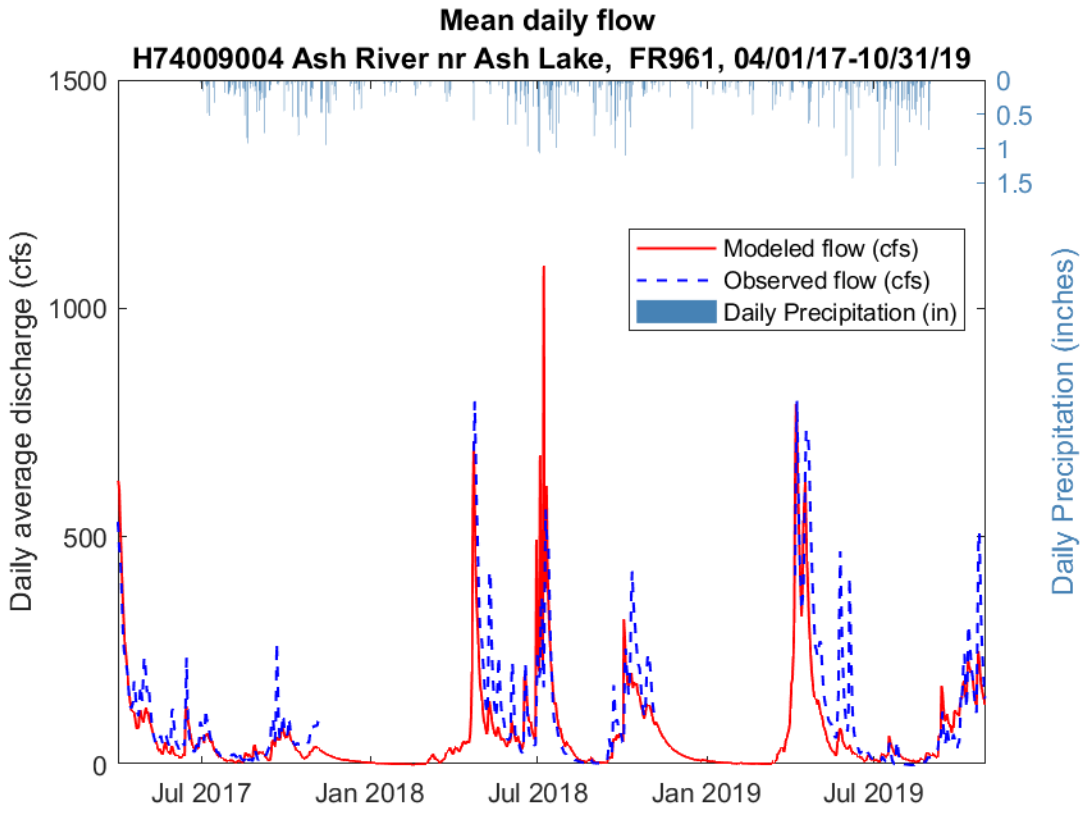

Figure A.10. Hydrograph comparison of observed and simulated daily average values at H74009004, Ash River near Ash Lake, FR961 (Rainy Lake model reach 101).

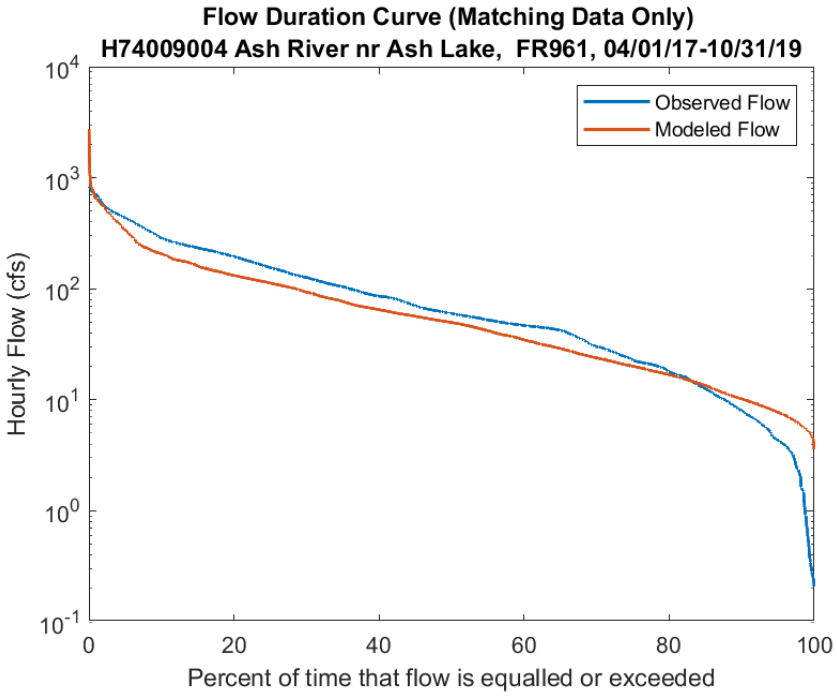

Figure A.11. Flow duration curves for simulated and observed data, H74009004, Ash River near Ash Lake, FR961 (Rainy Lake model reach 101).

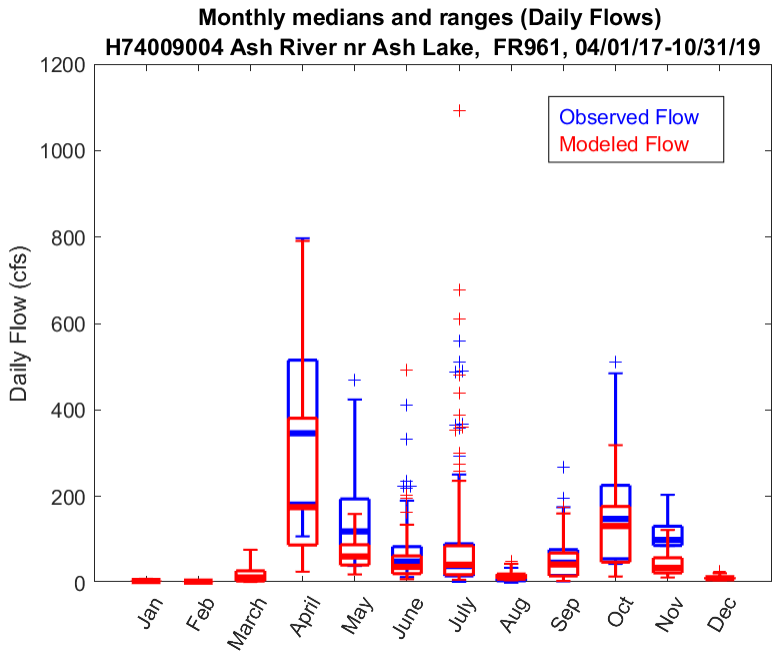

Figure A.12. Boxplots comparing simulated with observed flow by month (daily average flows) for Ash River near Ash Lake, FR961 (Rainy Lake model reach 101).

6.2 FULL WATER QUALITY CALIBRATION RESULTS

6.2.1 Rainy River Headwaters model

6.2.1.1 TSS

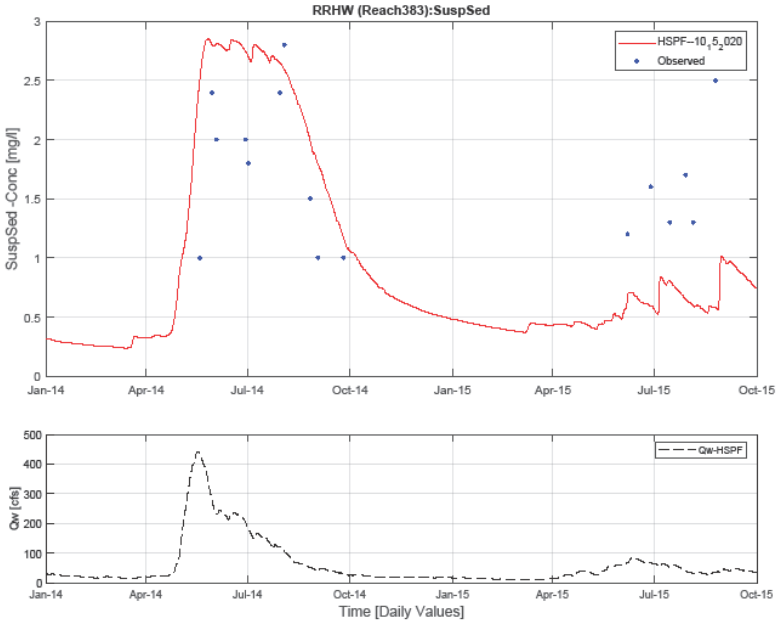

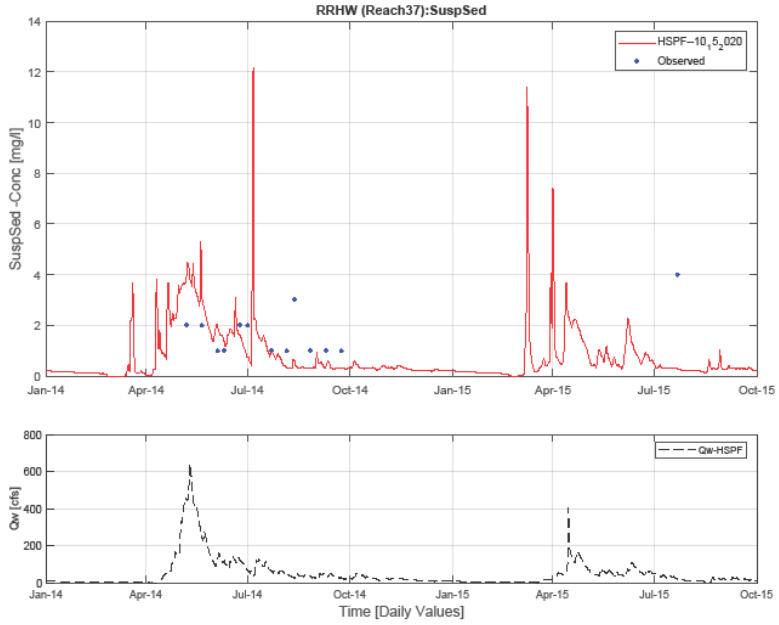

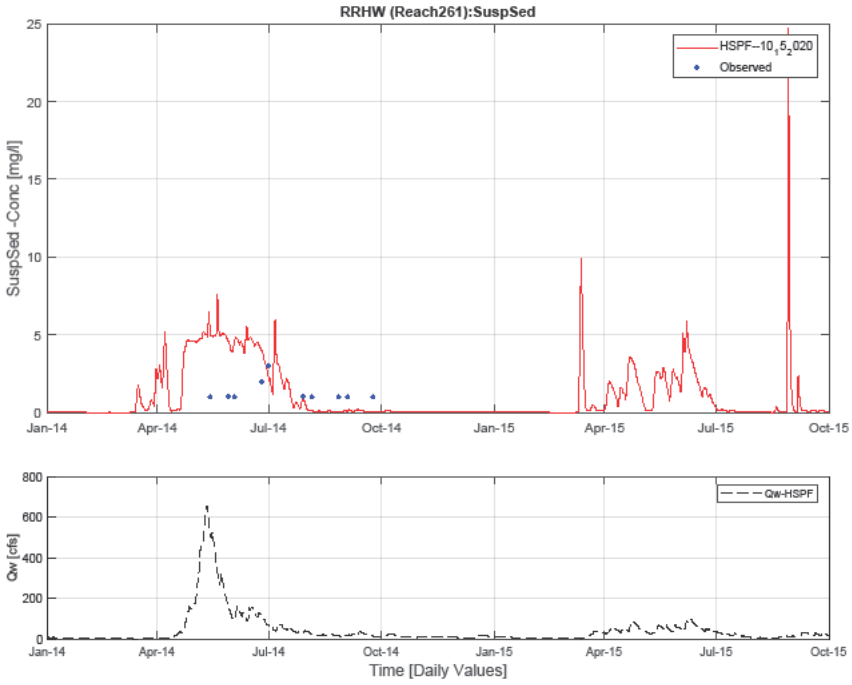
RRHW (Reach261):SuspSed
HSPF--10_1_5_2_020
Observed
SuspSed -Conc [mg/l]
Qw-HSPF
Qw [cfs]
Jan-14
Apr-14
Jul-14
Oct-14
Jan-15
Apr-15
Jul-15
Oct-15
Time [Daily Values]

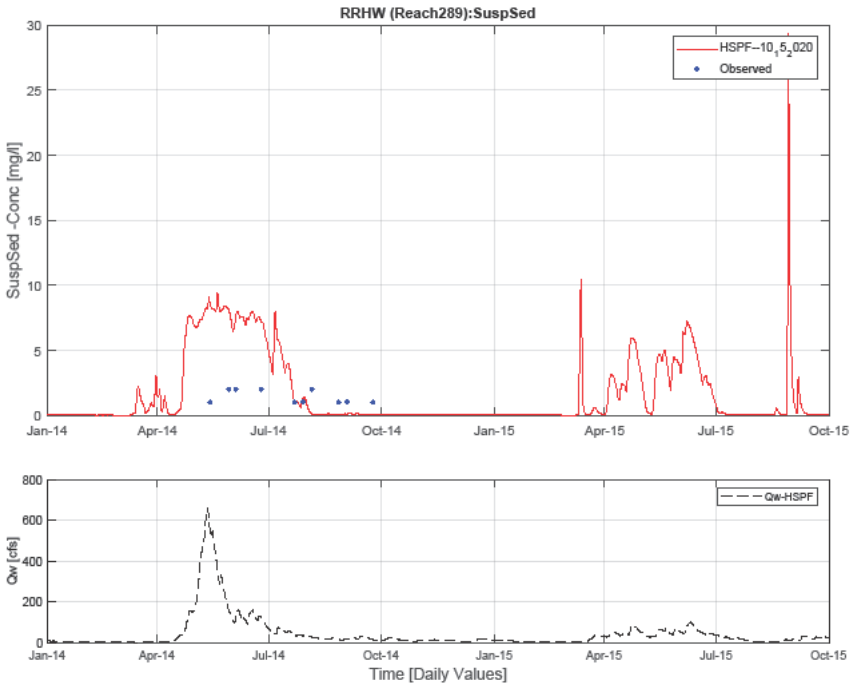
RRHW (Reach289):SuspSed
HSPF--10_1_5_2_020
Observed
SuspSed -Conc [mg/l]
Qw-HSPF
Qw [cfs]
Jan-14
Apr-14
Jul-14
Oct-14
Jan-15
Apr-15
Jul-15
Oct-15
Time [Daily Values]

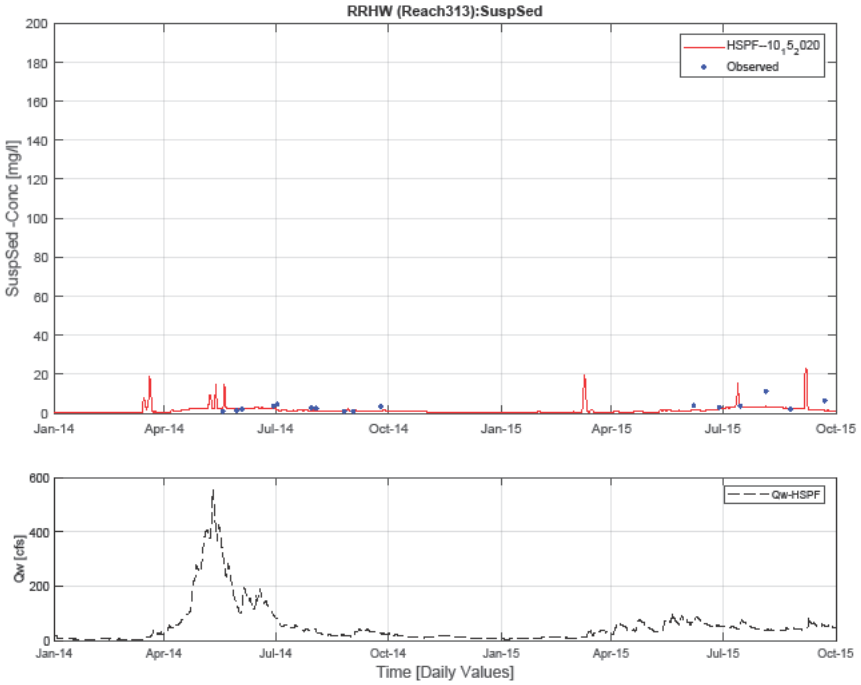
RRHW (Reach313):SuspSed
HSPF--10_5_020
Observed
SuspSed -Conc [mg/l]
Qw-HSPF
Qw [cfs]
Jan-14
Apr-14
Jul-14
Oct-14
Jan-15
Apr-15
Jul-15
Oct-15
Time [Daily Values]

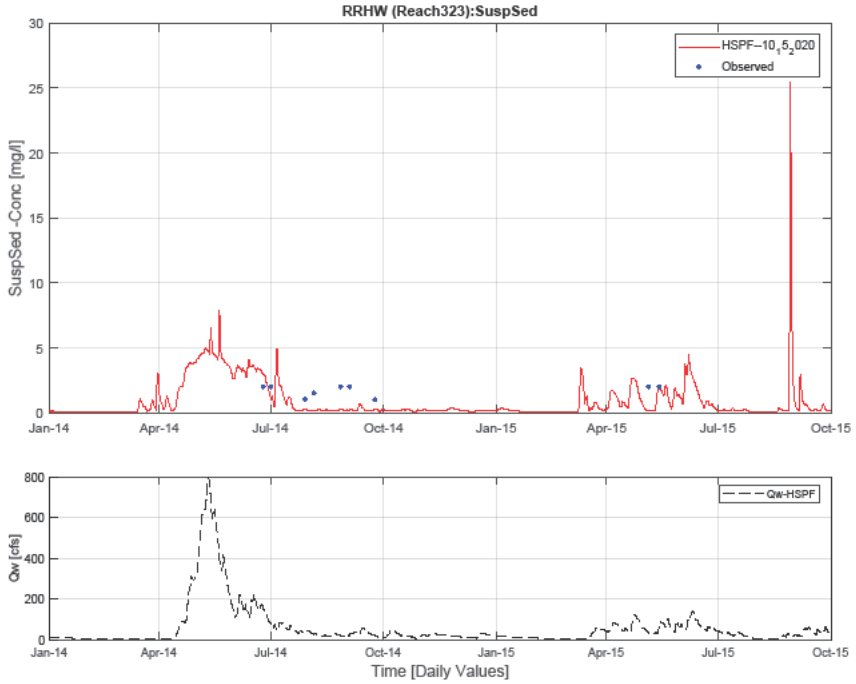
RRHW (Reach323):SuspSed
HSPF--10_5_020
Observed
SuspSed -Conc [mg/l]
Qw-HSPF
Qw [cfs]
Jan-14
Apr-14
Jul-14
Oct-14
Jan-15
Apr-15
Jul-15
Oct-15
Time [Daily Values]

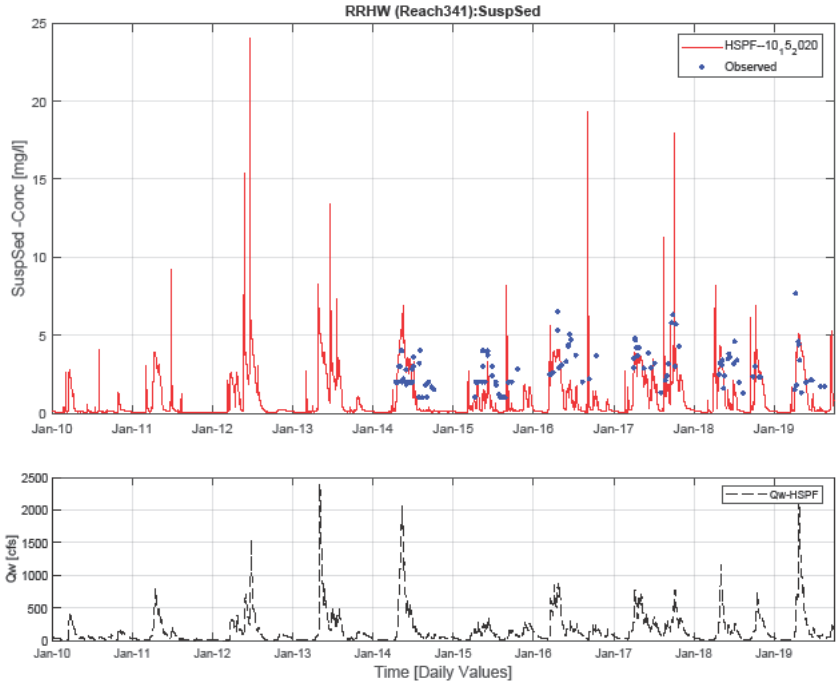
RRHW (Reach341):SuspSed
HSPF--10_5_020
Observed
SuspSed -Conc [mg/l]
Qw-HSPF
Qw [cfs]
Time [Daily Values]

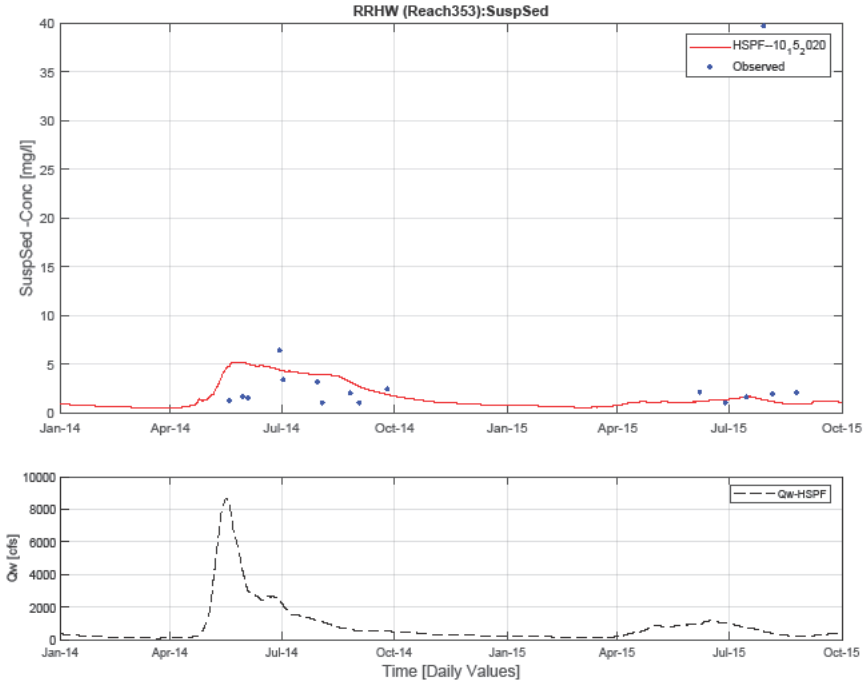
RRHW (Reach353):SuspSed
HSPF--10_5_020
Observed
SuspSed -Conc [mg/l]
Qw-HSPF
Qw [cfs]
Time [Daily Values]

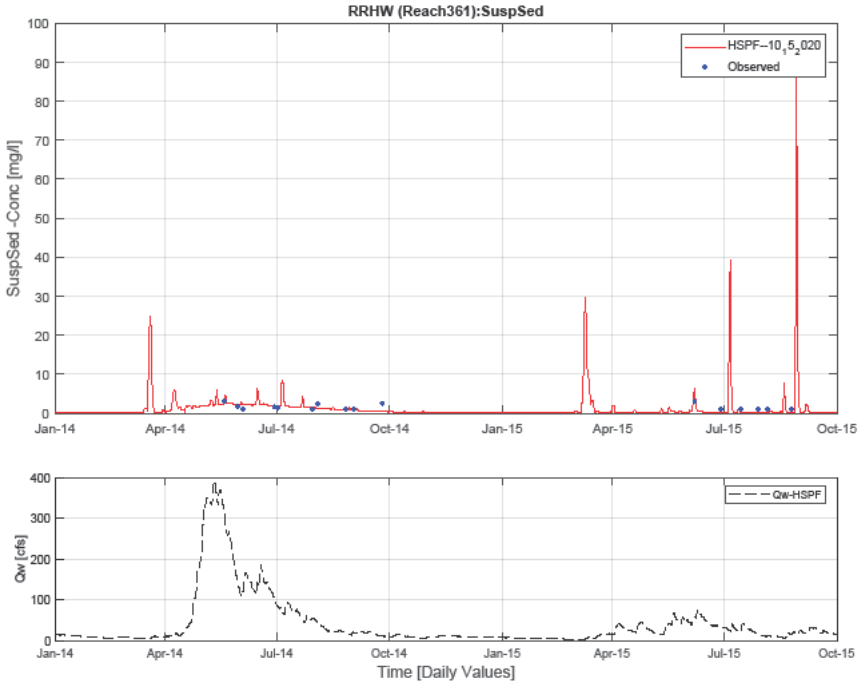
RRHW (Reach361):SuspSed
HSPF--10_5_020
Observed
SuspSed -Conc [mg/l]
Qw-HSPF
Qw [cfs]
Time [Daily Values]

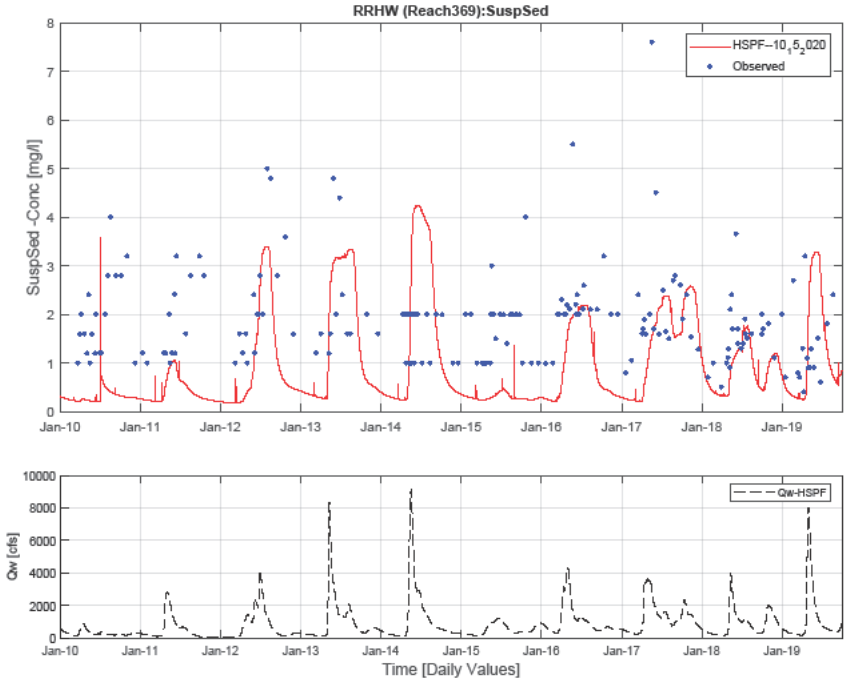
RRHW (Reach369):SuspSed
HSPF--10_5_020
Observed
SuspSed -Conc [mg/l]
Qw-HSPF
Qw [cfs]
Time [Daily Values]

6.2.1.2 PO_4

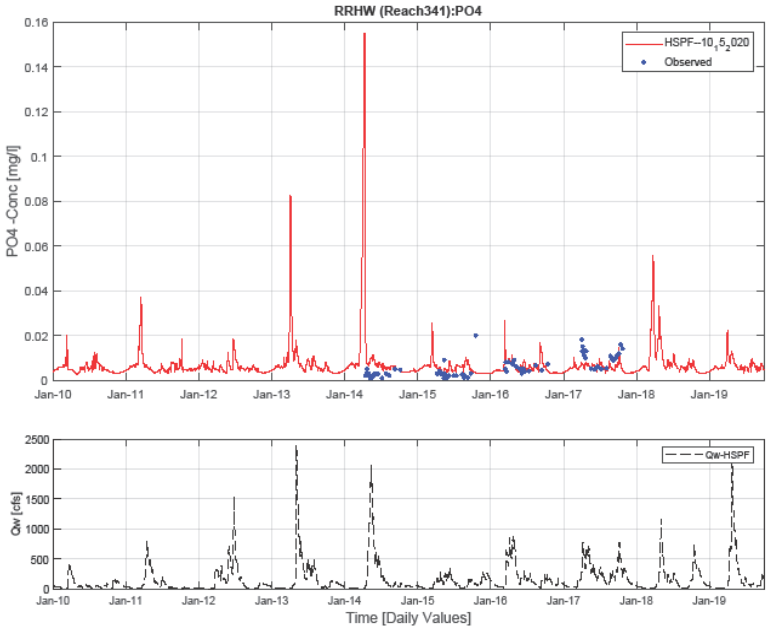
RRHW (Reach341):PO4
HSPF--10_1_5_020
Observed
PO4 -Conc [mg/l]
Qw-HSPF
Qw [cfs]
Time [Daily Values]

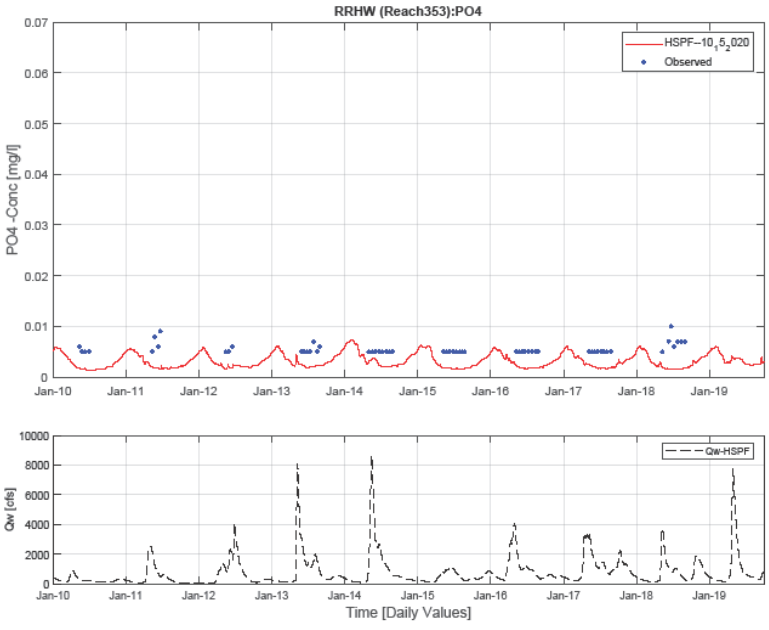
RRHW (Reach353):PO4
HSPF--10_1_5_020
Observed
PO4 -Conc [mg/l]
Qw-HSPF
Qw [cfs]
Time [Daily Values]

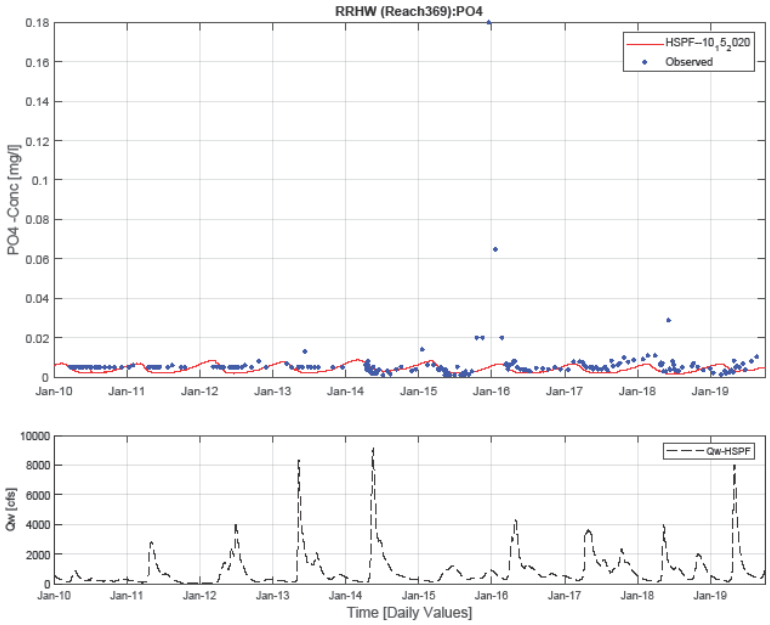
RRHW (Reach369):PO4
HSPF--10_5_020
Observed
PO4 -Conc [mg/l]
0.18
0.16
0.14
0.12
0.1
0.08
0.06
0.04
0.02
0
Jan-10
Jan-11
Jan-12
Jan-13
Jan-14
Jan-15
Jan-16
Jan-17
Jan-18
Jan-19
Qw-HSPF
Qw [cfs]
10000
8000
6000
4000
2000
0
Time [Daily Values]

6.2.1.3 TP

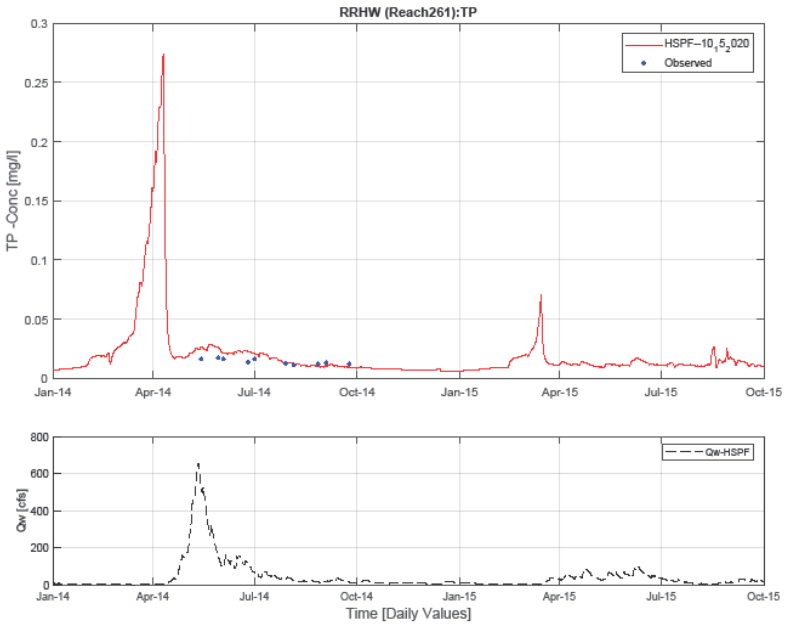
RRHW (Reach261):TP
HSPF--10_1_5_020
Observed
TP -Conc [mg/l]
0.3
0.25
0.2
0.15
0.1
0.05
0
Jan-14
Apr-14
Jul-14
Oct-14
Jan-15
Apr-15
Jul-15
Oct-15
Qw-HSPF
Qw [cfs]
800
600
400
200
0
Time [Daily Values]

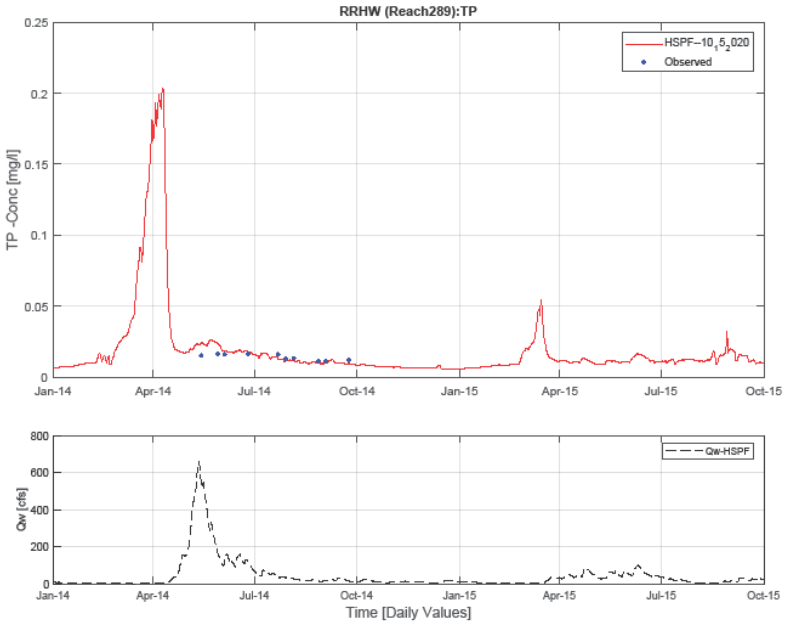
RRHW (Reach289):TP
HSPF--10_1_5_020
Observed
TP -Conc [mg/l]
0.25
0.2
0.15
0.1
0.05
0
Jan-14
Apr-14
Jul-14
Oct-14
Jan-15
Apr-15
Jul-15
Oct-15
Qw-HSPF
Qw [cfs]
800
600
400
200
0
Time [Daily Values]

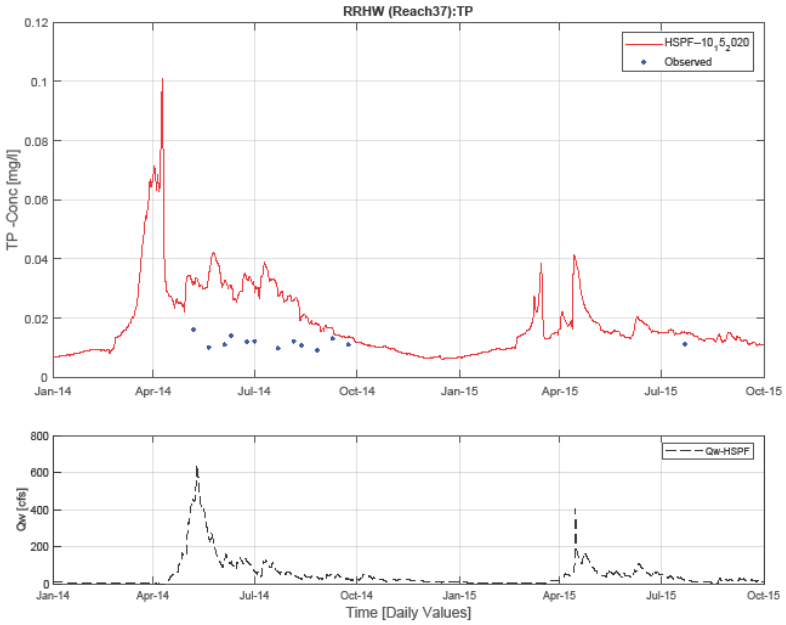
RRHW (Reach37):TP
HSPF--10_1_5_020
Observed
TP -Conc [mg/l]
Qw-HSPF
Qw [cfs]
Time [Daily Values]

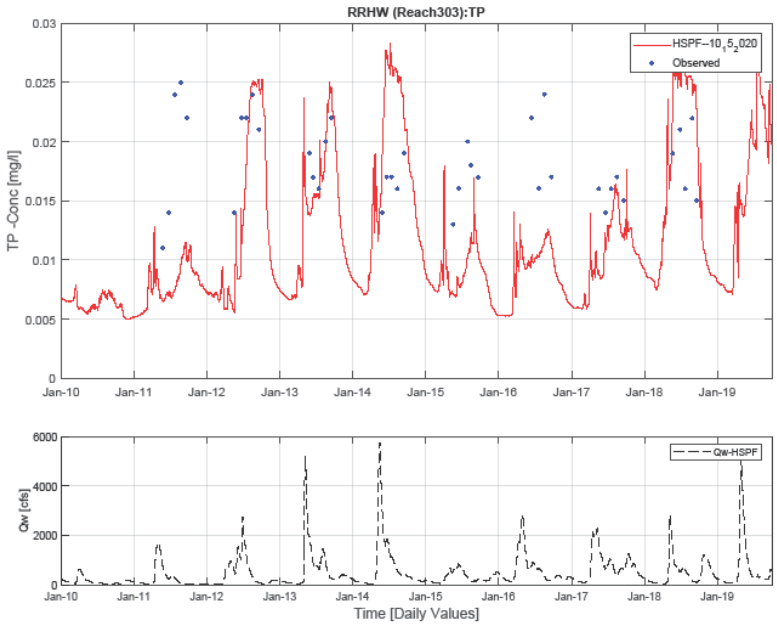
RRHW (Reach303):TP
HSPF--10_1_5_020
Observed
TP -Conc [mg/l]
Qw-HSPF
Qw [cfs]
Time [Daily Values]

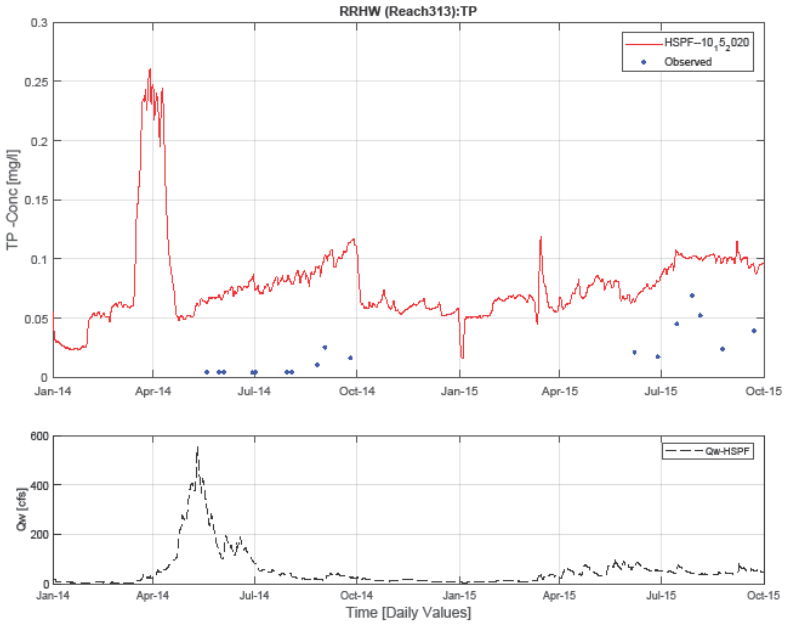
RRHW (Reach313):TP
HSPF--10_1_5_020
Observed
TP -Conc [mg/l]
0.3
0.25
0.2
0.15
0.1
0.05
0
Jan-14
Apr-14
Jul-14
Oct-14
Jan-15
Apr-15
Jul-15
Oct-15
Qw-HSPF
Qw [cfs]
600
400
200
0
Time [Daily Values]

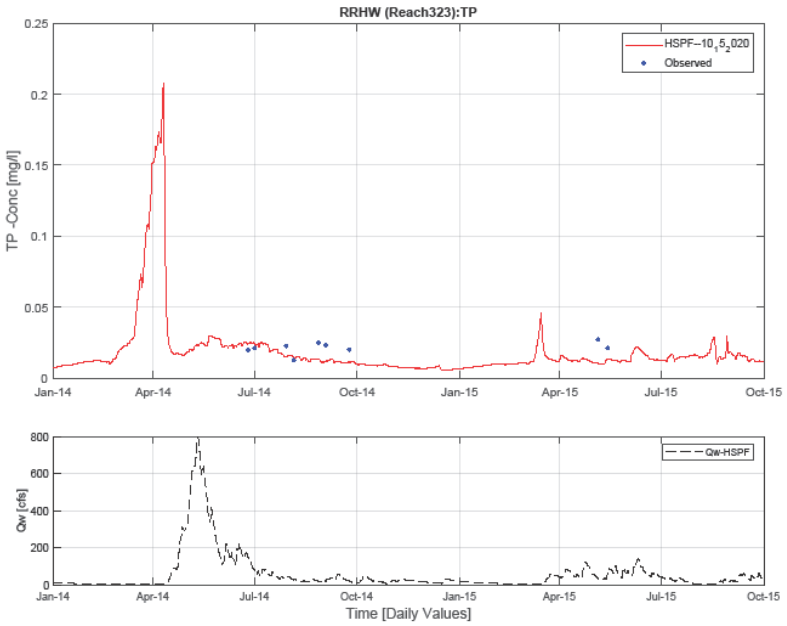
RRHW (Reach323):TP
HSPF--10_1_5_020
Observed
TP -Conc [mg/l]
0.25
0.2
0.15
0.1
0.05
0
Jan-14
Apr-14
Jul-14
Oct-14
Jan-15
Apr-15
Jul-15
Oct-15
Qw-HSPF
Qw [cfs]
800
600
400
200
0
Time [Daily Values]

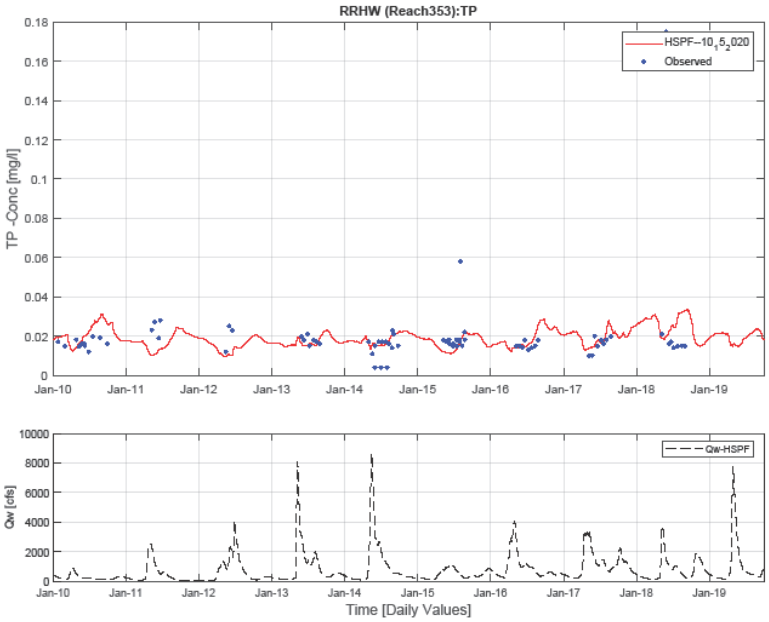
RRHW (Reach353):TP
HSPF--10_1_5_020
Observed
TP -Conc [mg/l]
Qw-HSPF
Qw [cfs]
Time [Daily Values]

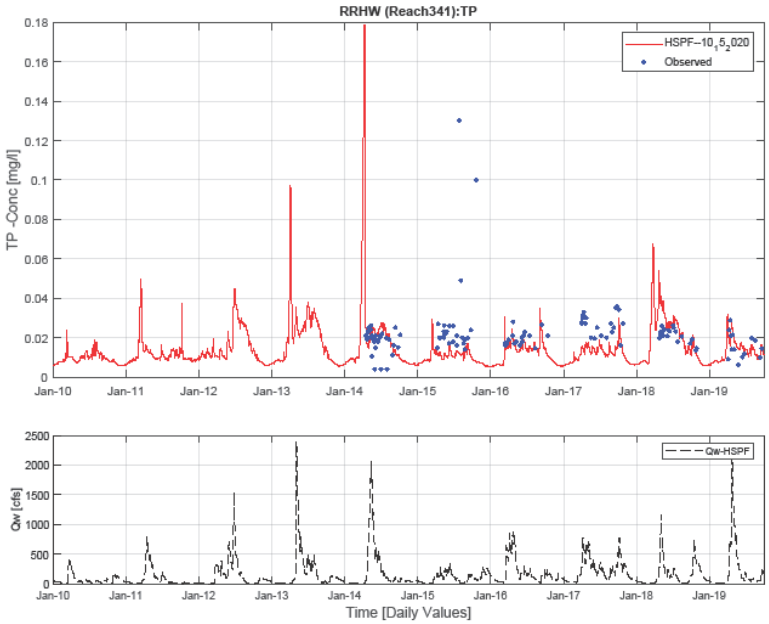
RRHW (Reach341):TP
HSPF--10_1_5_020
Observed
TP -Conc [mg/l]
Qw-HSPF
Qw [cfs]
Time [Daily Values]

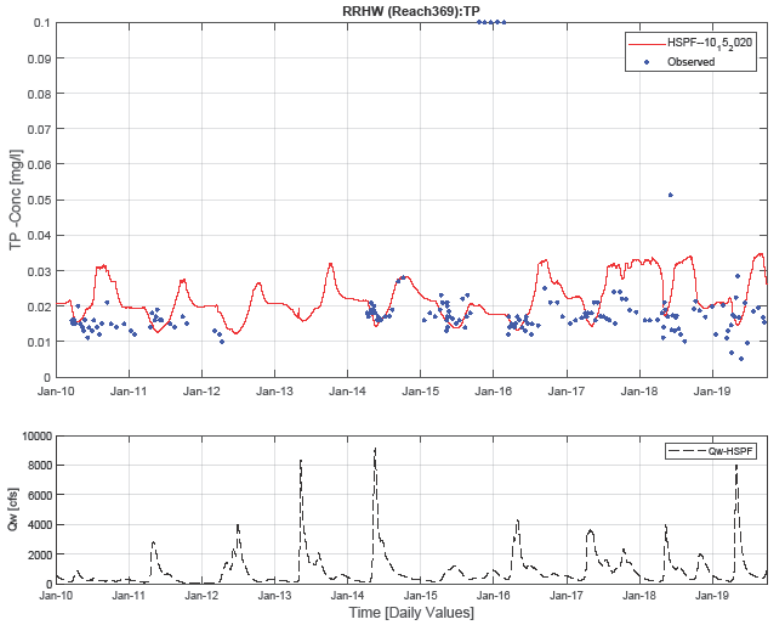
RRHW (Reach369):TP
HSPF--10_1_5_020
Observed
TP -Conc [mg/l]
Qw-HSPF
Qw [cfs]
Time [Daily Values]

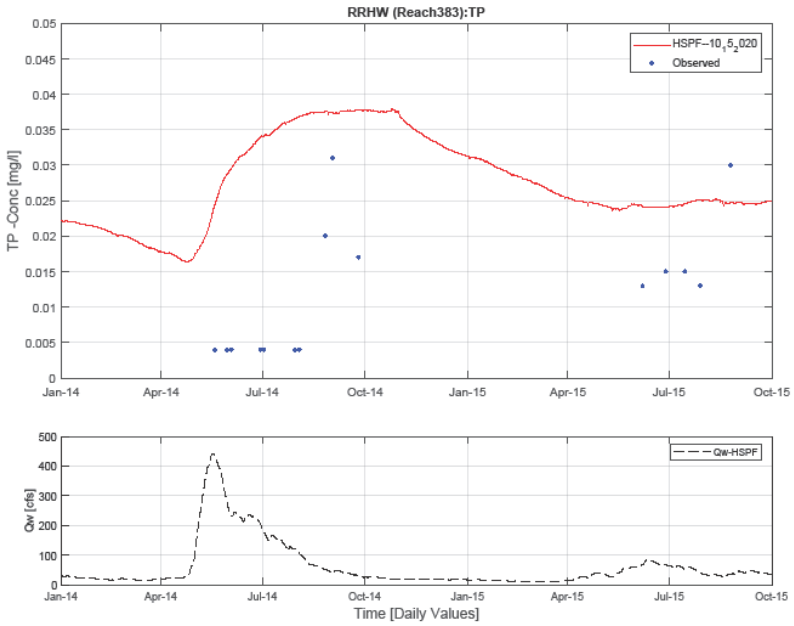
RRHW (Reach383):TP
HSPF--10_1_5_020
Observed
TP -Conc [mg/l]
Qw-HSPF
Qw [cfs]
Time [Daily Values]

6.2.1.4 NO_2+NO_3

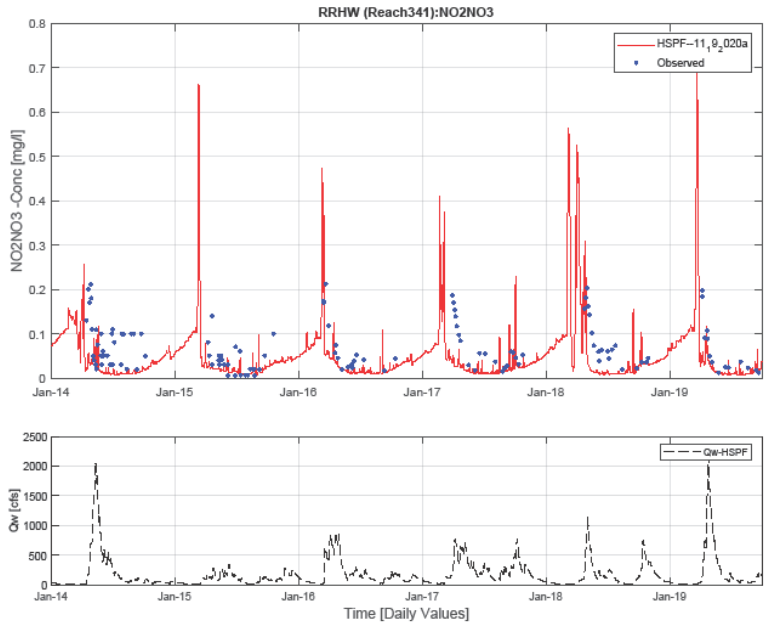
RRHW (Reach341):NO2NO3
HSPF--11_9_020a
Observed
NO2NO3 -Conc [mg/l]
Qw-HSPF
Qw [cfs]
Jan-14
Jan-15
Jan-16
Jan-17
Jan-18
Jan-19
Time [Daily Values]

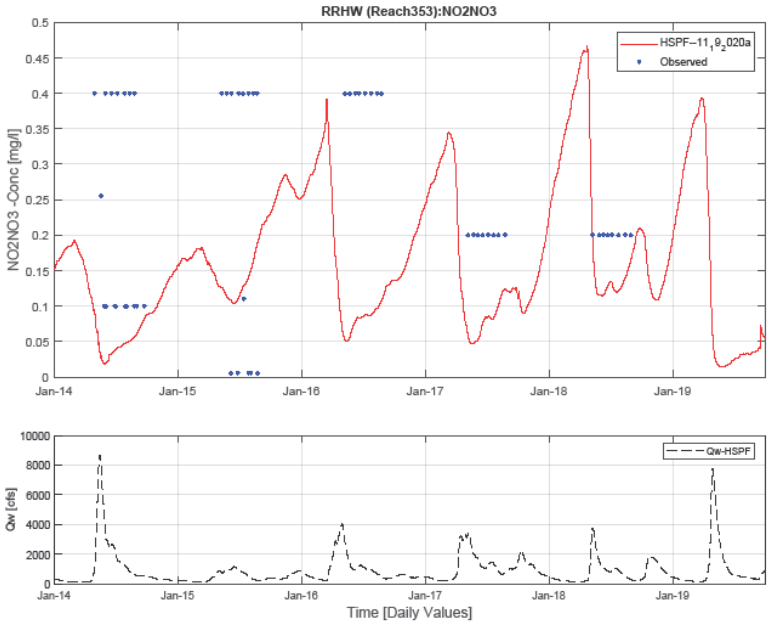
RRHW (Reach353):NO2NO3
HSPF--11_9_020a
Observed
NO2NO3 -Conc [mg/l]
Qw-HSPF
Qw [cfs]
Jan-14
Jan-15
Jan-16
Jan-17
Jan-18
Jan-19
Time [Daily Values]

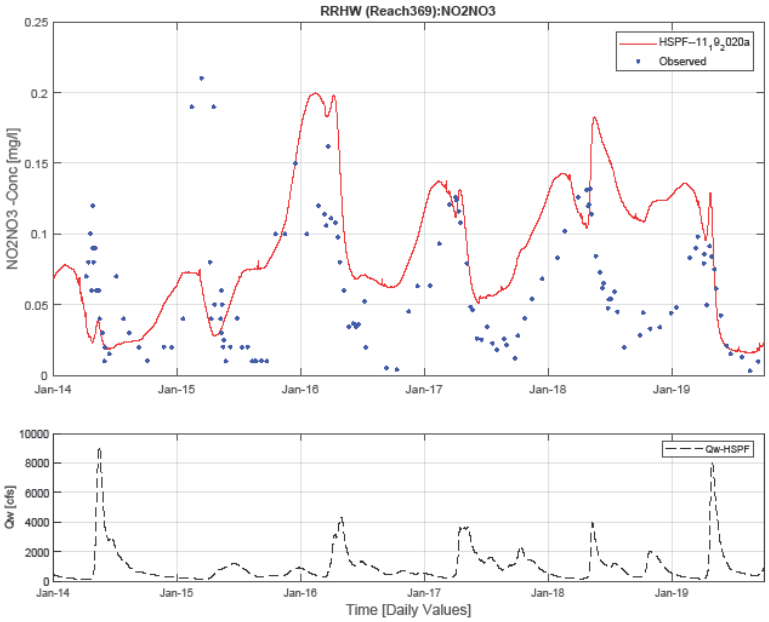
RRHW (Reach369):NO2NO3
HSPF--11_19_020a
Observed
NO2NO3 -Conc [mg/l]
0.25
0.2
0.15
0.1
0.05
0
Jan-14
Jan-15
Jan-16
Jan-17
Jan-18
Jan-19
Qw-HSPF
Qw [cfs]
10000
8000
6000
4000
2000
0
Time [Daily Values]

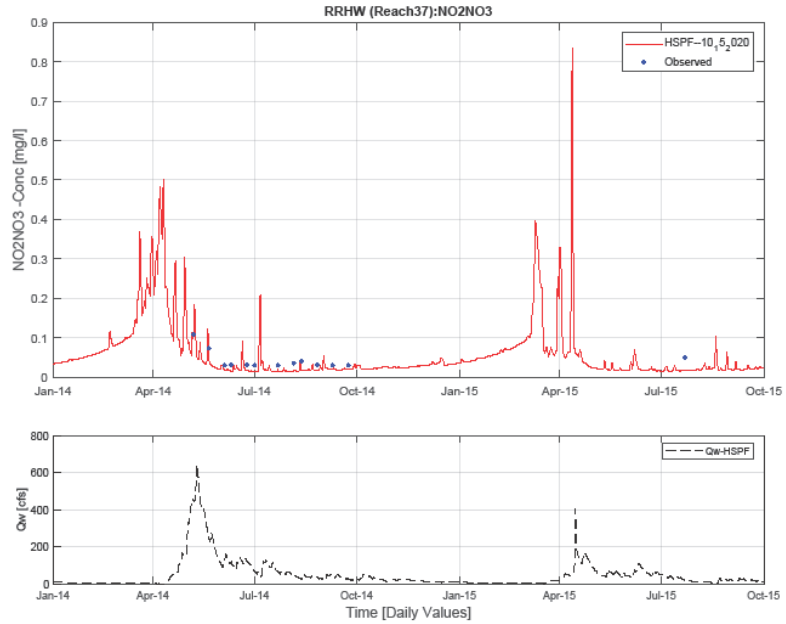
RRHW (Reach37):NO2NO3
HSPF--10_5_020
Observed
NO2NO3 -Conc [mg/l]
0.9
0.8
0.7
0.6
0.5
0.4
0.3
0.2
0.1
0
Jan-14
Apr-14
Jul-14
Oct-14
Jan-15
Apr-15
Jul-15
Oct-15
Qw-HSPF
Qw [cfs]
800
600
400
200
0
Time [Daily Values]

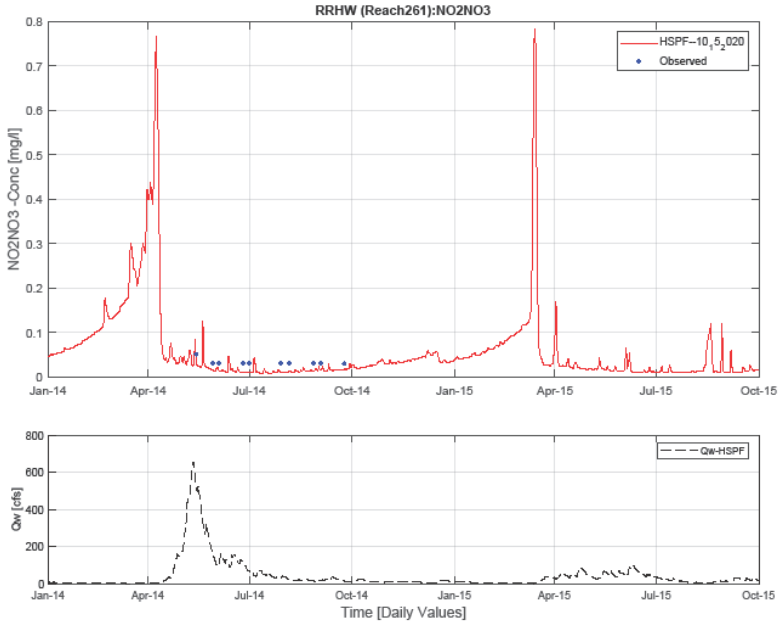
RRHW (Reach261):NO2NO3
HSPF--10_5_020
Observed
NO2NO3 -Conc [mg/l]
Qw-HSPF
Qw [cfs]
Jan-14
Apr-14
Jul-14
Oct-14
Jan-15
Apr-15
Jul-15
Oct-15
Time [Daily Values]

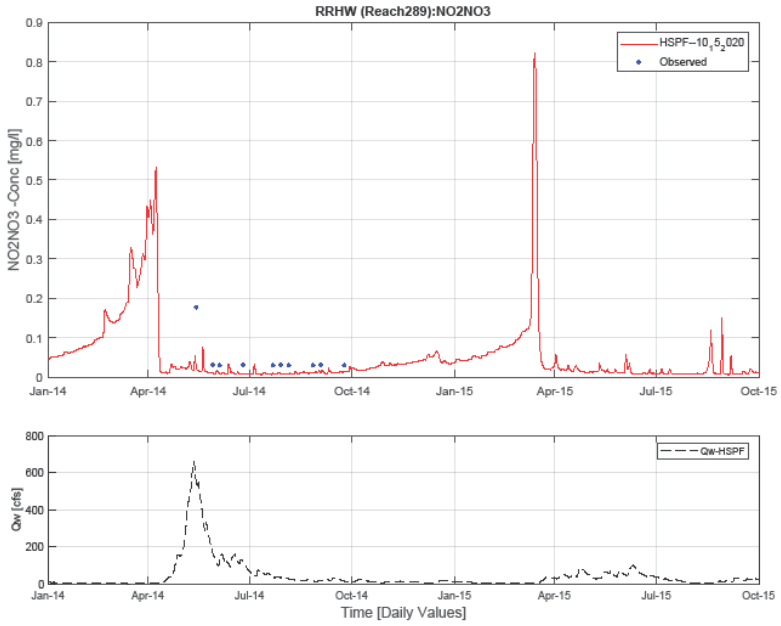
RRHW (Reach289):NO2NO3
HSPF--10_5_020
Observed
NO2NO3 -Conc [mg/l]
Qw-HSPF
Qw [cfs]
Jan-14
Apr-14
Jul-14
Oct-14
Jan-15
Apr-15
Jul-15
Oct-15
Time [Daily Values]

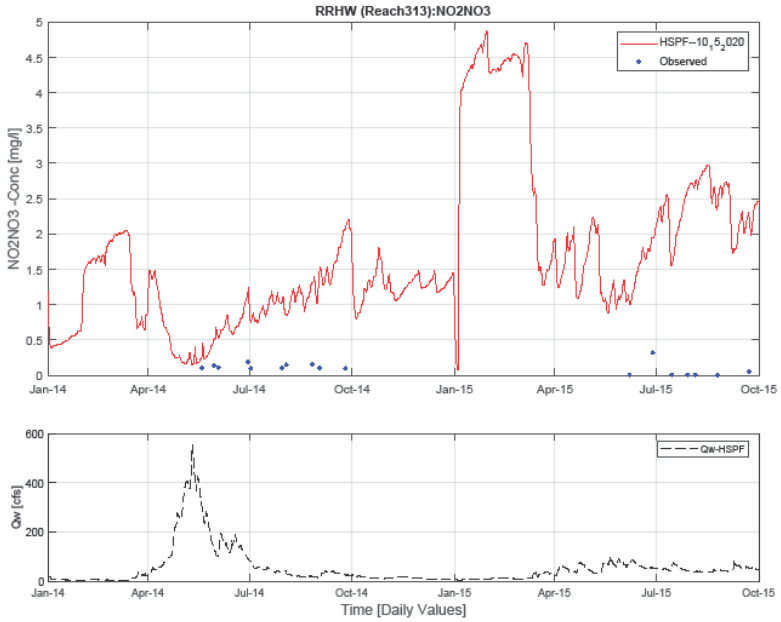
RRHW (Reach313):NO2NO3
HSPF--10_5_020
Observed
NO2NO3 -Conc [mg/l]
Qw-HSPF
Qw [cfs]
Jan-14
Apr-14
Jul-14
Oct-14
Jan-15
Apr-15
Jul-15
Oct-15
Time [Daily Values]

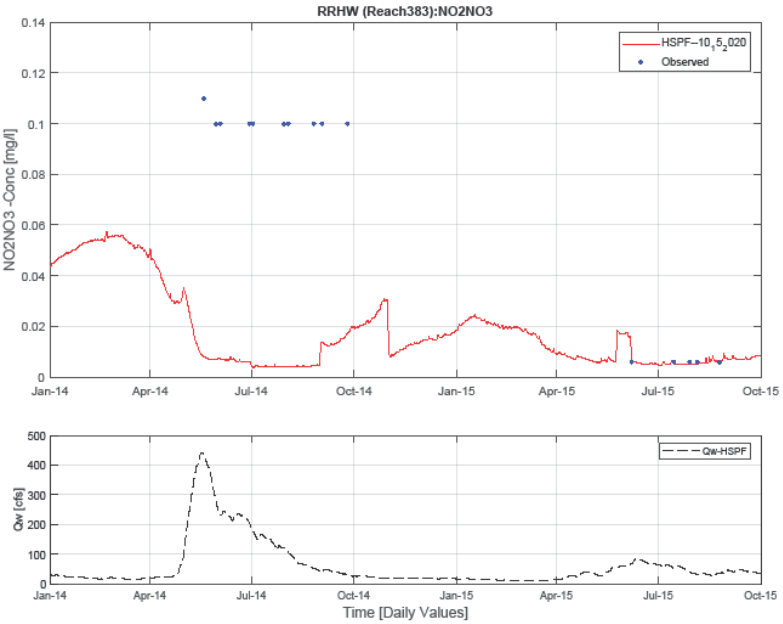
RRHW (Reach383):NO2NO3
HSPF--10_5_020
Observed
NO2NO3 -Conc [mg/l]
Qw-HSPF
Qw [cfs]
Jan-14
Apr-14
Jul-14
Oct-14
Jan-15
Apr-15
Jul-15
Oct-15
Time [Daily Values]

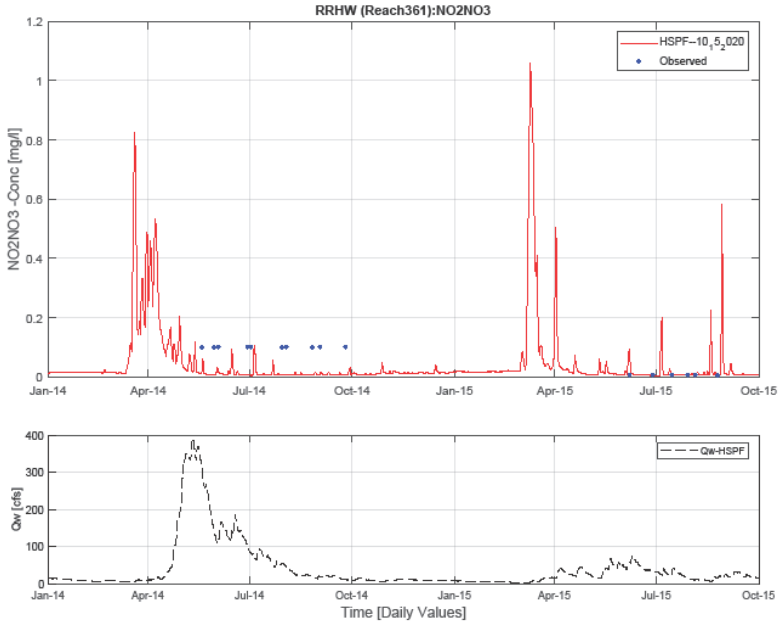
RRHW (Reach361):NO2NO3
HSPF--10_5_020
Observed
NO2NO3 -Conc [mg/l]
Qw-HSPF
Qw [cfs]
Jan-14
Apr-14
Jul-14
Oct-14
Jan-15
Apr-15
Jul-15
Oct-15
Time [Daily Values]

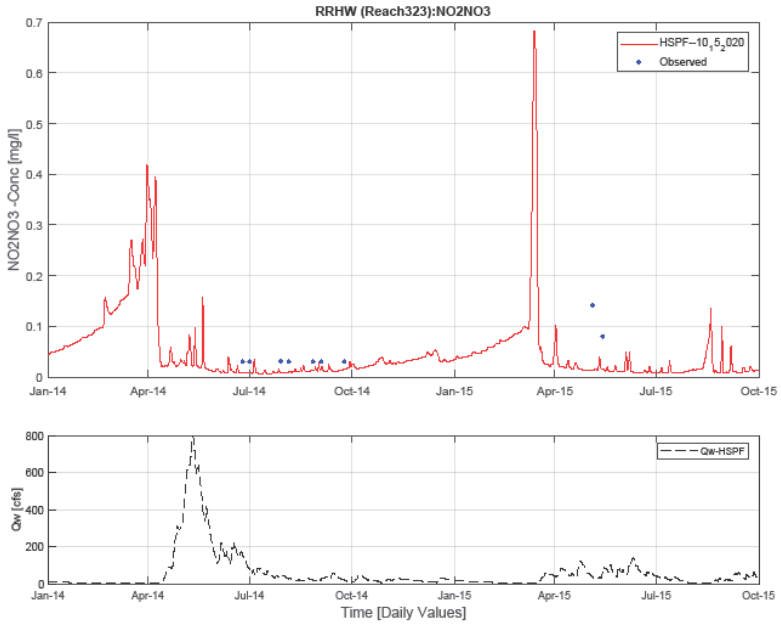
RRHW (Reach323):NO2NO3
HSPF--10_5_020
Observed
NO2NO3 -Conc [mg/l]
Qw-HSPF
Qw [cfs]
Jan-14
Apr-14
Jul-14
Oct-14
Jan-15
Apr-15
Jul-15
Oct-15
Time [Daily Values]

6.2.1.5 TAM

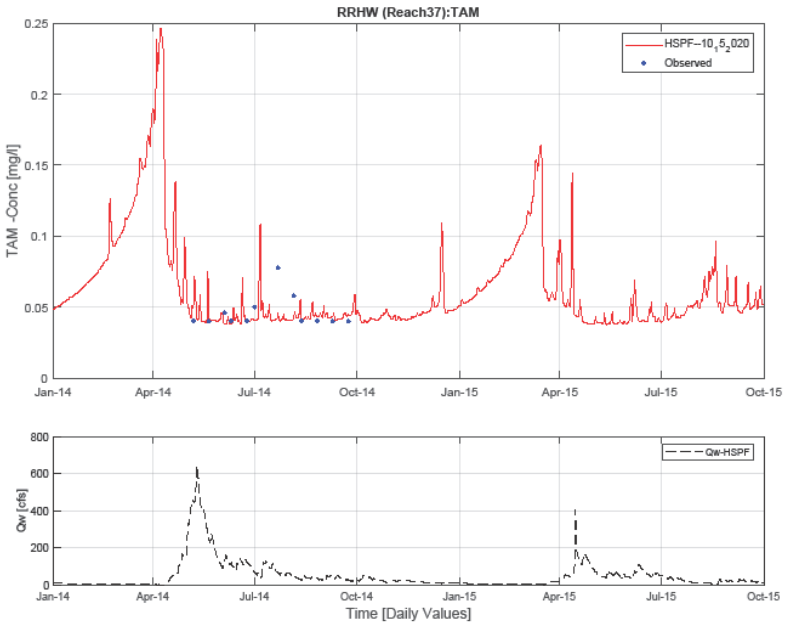
RRHW (Reach37):TAM
HSPF--10_5_020
Observed
TAM -Conc [mg/l]
0.25
0.2
0.15
0.1
0.05
0
Jan-14
Apr-14
Jul-14
Oct-14
Jan-15
Apr-15
Jul-15
Oct-15
Qw-HSPF
Qw [cfs]
800
600
400
200
0
Time [Daily Values]

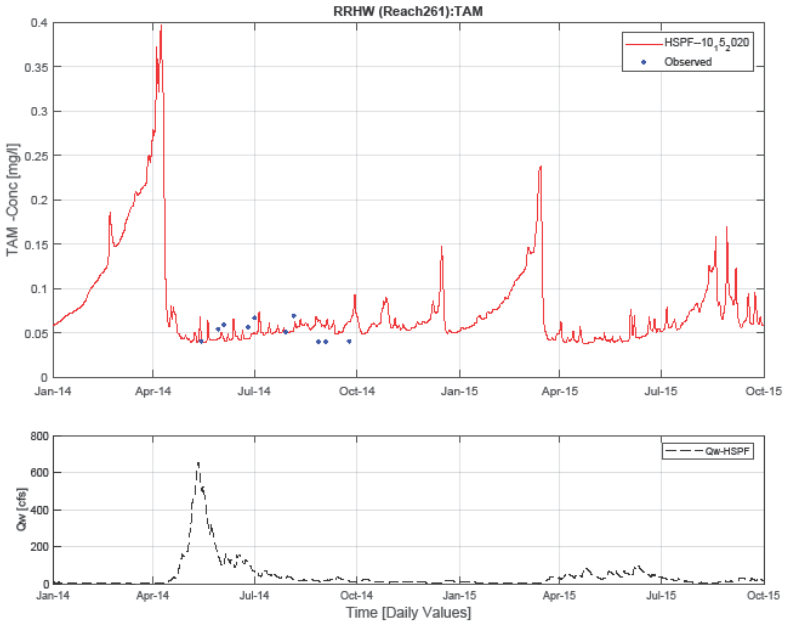
RRHW (Reach261):TAM
HSPF--10_5_020
Observed
TAM -Conc [mg/l]
0.4
0.35
0.3
0.25
0.2
0.15
0.1
0.05
0
Jan-14
Apr-14
Jul-14
Oct-14
Jan-15
Apr-15
Jul-15
Oct-15
Qw-HSPF
Qw [cfs]
800
600
400
200
0
Time [Daily Values]

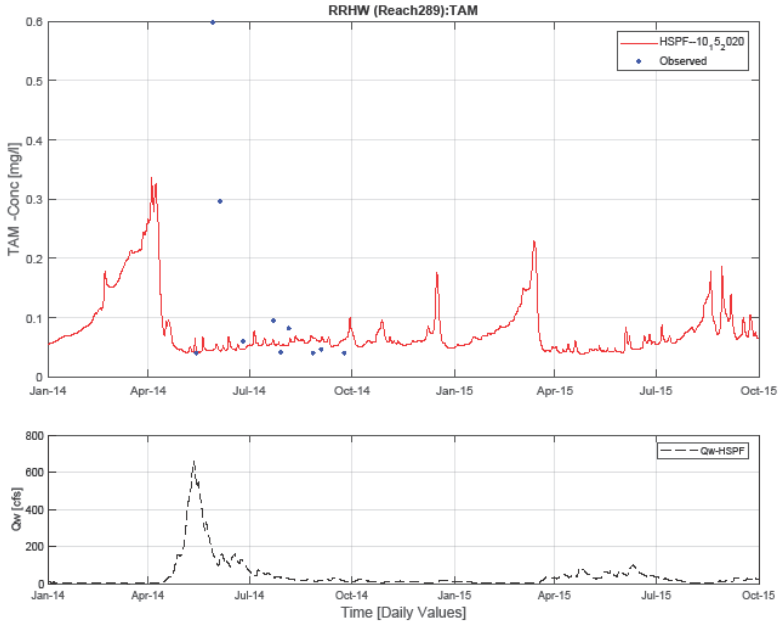
RRHW (Reach289):TAM
HSPF--10_1_5_020
Observed
TAM -Conc [mg/l]
Qw-HSPF
Qw [cfs]
Jan-14
Apr-14
Jul-14
Oct-14
Jan-15
Apr-15
Jul-15
Oct-15
Time [Daily Values]

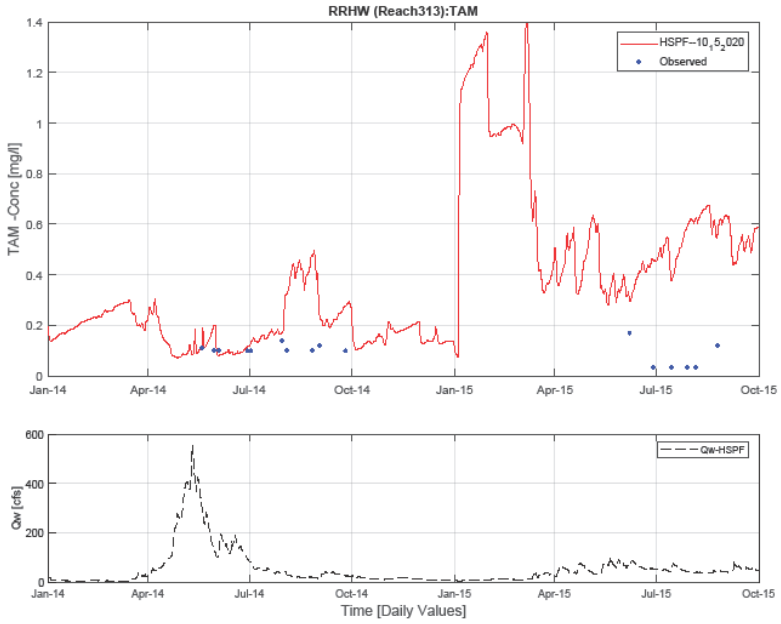
RRHW (Reach313):TAM
HSPF--10_1_5_020
Observed
TAM -Conc [mg/l]
Qw-HSPF
Qw [cfs]
Jan-14
Apr-14
Jul-14
Oct-14
Jan-15
Apr-15
Jul-15
Oct-15
Time [Daily Values]

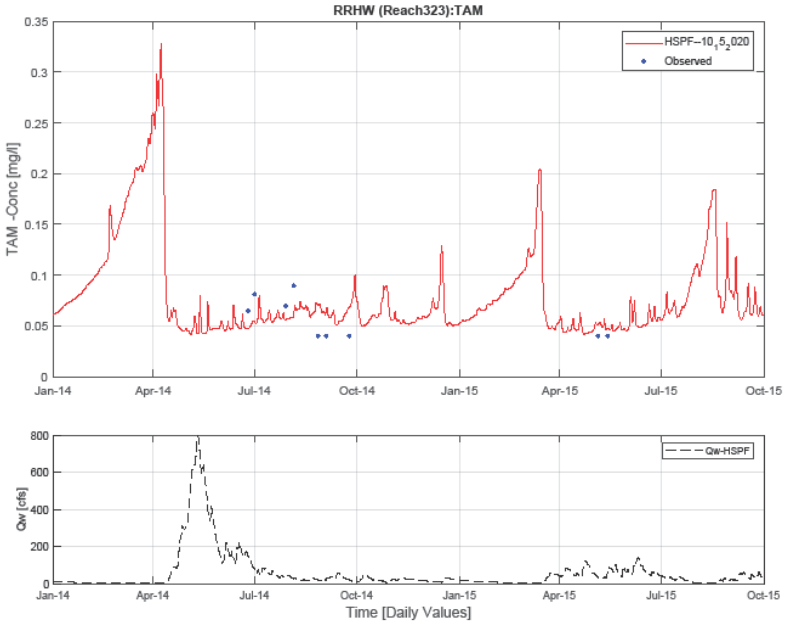
RRHW (Reach323):TAM
HSPF--10_1_5_020
Observed
TAM -Conc [mg/l]
0.35
0.3
0.25
0.2
0.15
0.1
0.05
0
Jan-14
Apr-14
Jul-14
Oct-14
Jan-15
Apr-15
Jul-15
Oct-15
Qw-HSPF
Qw [cfs]
800
600
400
200
0
Time [Daily Values]

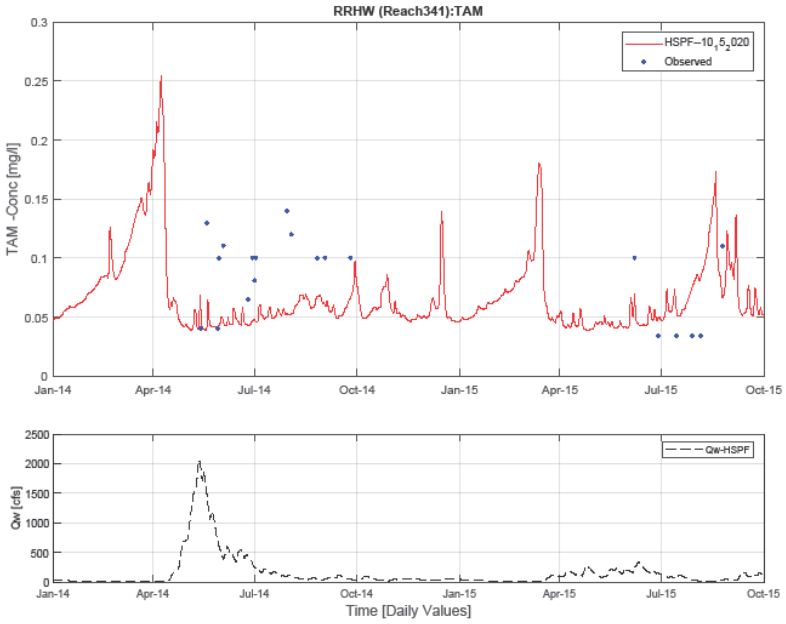
RRHW (Reach341):TAM
HSPF--10_1_5_020
Observed
TAM -Conc [mg/l]
0.3
0.25
0.2
0.15
0.1
0.05
0
Jan-14
Apr-14
Jul-14
Oct-14
Jan-15
Apr-15
Jul-15
Oct-15
Qw-HSPF
Qw [cfs]
2500
2000
1500
1000
500
0
Time [Daily Values]

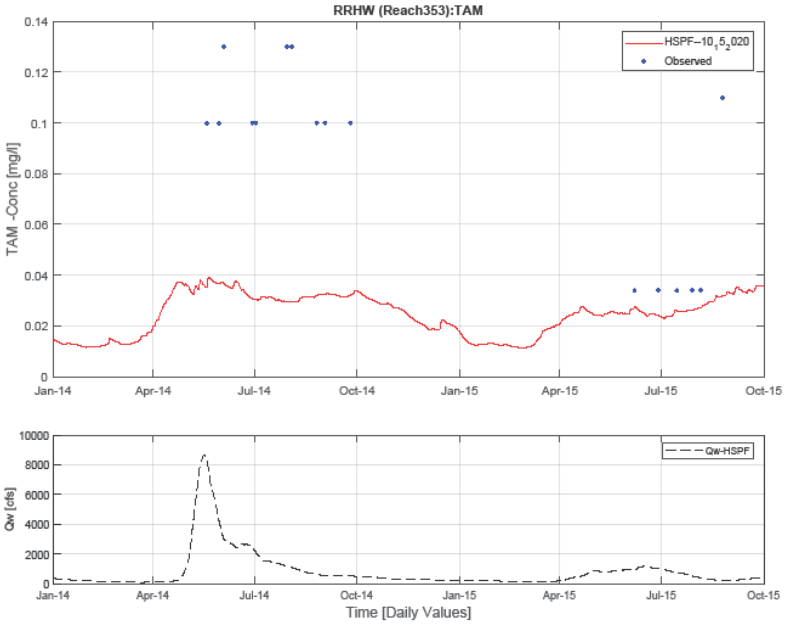
RRHW (Reach353):TAM
HSPF--10_1_5_020
Observed
TAM -Conc [mg/l]
Qw-HSPF
Qw [cfs]
Jan-14
Apr-14
Jul-14
Oct-14
Jan-15
Apr-15
Jul-15
Oct-15
Time [Daily Values]

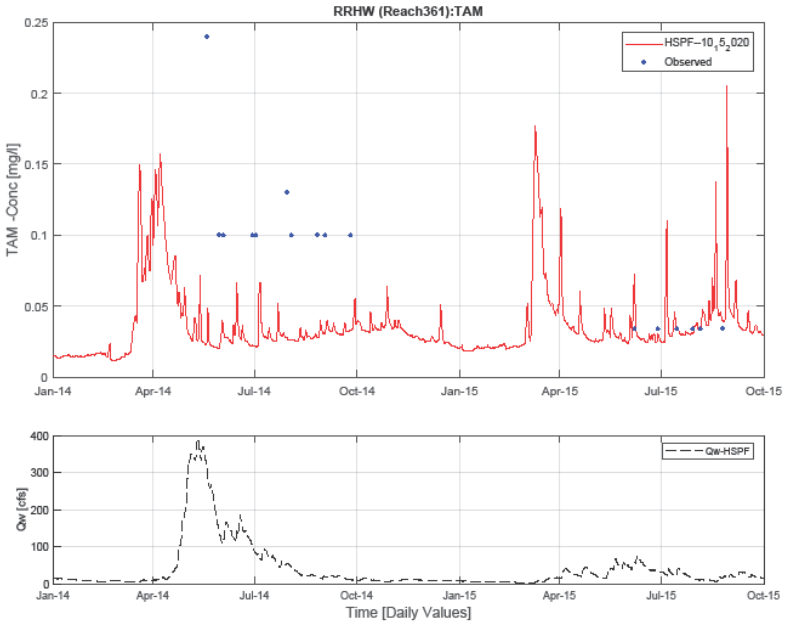
RRHW (Reach361):TAM
HSPF--10_1_5_020
Observed
TAM -Conc [mg/l]
Qw-HSPF
Qw [cfs]
Jan-14
Apr-14
Jul-14
Oct-14
Jan-15
Apr-15
Jul-15
Oct-15
Time [Daily Values]

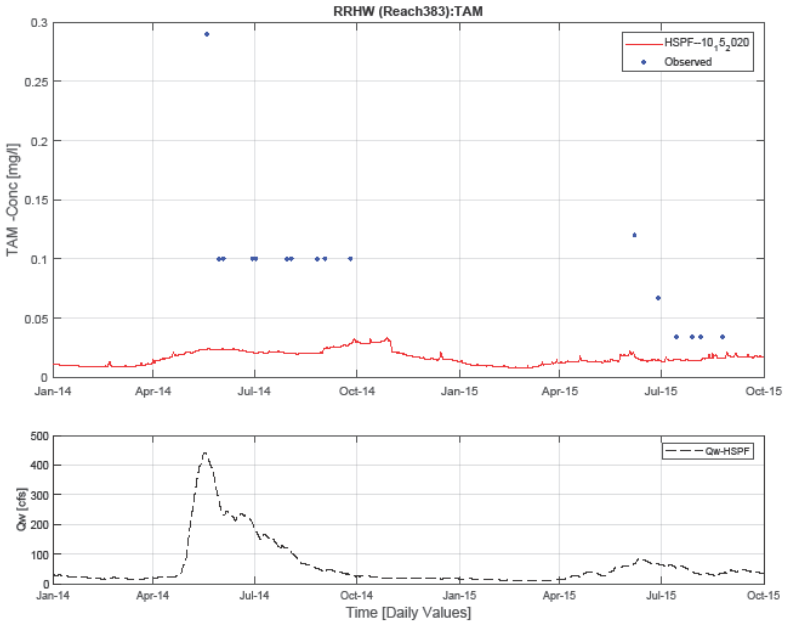
RRHW (Reach383):TAM
HSPF--10_1_5_020
Observed
TAM -Conc [mg/l]
Qw-HSPF
Qw [cfs]
Jan-14
Apr-14
Jul-14
Oct-14
Jan-15
Apr-15
Jul-15
Oct-15
Time [Daily Values]

6.2.1.6 Chl-*a*

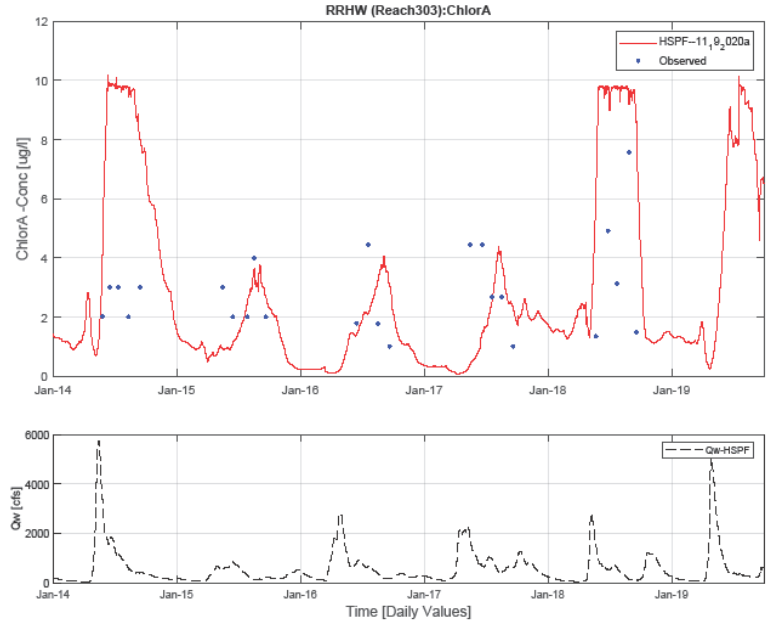
RRHW (Reach303):ChlorA
HSPF--11_1_9_020a
Observed
ChlorA -Conc [ug/l]
Qw-HSPF
Qw [cfs]
Jan-14
Jan-15
Jan-16
Jan-17
Jan-18
Jan-19
Time [Daily Values]

6.2.2 Vermilion River model

6.2.2.1 TSS

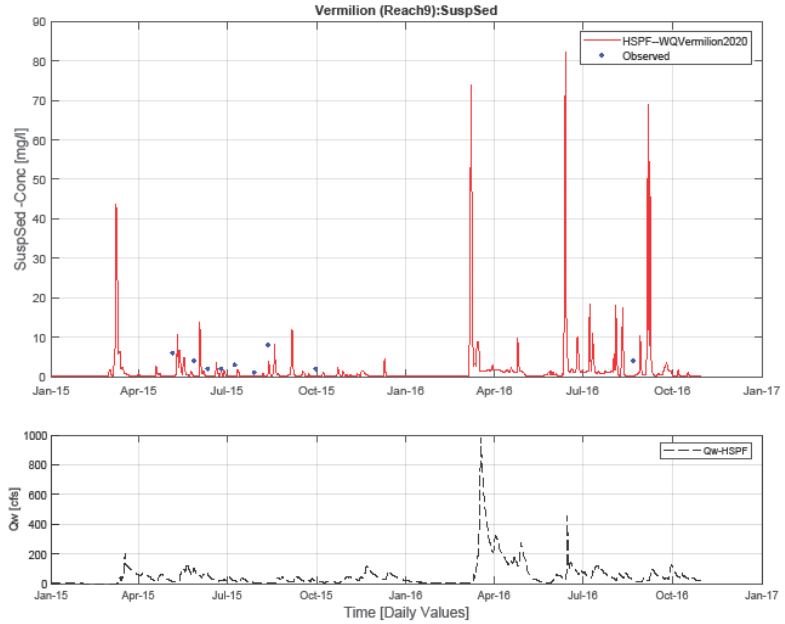

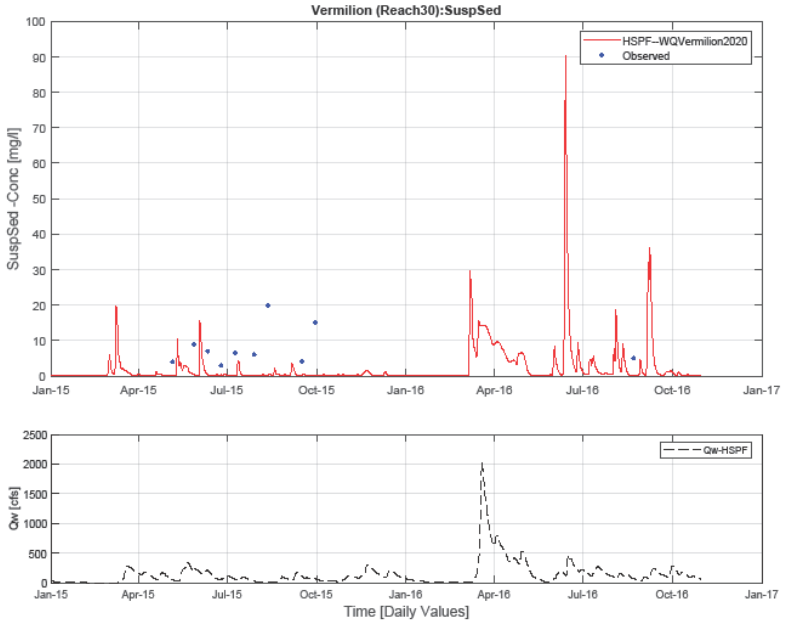

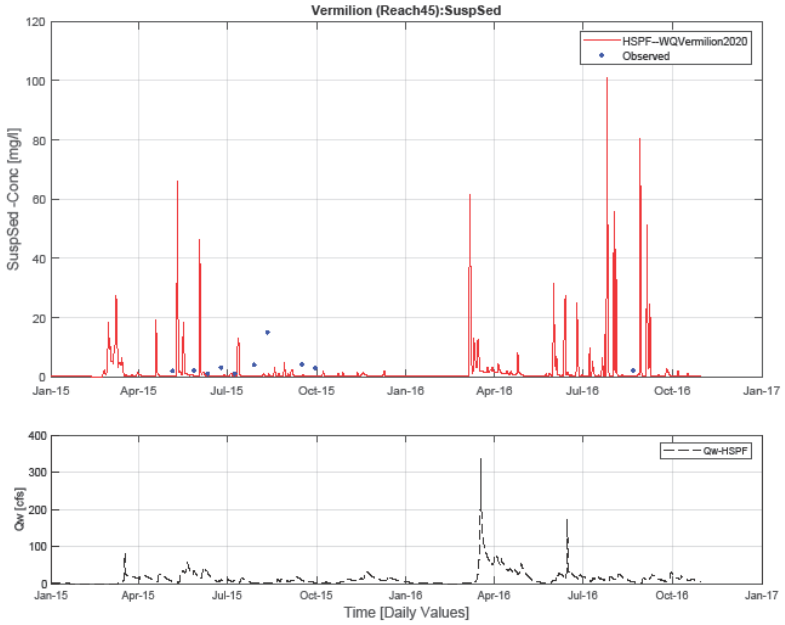
Vermilion (Reach45):SuspSed
HSPF--WQVermilion2020
Observed
SuspSed -Conc [mg/l]
Qw-HSPF
Qw [cfs]
Jan-15
Apr-15
Jul-15
Oct-15
Jan-16
Apr-16
Jul-16
Oct-16
Jan-17
Time [Daily Values]

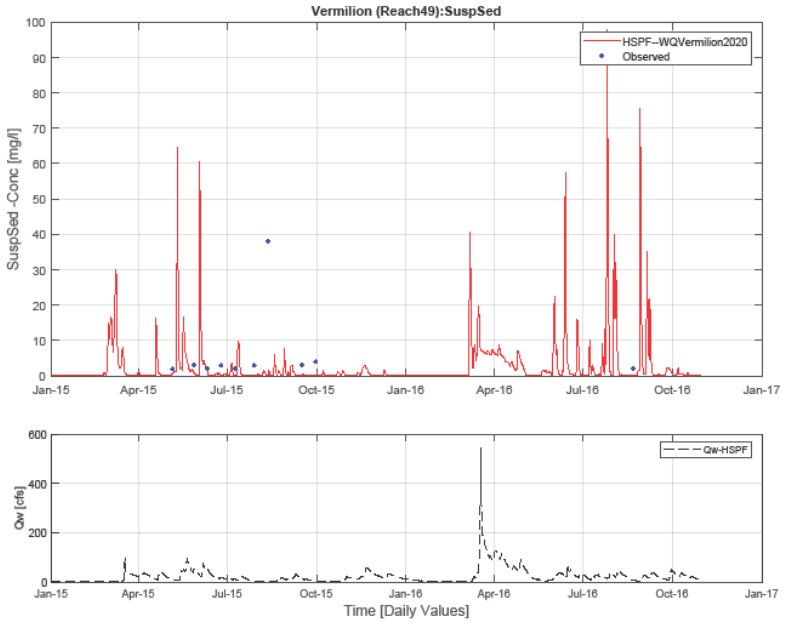
Vermilion (Reach49):SuspSed
HSPF--WQVermilion2020
Observed
SuspSed -Conc [mg/l]
Qw-HSPF
Qw [cfs]
Jan-15
Apr-15
Jul-15
Oct-15
Jan-16
Apr-16
Jul-16
Oct-16
Jan-17
Time [Daily Values]

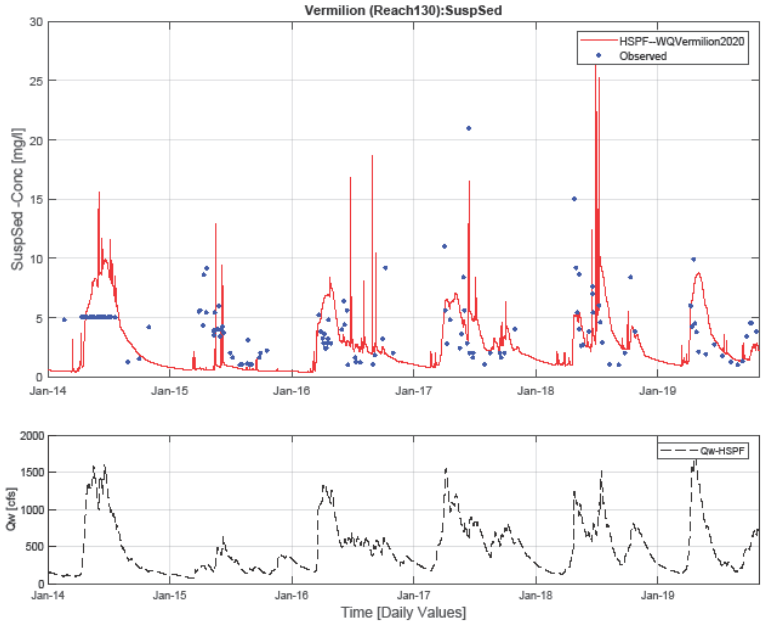
Vermilion (Reach130):SuspSed
HSPF--WQVermilion2020
Observed
SuspSed -Conc [mg/l]
Qw-HSPF
Qw [cfs]
Time [Daily Values]

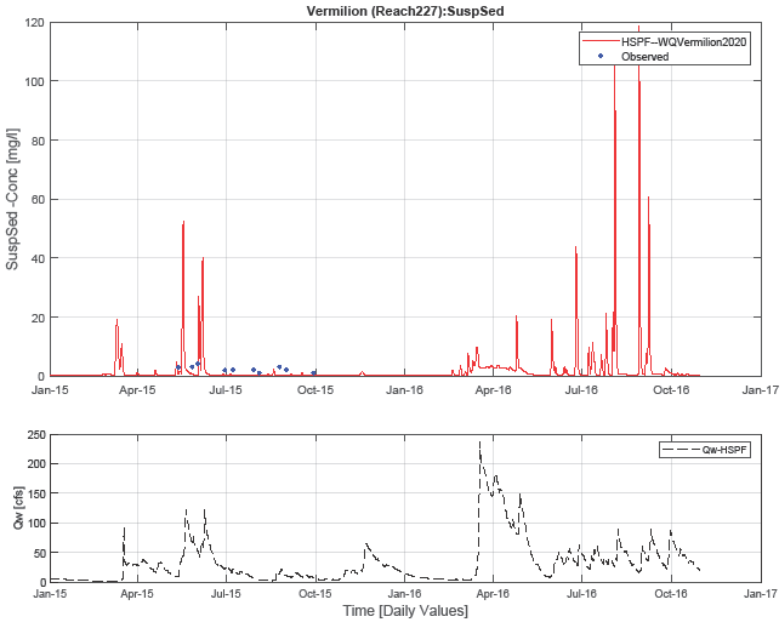
Vermilion (Reach227):SuspSed
HSPF--WQVermilion2020
Observed
SuspSed -Conc [mg/l]
Qw-HSPF
Qw [cfs]
Time [Daily Values]

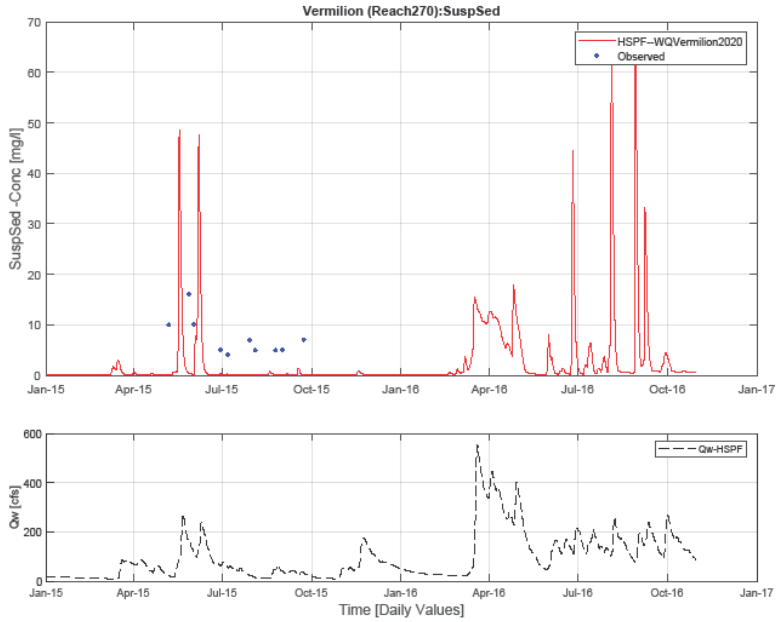
Vermilion (Reach270):SuspSed
HSPF--WQVermilion2020
Observed
SuspSed -Conc [mg/l]
Qw-HSPF
Qw [cfs]
Jan-15
Apr-15
Jul-15
Oct-15
Jan-16
Apr-16
Jul-16
Oct-16
Jan-17
Time [Daily Values]

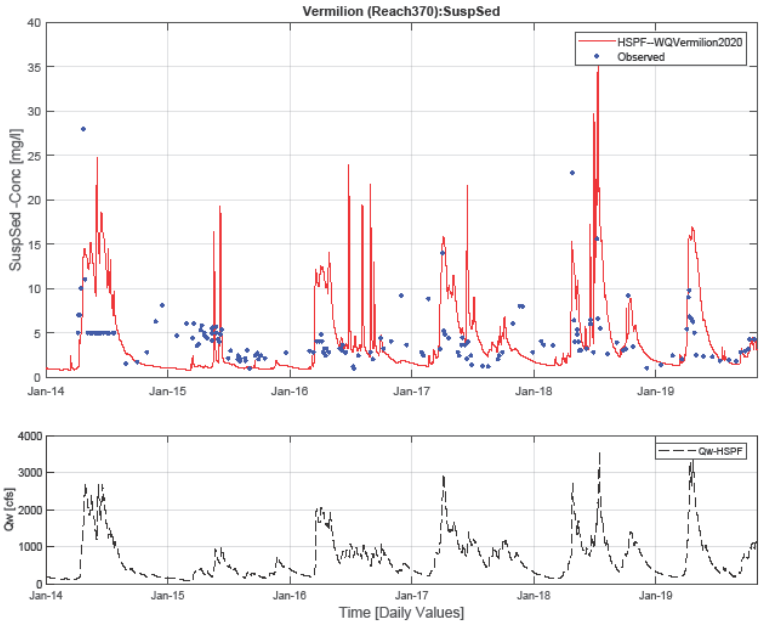
Vermilion (Reach370):SuspSed
HSPF--WQVermilion2020
Observed
SuspSed -Conc [mg/l]
Qw-HSPF
Qw [cfs]
Jan-14
Jan-15
Jan-16
Jan-17
Jan-18
Jan-19
Time [Daily Values]

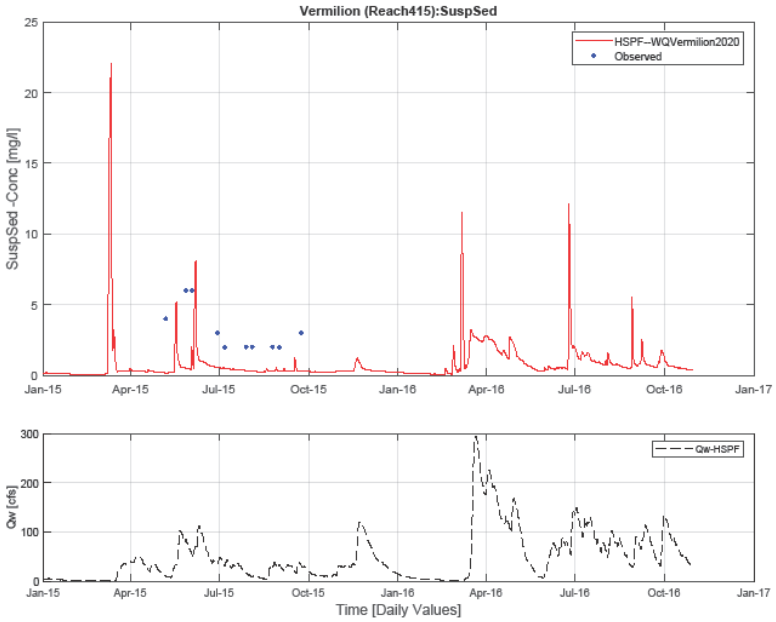
Vermilion (Reach415):SuspSed
HSPF--WQVermilion2020
Observed
SuspSed -Conc [mg/l]
25
20
15
10
5
0
Jan-15
Apr-15
Jul-15
Oct-15
Jan-16
Apr-16
Jul-16
Oct-16
Jan-17
Qw-HSPF
Qw [cfs]
300
200
100
0
Time [Daily Values]

6.2.2.2 PO_4

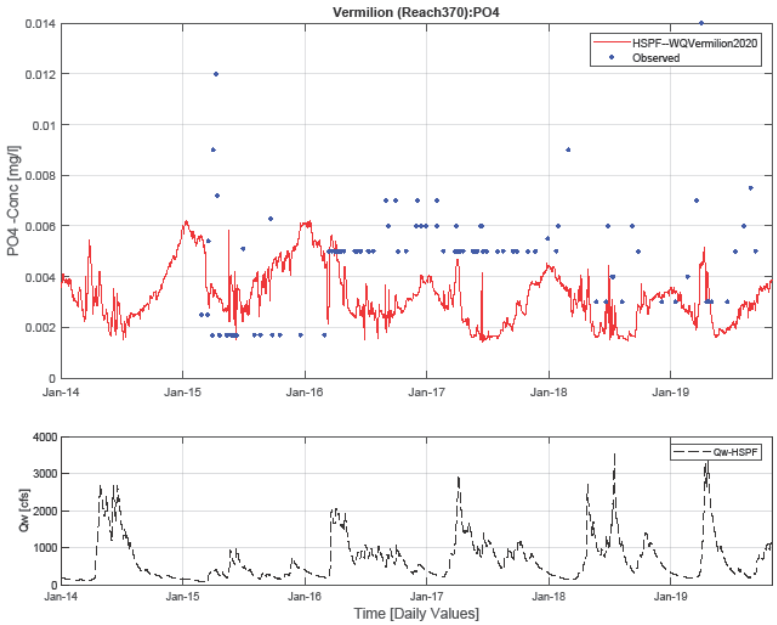
Vermilion (Reach370):PO4
HSPF--WQVermilion2020
Observed
PO4 -Conc [mg/l]
Qw-HSPF
Qw [cfs]
Jan-14
Jan-15
Jan-16
Jan-17
Jan-18
Jan-19
Time [Daily Values]

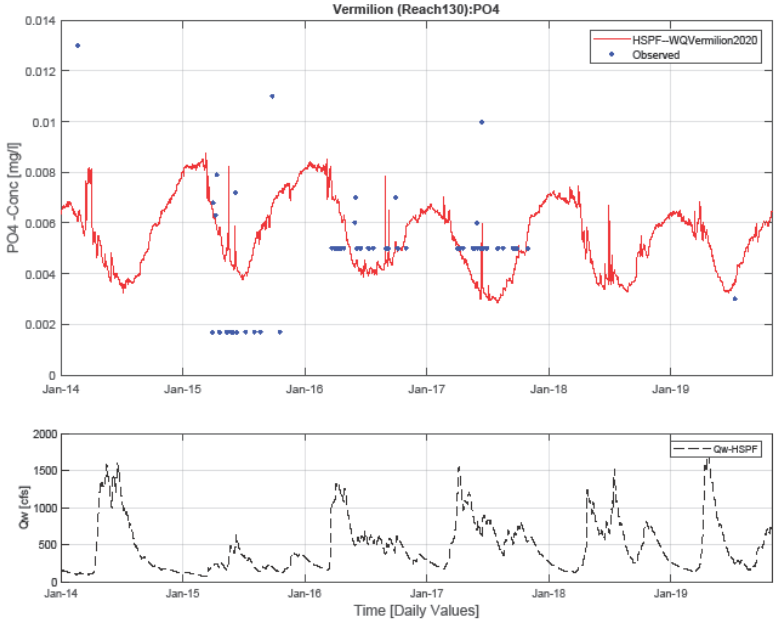
Vermilion (Reach130):PO4
HSPF--WQVermilion2020
Observed
PO4 -Conc [mg/l]
Qw-HSPF
Qw [cfs]
Jan-14
Jan-15
Jan-16
Jan-17
Jan-18
Jan-19
Time [Daily Values]

6.2.2.3 TP

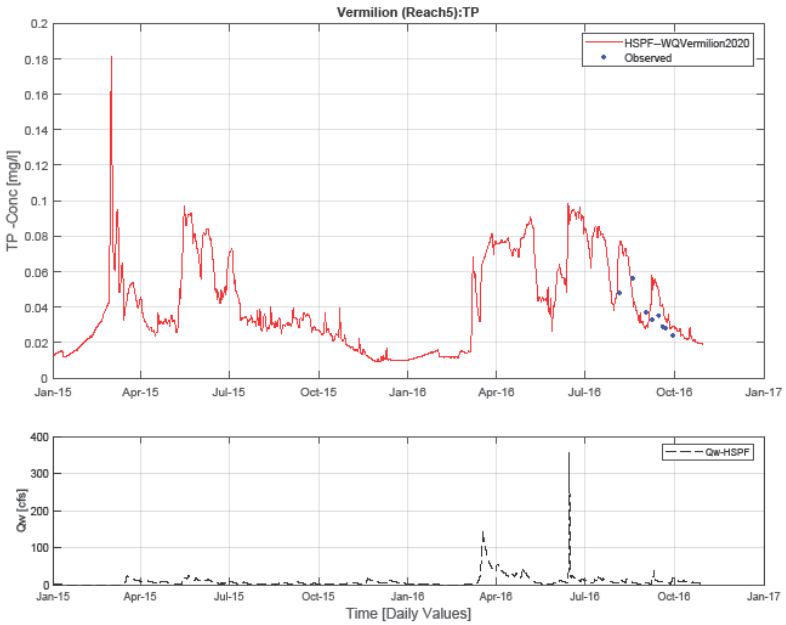
Vermilion (Reach5):TP
HSPF--WQVermilion2020
Observed
TP -Conc [mg/l]
Qw-HSPF
Qw [cfs]
Time [Daily Values]
Jan-15
Apr-15
Jul-15
Oct-15
Jan-16
Apr-16
Jul-16
Oct-16
Jan-17

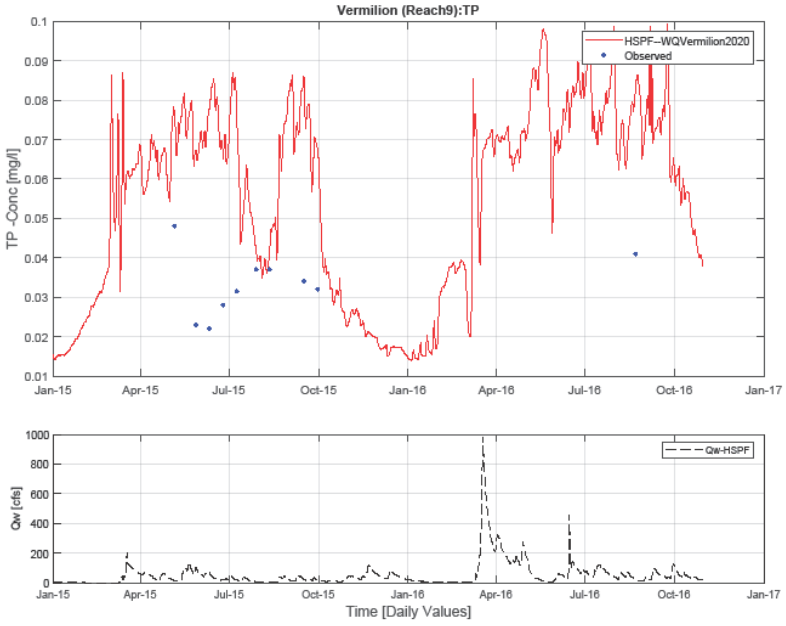
Vermilion (Reach9):TP
HSPF--WQVermilion2020
Observed
TP -Conc [mg/l]
Qw-HSPF
Qw [cfs]
Time [Daily Values]
Jan-15
Apr-15
Jul-15
Oct-15
Jan-16
Apr-16
Jul-16
Oct-16
Jan-17

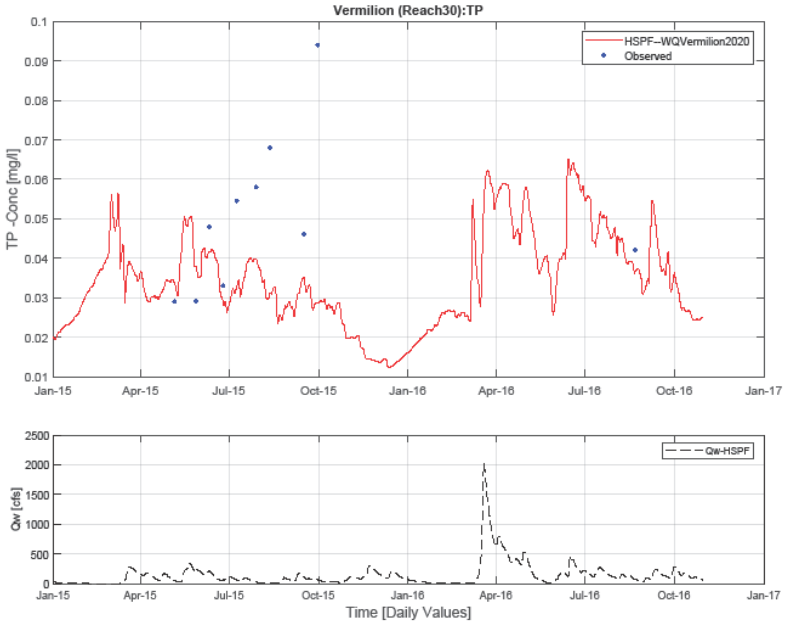
Vermilion (Reach30):TP
HSPF--WQVermilion2020
Observed
TP -Conc [mg/l]
Qw-HSPF
Qw [cfs]
Jan-15
Apr-15
Jul-15
Oct-15
Jan-16
Apr-16
Jul-16
Oct-16
Jan-17
Time [Daily Values]

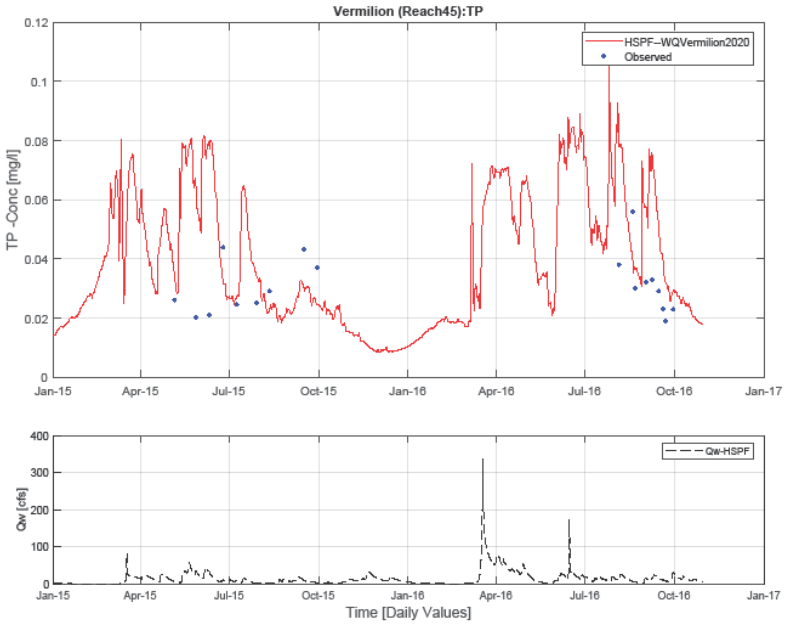
Vermilion (Reach45):TP
HSPF--WQVermilion2020
Observed
TP -Conc [mg/l]
Qw-HSPF
Qw [cfs]
Jan-15
Apr-15
Jul-15
Oct-15
Jan-16
Apr-16
Jul-16
Oct-16
Jan-17
Time [Daily Values]

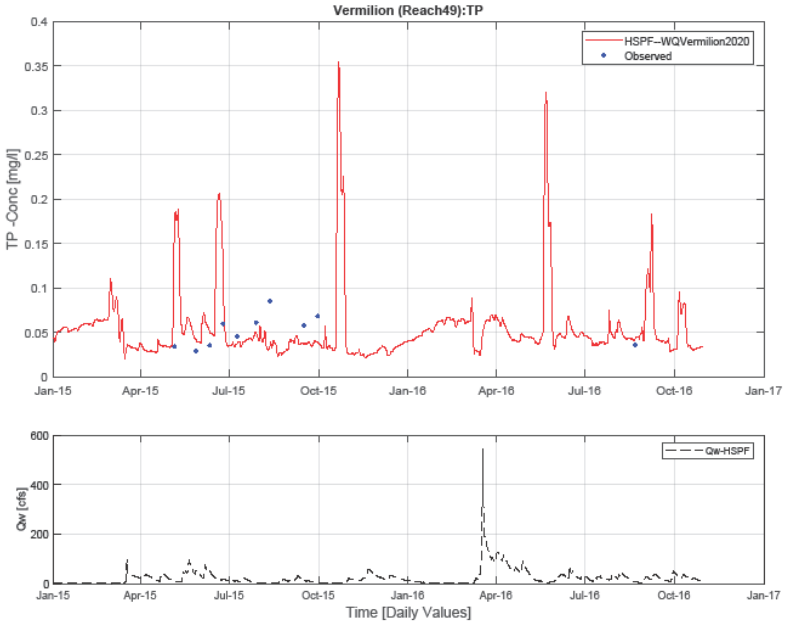
Vermilion (Reach49):TP
HSPF--WQVermilion2020
Observed
TP -Conc [mg/l]
Qw-HSPF
Qw [cfs]
Jan-15
Apr-15
Jul-15
Oct-15
Jan-16
Apr-16
Jul-16
Oct-16
Jan-17
Time [Daily Values]

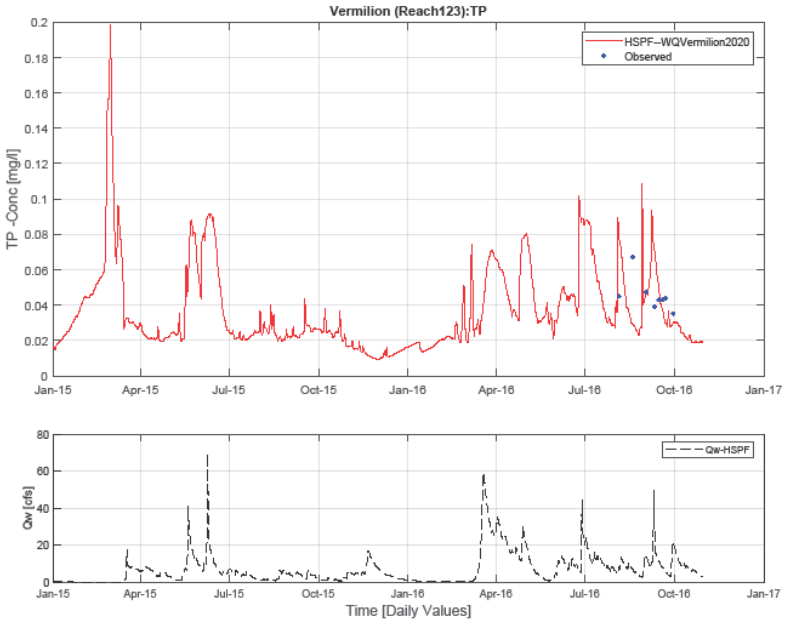
Vermilion (Reach123):TP
HSPF--WQVermilion2020
Observed
TP -Conc [mg/l]
Qw-HSPF
Qw [cfs]
Jan-15
Apr-15
Jul-15
Oct-15
Jan-16
Apr-16
Jul-16
Oct-16
Jan-17
Time [Daily Values]

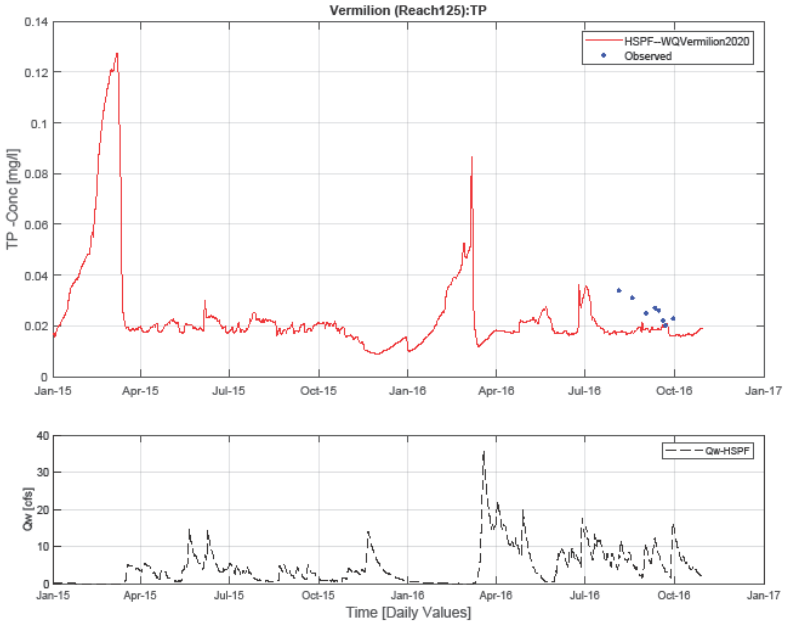
Vermilion (Reach125):TP
HSPF--WQVermilion2020
Observed
TP -Conc [mg/l]
Qw-HSPF
Qw [cfs]
Jan-15
Apr-15
Jul-15
Oct-15
Jan-16
Apr-16
Jul-16
Oct-16
Jan-17
Time [Daily Values]

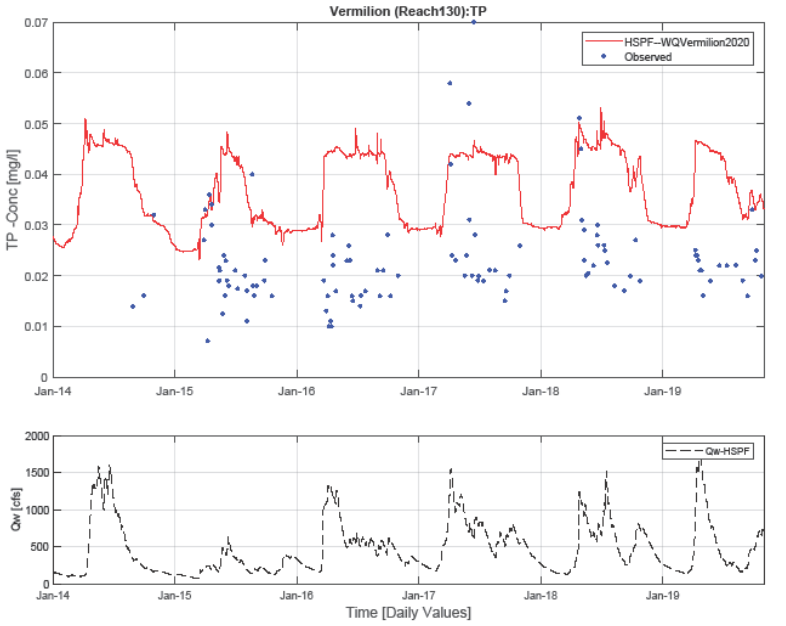
Vermilion (Reach130):TP
HSPF--WQVermilion2020
Observed
TP -Conc [mg/l]
Qw-HSPF
Qw [cfs]
Jan-14
Jan-15
Jan-16
Jan-17
Jan-18
Jan-19
Time [Daily Values]

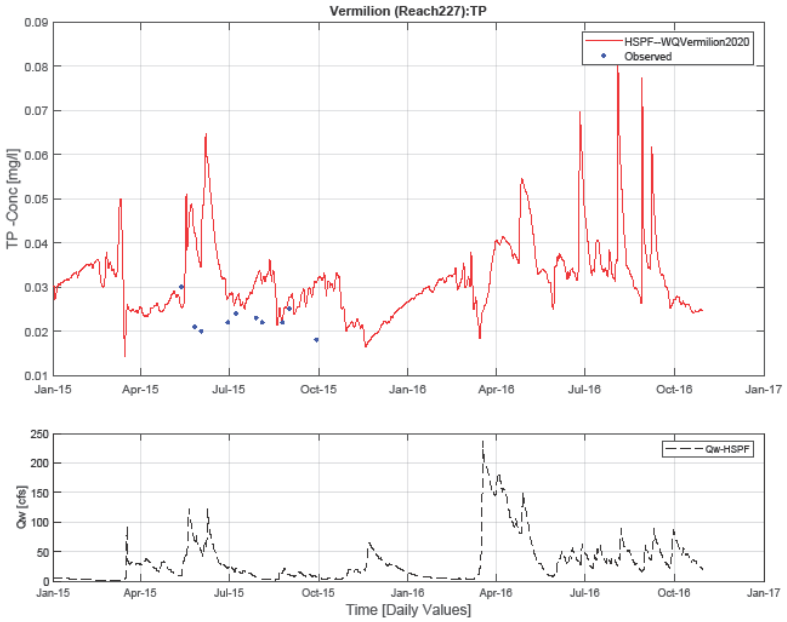
Vermilion (Reach227):TP
HSPF--WQVermilion2020
Observed
TP -Conc [mg/l]
Qw-HSPF
Qw [cfs]
Jan-15
Apr-15
Jul-15
Oct-15
Jan-16
Apr-16
Jul-16
Oct-16
Jan-17
Time [Daily Values]

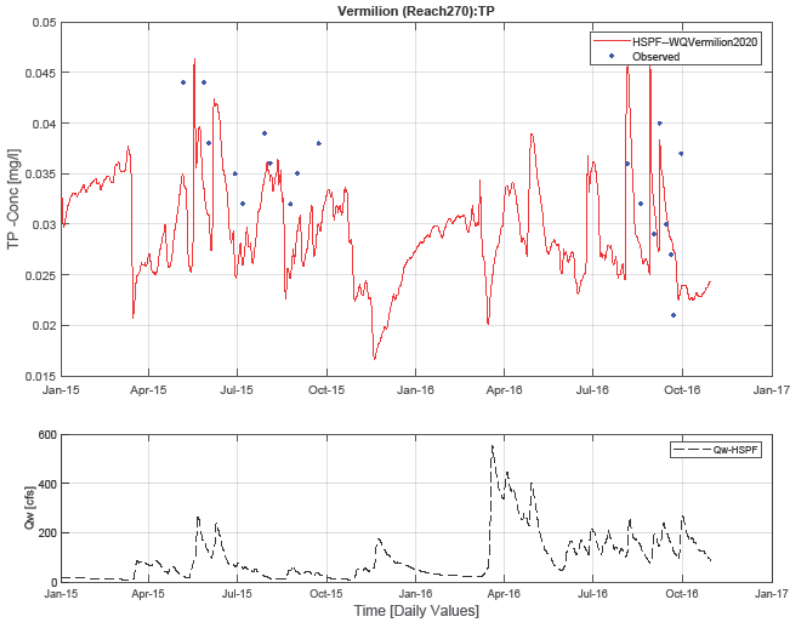
Vermilion (Reach270):TP
HSPF--WQVermilion2020
Observed
TP -Conc [mg/l]
Qw-HSPF
Qw [cfs]
Jan-15
Apr-15
Jul-15
Oct-15
Jan-16
Apr-16
Jul-16
Oct-16
Jan-17
Time [Daily Values]

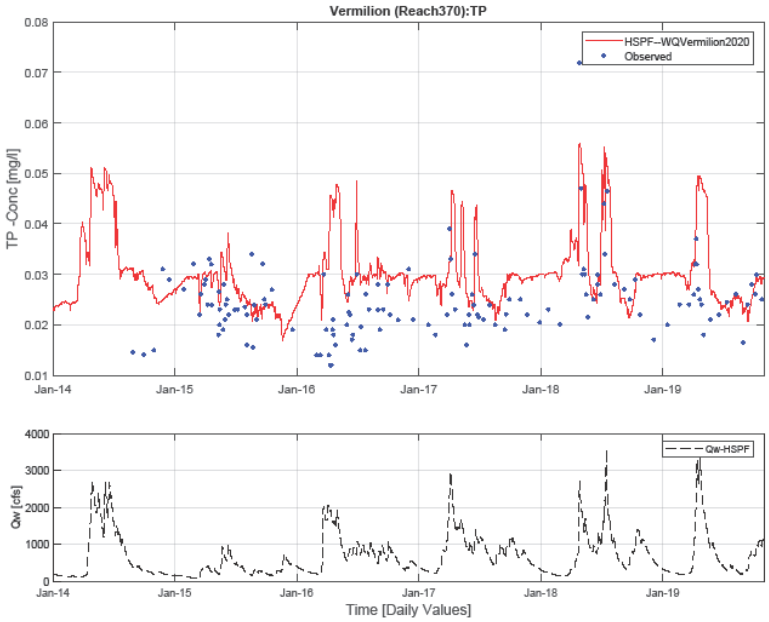
Vermilion (Reach370):TP
HSPF--WQVermilion2020
Observed
TP -Conc [mg/l]
0.08
0.07
0.06
0.05
0.04
0.03
0.02
0.01
Jan-14
Jan-15
Jan-16
Jan-17
Jan-18
Jan-19
Qw-HSPF
Qw [cfs]
4000
3000
2000
1000
0
Time [Daily Values]

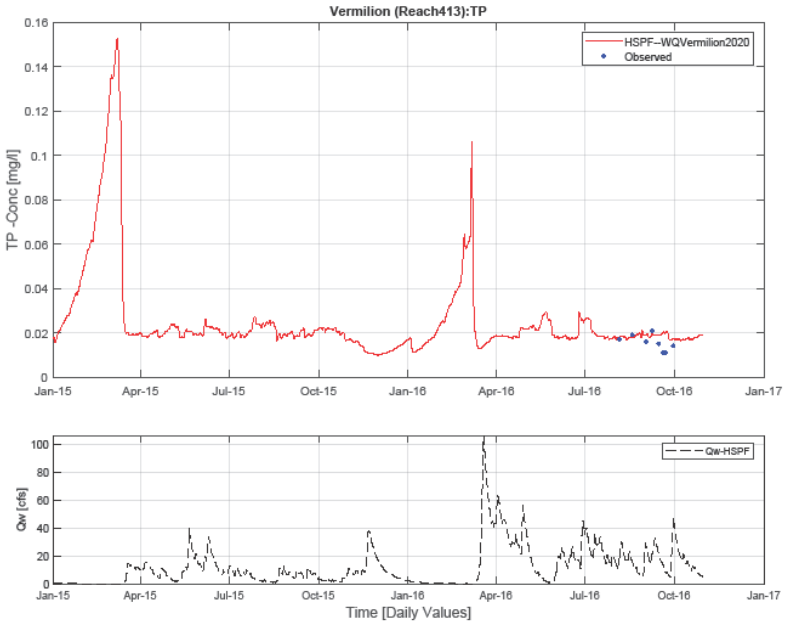
Vermilion (Reach413):TP
HSPF--WQVermilion2020
Observed
TP -Conc [mg/l]
0.16
0.14
0.12
0.1
0.08
0.06
0.04
0.02
0
Jan-15
Apr-15
Jul-15
Oct-15
Jan-16
Apr-16
Jul-16
Oct-16
Jan-17
Qw-HSPF
Qw [cfs]
100
80
60
40
20
0
Time [Daily Values]

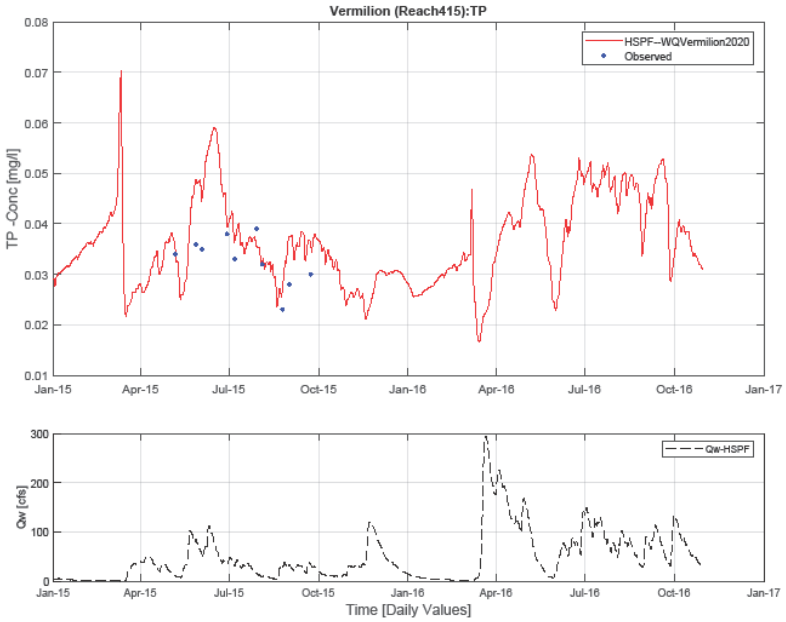
Vermilion (Reach415):TP
HSPF--WQVermilion2020
Observed
TP -Conc [mg/l]
0.08
0.07
0.06
0.05
0.04
0.03
0.02
0.01
Jan-15
Apr-15
Jul-15
Oct-15
Jan-16
Apr-16
Jul-16
Oct-16
Jan-17
Qw-HSPF
Qw [cfs]
300
200
100
0
Time [Daily Values]

6.2.2.4 TAM

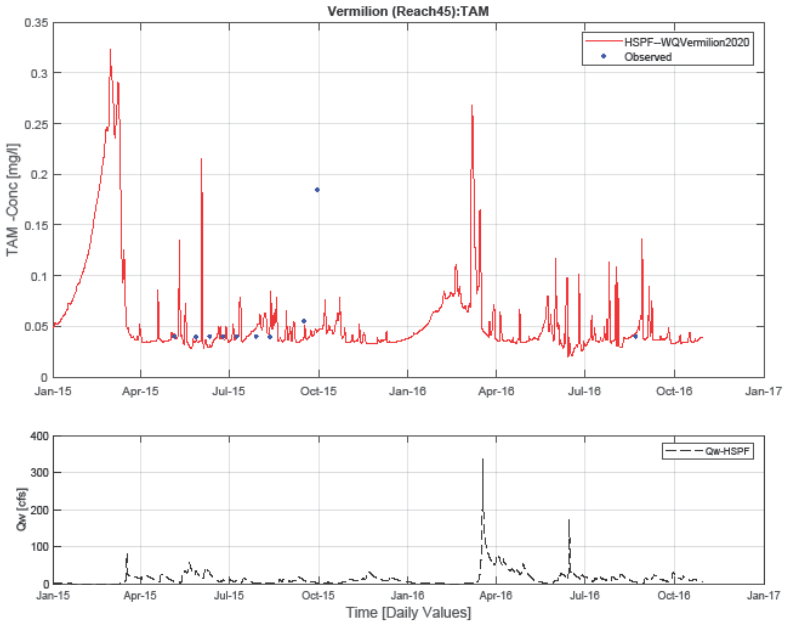
Vermilion (Reach45):TAM
HSPF--WQVermilion2020
Observed
TAM -Conc [mg/l]
0.35
0.3
0.25
0.2
0.15
0.1
0.05
0
Jan-15
Apr-15
Jul-15
Oct-15
Jan-16
Apr-16
Jul-16
Oct-16
Jan-17
Qw-HSPF
Qw [cfs]
400
300
200
100
0
Time [Daily Values]

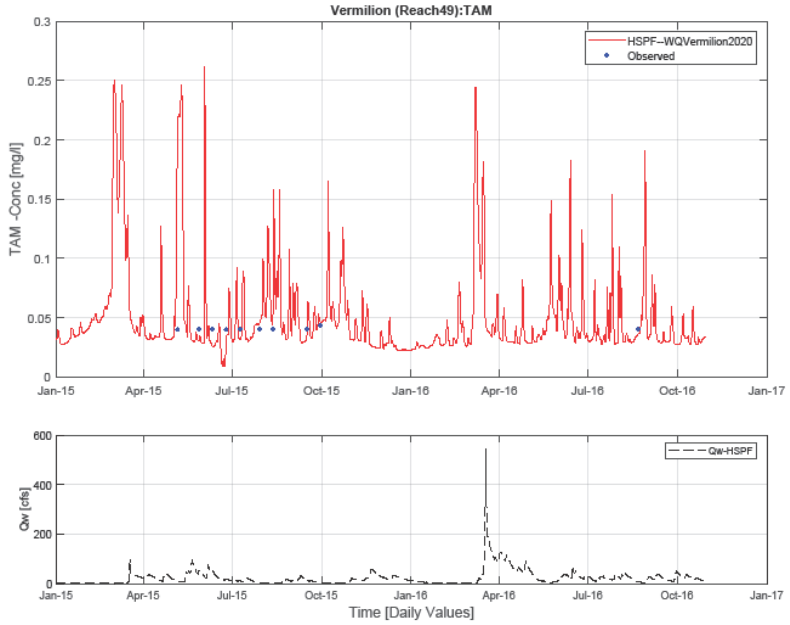
Vermilion (Reach49):TAM
HSPF--WQVermilion2020
Observed
TAM -Conc [mg/l]
Qw-HSPF
Qw [cfs]
Time [Daily Values]
Jan-15
Apr-15
Jul-15
Oct-15
Jan-16
Apr-16
Jul-16
Oct-16
Jan-17

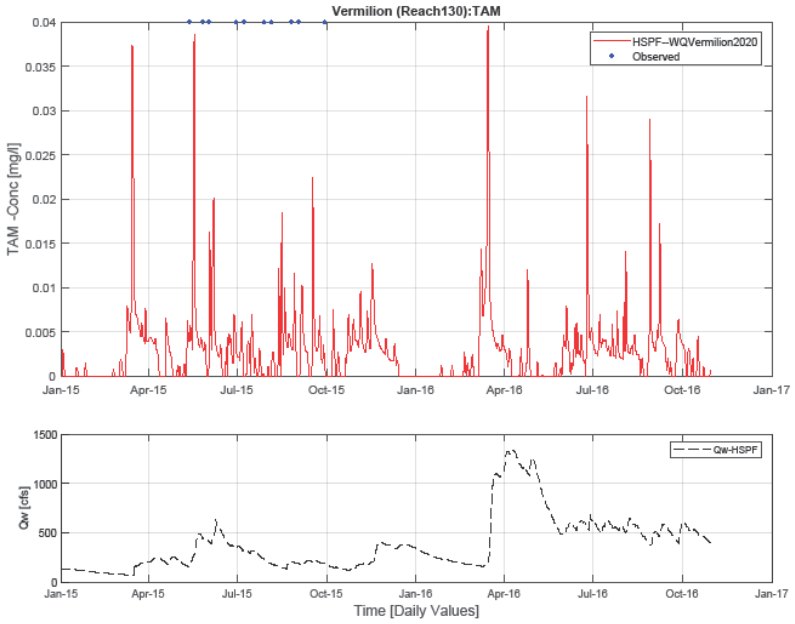
Vermilion (Reach130):TAM
HSPF--WQVermilion2020
Observed
TAM -Conc [mg/l]
Qw-HSPF
Qw [cfs]
Time [Daily Values]
Jan-15
Apr-15
Jul-15
Oct-15
Jan-16
Apr-16
Jul-16
Oct-16
Jan-17

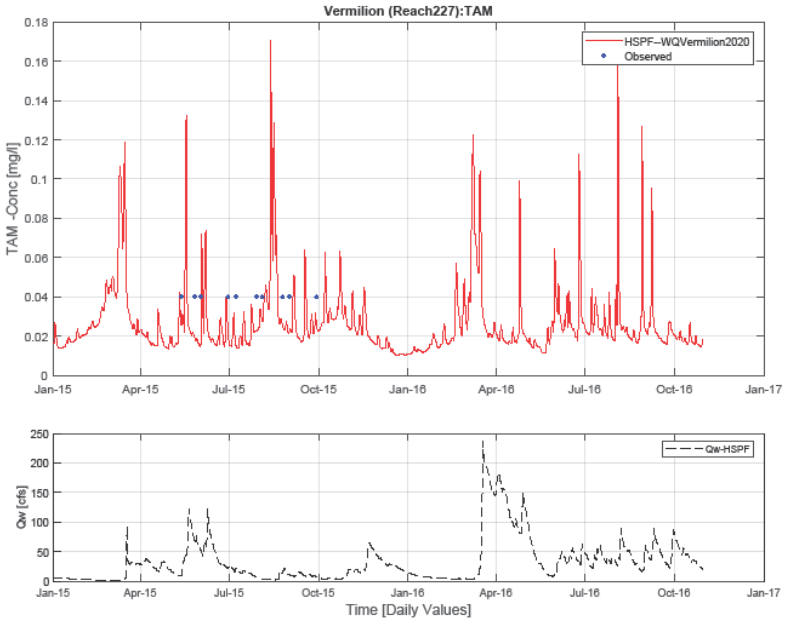
Vermilion (Reach227):TAM
HSPF--WQVermilion2020
Observed
TAM -Conc [mg/l]
Qw-HSPF
Qw [cfs]
Jan-15
Apr-15
Jul-15
Oct-15
Jan-16
Apr-16
Jul-16
Oct-16
Jan-17
Time [Daily Values]

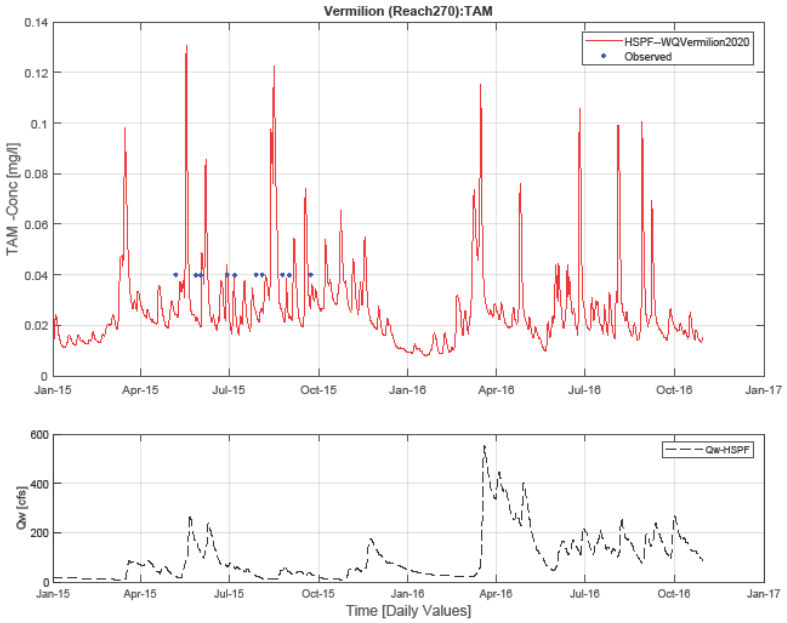
Vermilion (Reach270):TAM
HSPF--WQVermilion2020
Observed
TAM -Conc [mg/l]
Qw-HSPF
Qw [cfs]
Jan-15
Apr-15
Jul-15
Oct-15
Jan-16
Apr-16
Jul-16
Oct-16
Jan-17
Time [Daily Values]

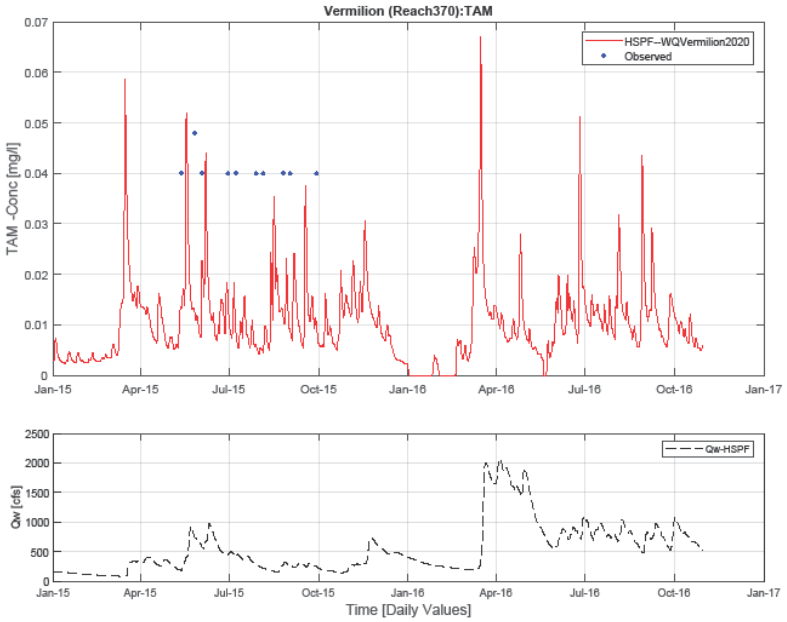
Vermilion (Reach370):TAM
HSPF--WQVermilion2020
Observed
TAM -Conc [mg/l]
0.07
0.06
0.05
0.04
0.03
0.02
0.01
0
Jan-15
Apr-15
Jul-15
Oct-15
Jan-16
Apr-16
Jul-16
Oct-16
Jan-17
Qw-HSPF
Qw [cfs]
2500
2000
1500
1000
500
0
Time [Daily Values]

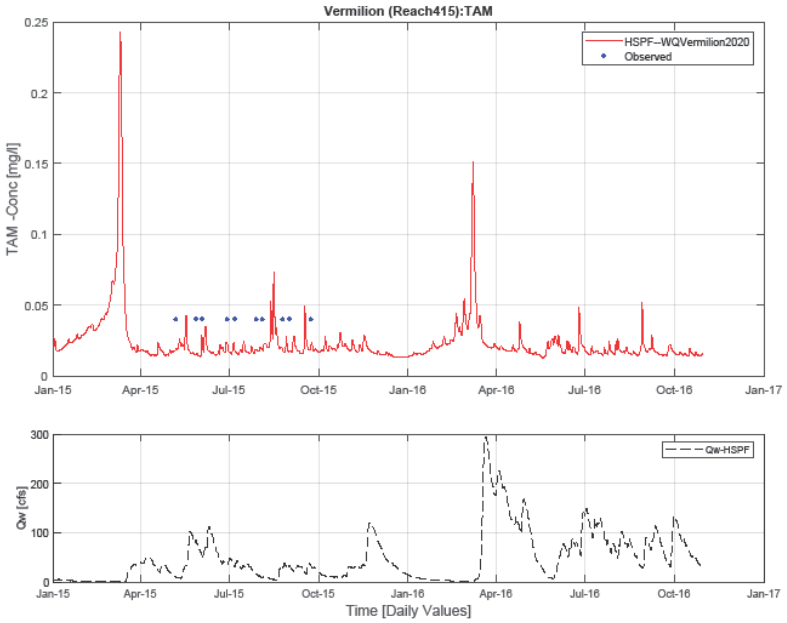
Vermilion (Reach415):TAM
HSPF--WQVermilion2020
Observed
TAM -Conc [mg/l]
0.25
0.2
0.15
0.1
0.05
0
Jan-15
Apr-15
Jul-15
Oct-15
Jan-16
Apr-16
Jul-16
Oct-16
Jan-17
Qw-HSPF
Qw [cfs]
300
200
100
0
Time [Daily Values]

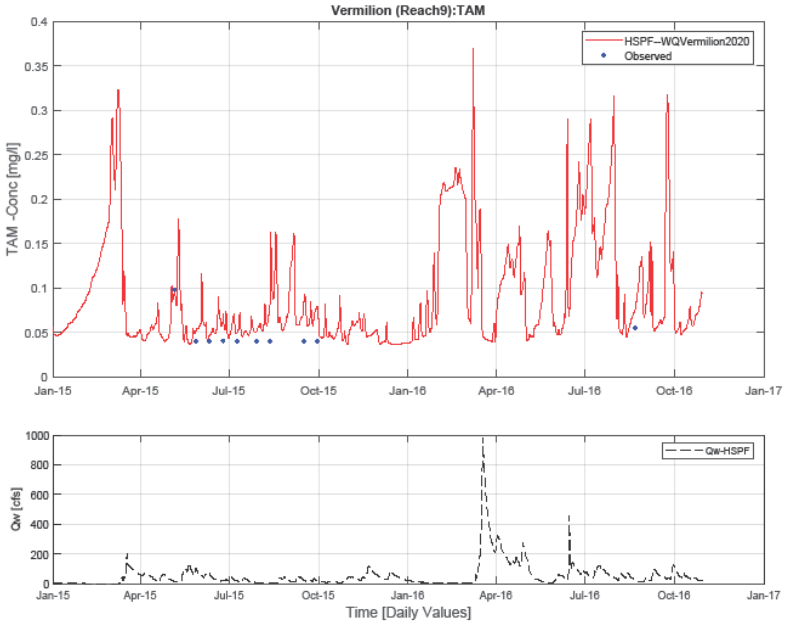
Vermilion (Reach9):TAM
HSPF--WQVermilion2020
Observed
TAM -Conc [mg/l]
Qw-HSPF
Qw [cfs]
Jan-15
Apr-15
Jul-15
Oct-15
Jan-16
Apr-16
Jul-16
Oct-16
Jan-17
Time [Daily Values]

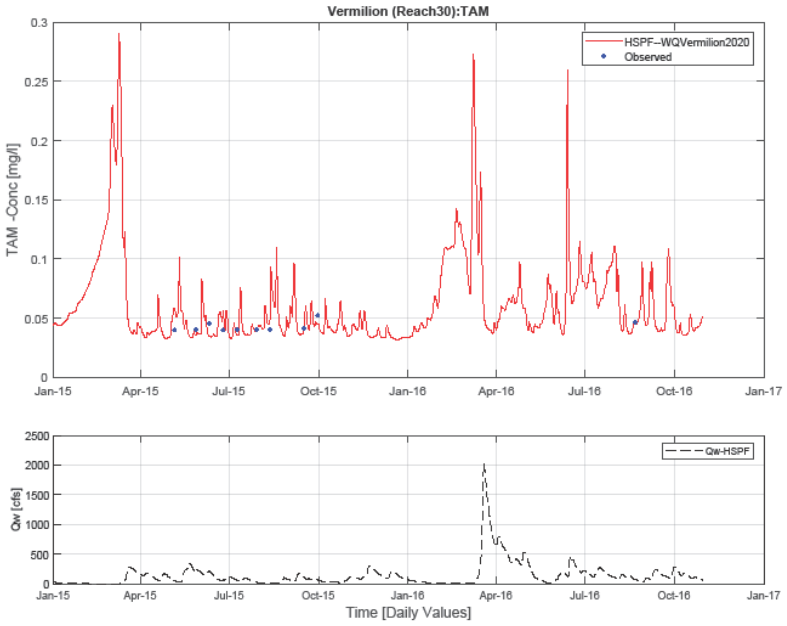
Vermilion (Reach30):TAM
HSPF--WQVermilion2020
Observed
TAM -Conc [mg/l]
Qw-HSPF
Qw [cfs]
Jan-15
Apr-15
Jul-15
Oct-15
Jan-16
Apr-16
Jul-16
Oct-16
Jan-17
Time [Daily Values]

6.2.2.5 $NO_2 + NO_3$

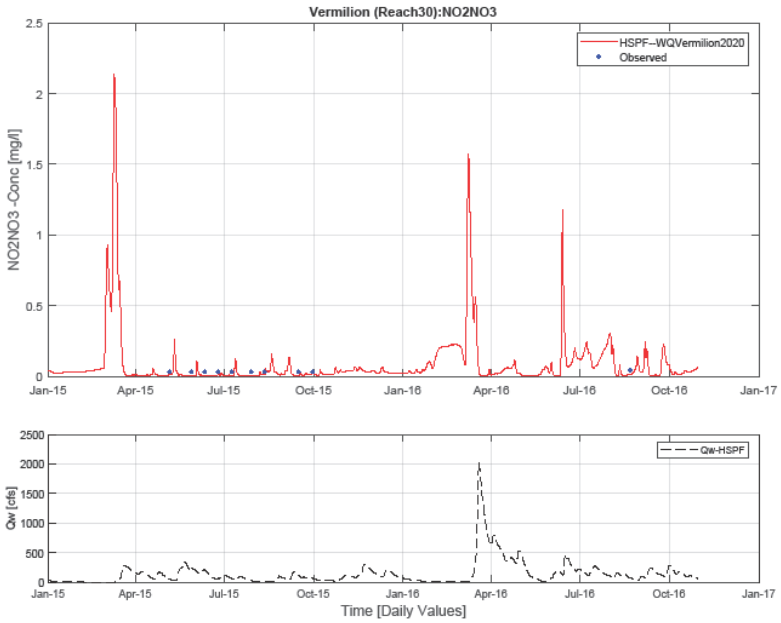
Vermilion (Reach30):NO2NO3
HSPF--WQVermilion2020
Observed
NO2NO3 -Conc [mg/l]
Qw-HSPF
Qw [cfs]
Jan-15
Apr-15
Jul-15
Oct-15
Jan-16
Apr-16
Jul-16
Oct-16
Jan-17
Time [Daily Values]

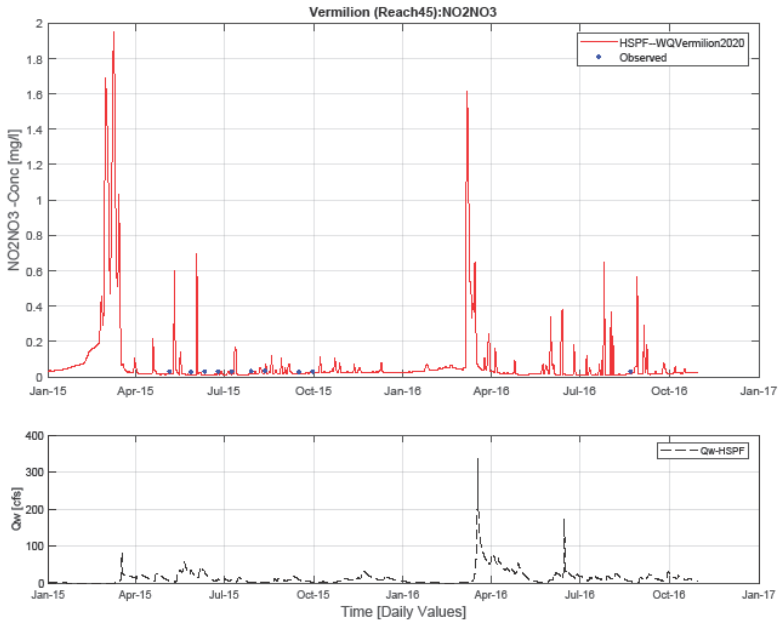
Vermilion (Reach45):NO2NO3
HSPF--WQVermilion2020
Observed
NO2NO3 -Conc [mg/l]
Qw-HSPF
Qw [cfs]
Jan-15
Apr-15
Jul-15
Oct-15
Jan-16
Apr-16
Jul-16
Oct-16
Jan-17
Time [Daily Values]

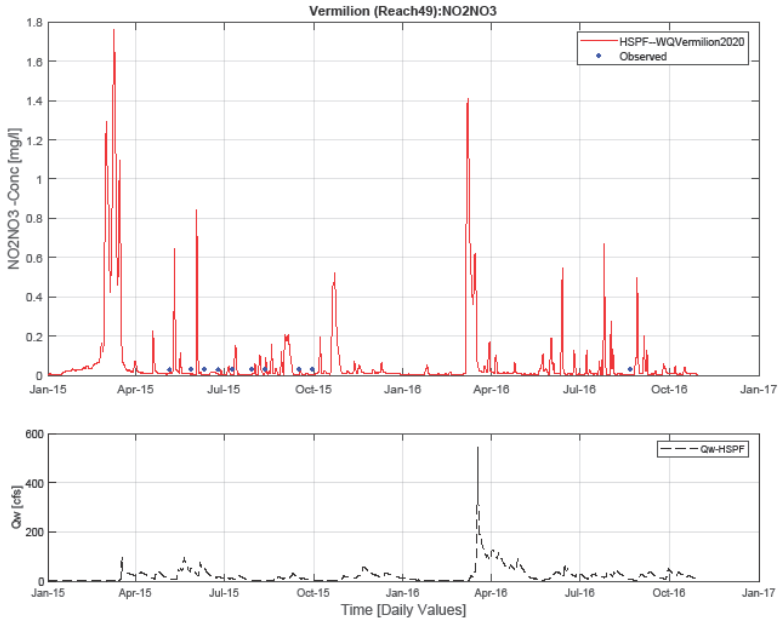
Vermilion (Reach49):NO2NO3
HSPF--WQVermilion2020
Observed
NO2NO3 -Conc [mg/l]
Qw-HSPF
Qw [cfs]
Jan-15
Apr-15
Jul-15
Oct-15
Jan-16
Apr-16
Jul-16
Oct-16
Jan-17
Time [Daily Values]

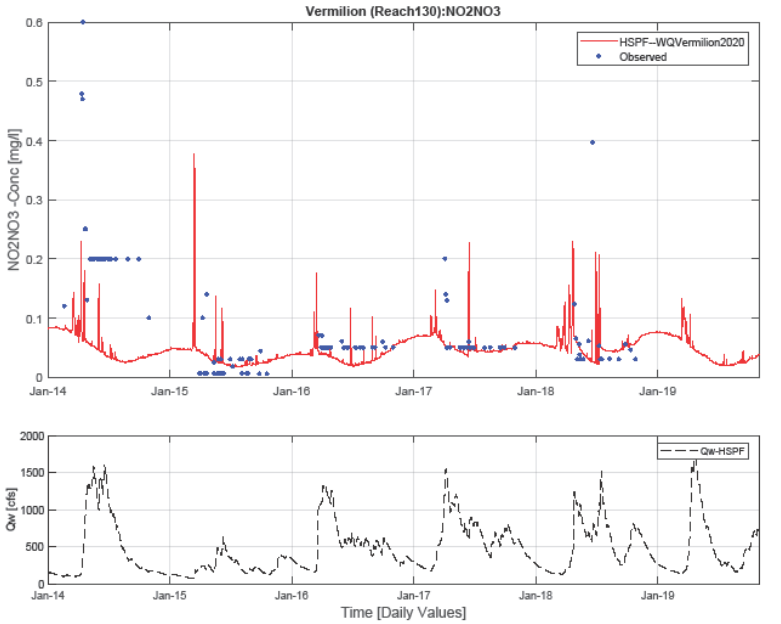
Vermilion (Reach130):NO2NO3
HSPF--WQVermilion2020
Observed
NO2NO3 -Conc [mg/l]
Qw-HSPF
Qw [cfs]
Jan-14
Jan-15
Jan-16
Jan-17
Jan-18
Jan-19
Time [Daily Values]

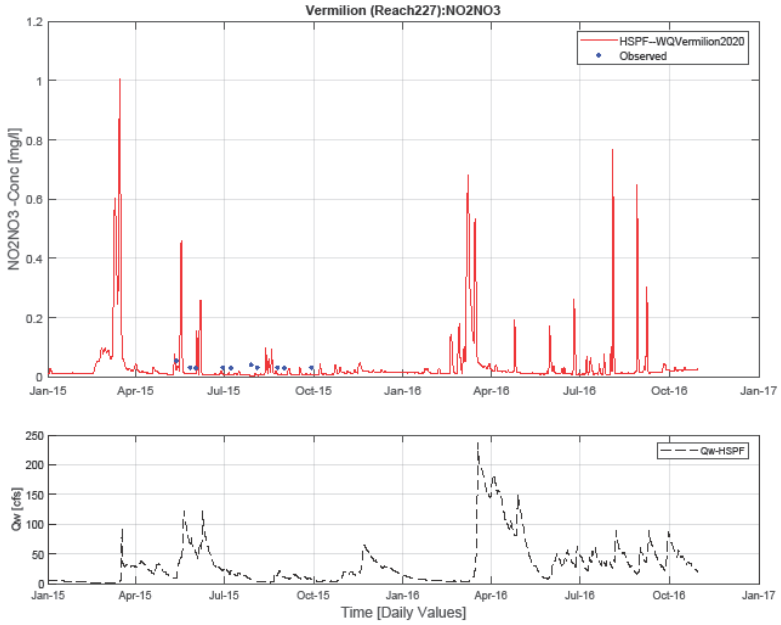
Vermilion (Reach227):NO2NO3
HSPF--WQVermilion2020
Observed
NO2NO3 -Conc [mg/l]
Qw-HSPF
Qw [cfs]
Jan-15
Apr-15
Jul-15
Oct-15
Jan-16
Apr-16
Jul-16
Oct-16
Jan-17
Time [Daily Values]

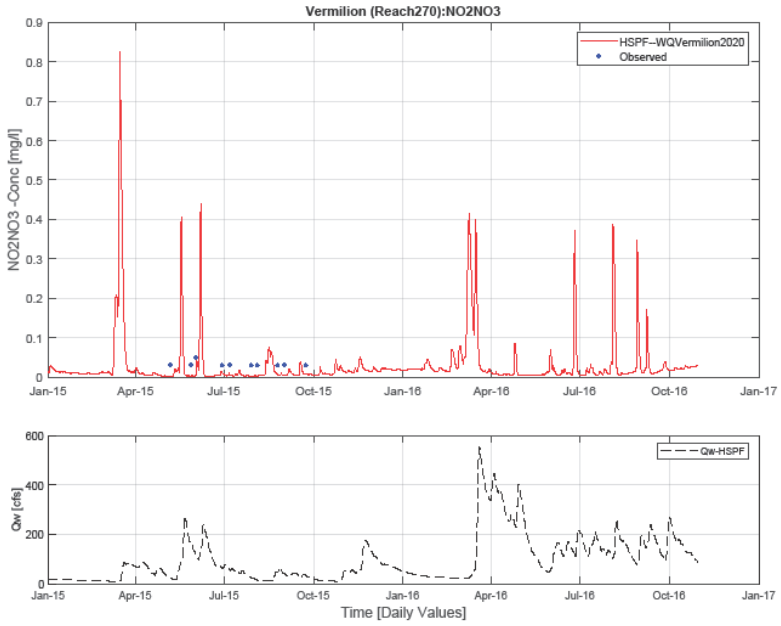
Vermilion (Reach270):NO2NO3
HSPF--WQVermilion2020
Observed
NO2NO3 -Conc [mg/l]
Qw-HSPF
Qw [cfs]
Jan-15
Apr-15
Jul-15
Oct-15
Jan-16
Apr-16
Jul-16
Oct-16
Jan-17
Time [Daily Values]

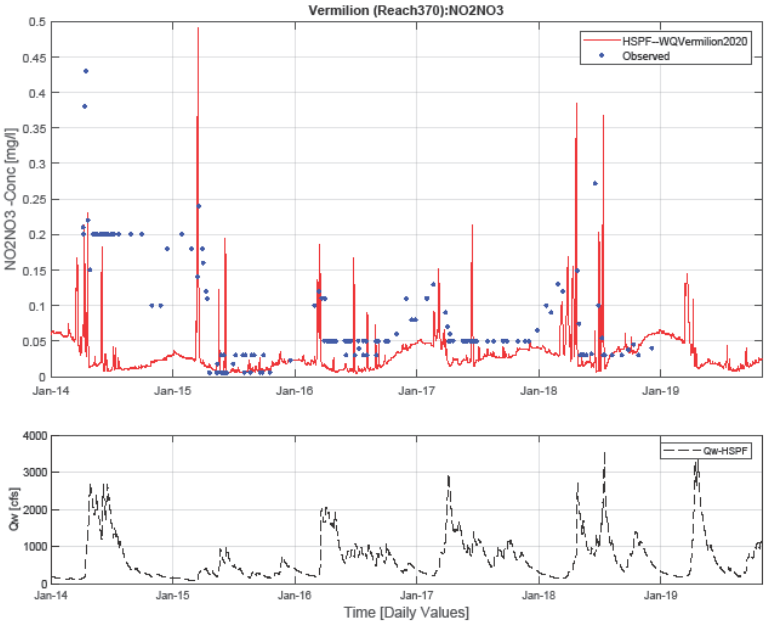
Vermilion (Reach370):NO2NO3
HSPF--WQVermilion2020
Observed
NO2NO3 -Conc [mg/l]
Qw-HSPF
Qw [cfs]
Jan-14
Jan-15
Jan-16
Jan-17
Jan-18
Jan-19
Time [Daily Values]

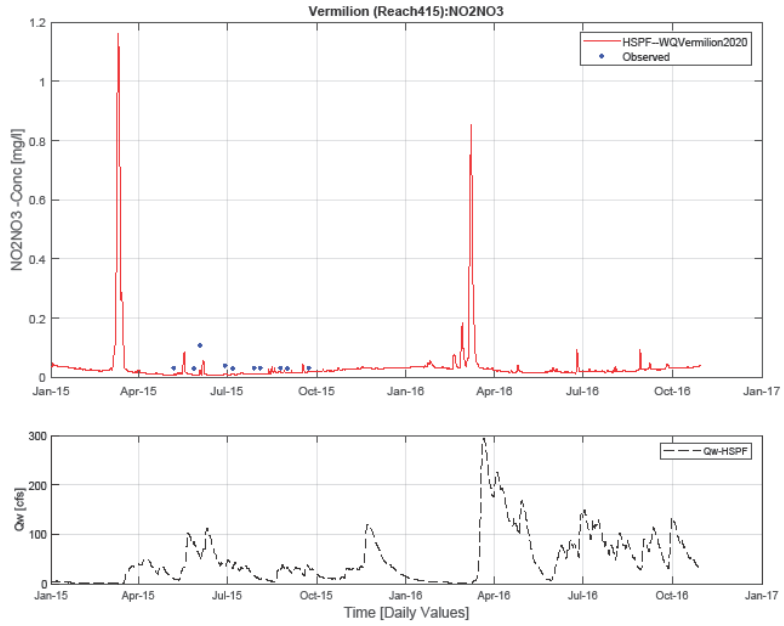
Vermilion (Reach415):NO2NO3
HSPF--WQVermilion2020
Observed
NO2NO3 -Conc [mg/l]
Qw-HSPF
Qw [cfs]
Jan-15
Apr-15
Jul-15
Oct-15
Jan-16
Apr-16
Jul-16
Oct-16
Jan-17
Time [Daily Values]

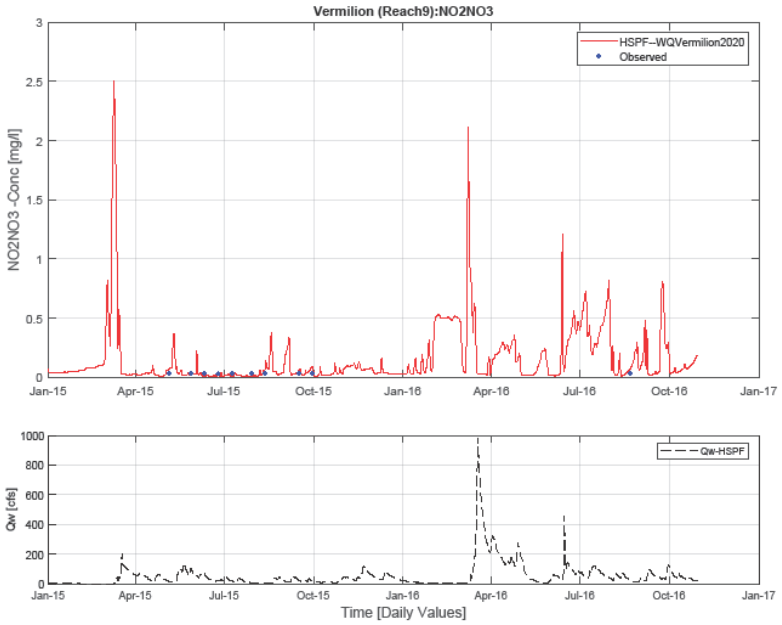
Vermilion (Reach9):NO2NO3
HSPF--WQVermilion2020
Observed
NO2NO3 -Conc [mg/l]
Qw-HSPF
Qw [cfs]
Jan-15
Apr-15
Jul-15
Oct-15
Jan-16
Apr-16
Jul-16
Oct-16
Jan-17
Time [Daily Values]

6.2.2.6 TKN

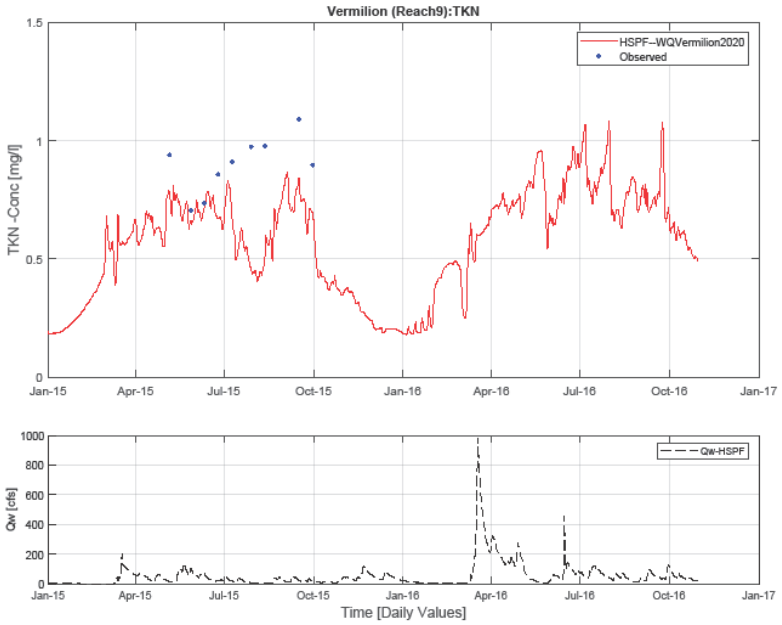
Vermilion (Reach9):TKN
HSPF--WQVermilion2020
Observed
TKN -Conc [mg/l]
Qw-HSPF
Qw [cfs]
Jan-15
Apr-15
Jul-15
Oct-15
Jan-16
Apr-16
Jul-16
Oct-16
Jan-17
Time [Daily Values]

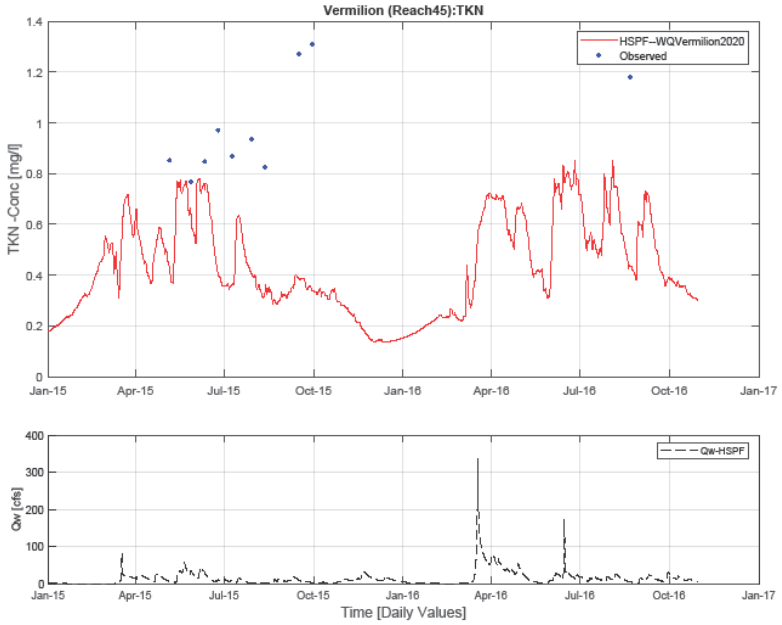
Vermilion (Reach45):TKN
HSPF--WQVermilion2020
Observed
TKN -Conc [mg/l]
Qw-HSPF
Qw [cfs]
Time [Daily Values]
Jan-15
Apr-15
Jul-15
Oct-15
Jan-16
Apr-16
Jul-16
Oct-16
Jan-17

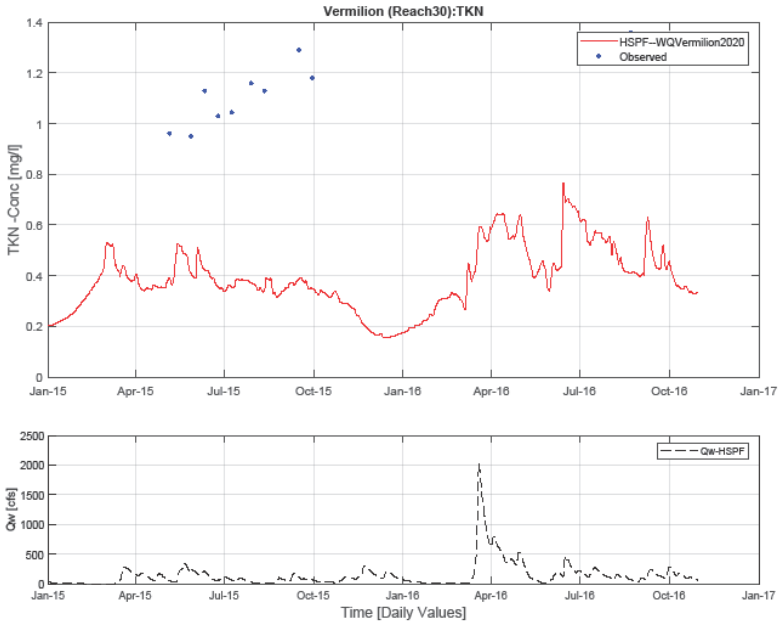
Vermilion (Reach30):TKN
HSPF--WQVermilion2020
Observed
TKN -Conc [mg/l]
Qw-HSPF
Qw [cfs]
Time [Daily Values]
Jan-15
Apr-15
Jul-15
Oct-15
Jan-16
Apr-16
Jul-16
Oct-16
Jan-17

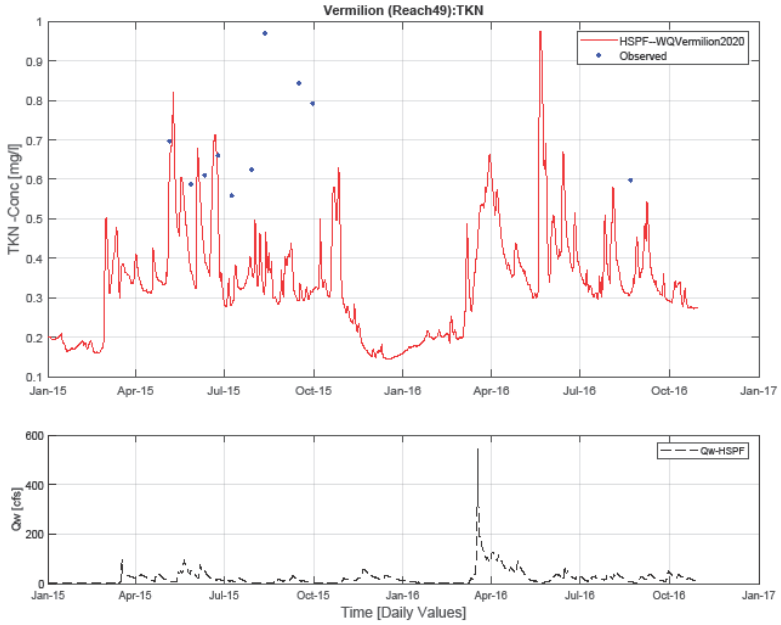
Vermilion (Reach49):TKN
HSPF--WQVermilion2020
Observed
TKN -Conc [mg/l]
Qw-HSPF
Qw [cfs]
Jan-15
Apr-15
Jul-15
Oct-15
Jan-16
Apr-16
Jul-16
Oct-16
Jan-17
Time [Daily Values]

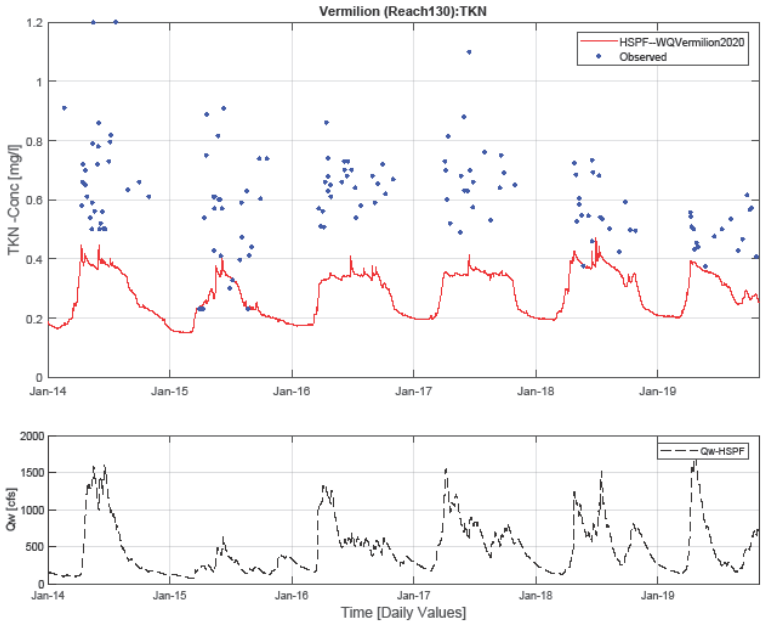
Vermilion (Reach130):TKN
HSPF--WQVermilion2020
Observed
TKN -Conc [mg/l]
Qw-HSPF
Qw [cfs]
Jan-14
Jan-15
Jan-16
Jan-17
Jan-18
Jan-19
Time [Daily Values]

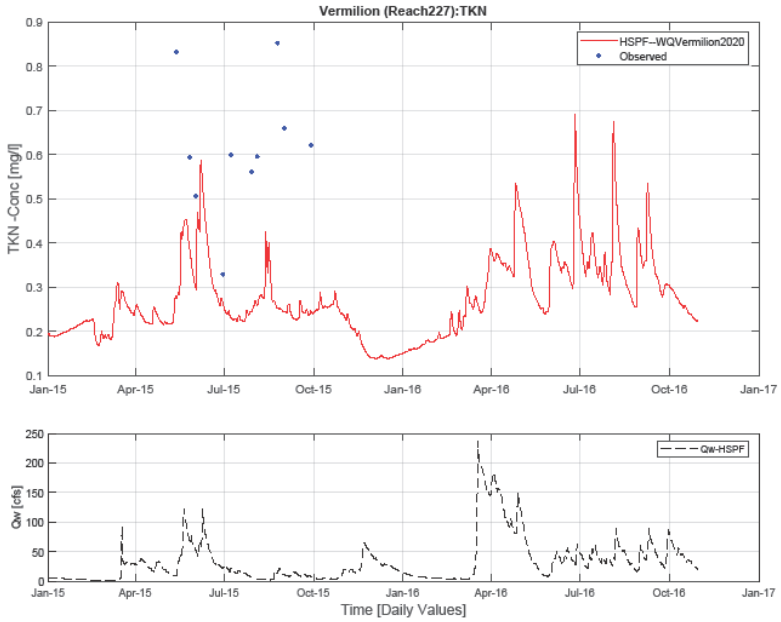
Vermilion (Reach227):TKN
HSPF--WQVermilion2020
Observed
TKN -Conc [mg/l]
Qw-HSPF
Qw [cfs]
Jan-15
Apr-15
Jul-15
Oct-15
Jan-16
Apr-16
Jul-16
Oct-16
Jan-17
Time [Daily Values]

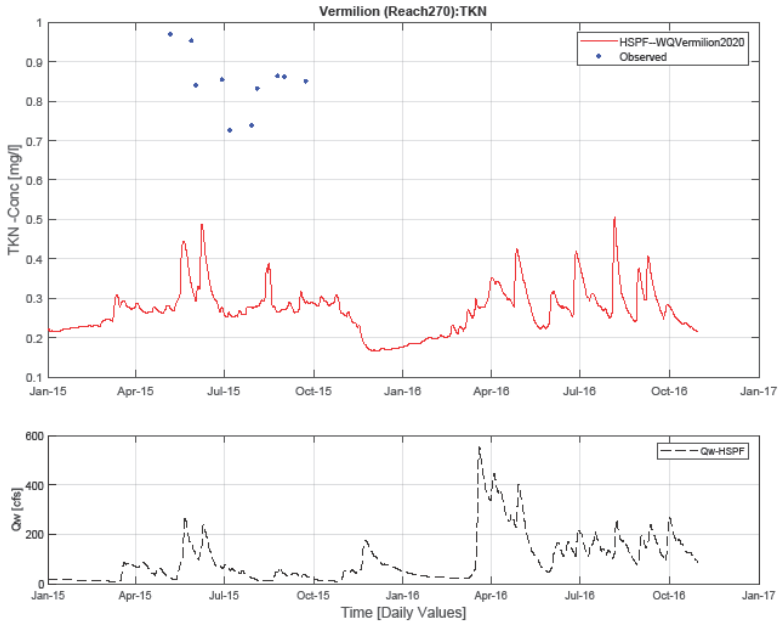
Vermilion (Reach270):TKN
HSPF--WQVermilion2020
Observed
TKN -Conc [mg/l]
Qw-HSPF
Qw [cfs]
Jan-15
Apr-15
Jul-15
Oct-15
Jan-16
Apr-16
Jul-16
Oct-16
Jan-17
Time [Daily Values]

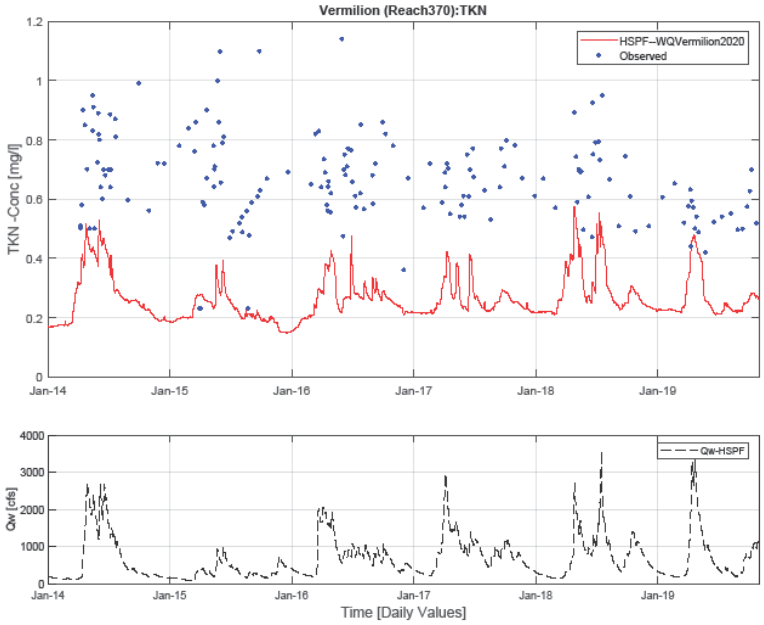
Vermilion (Reach370):TKN
HSPF--WQVermilion2020
Observed
TKN -Conc [mg/l]
Qw-HSPF
Qw [cfs]
Jan-14
Jan-15
Jan-16
Jan-17
Jan-18
Jan-19
Time [Daily Values]

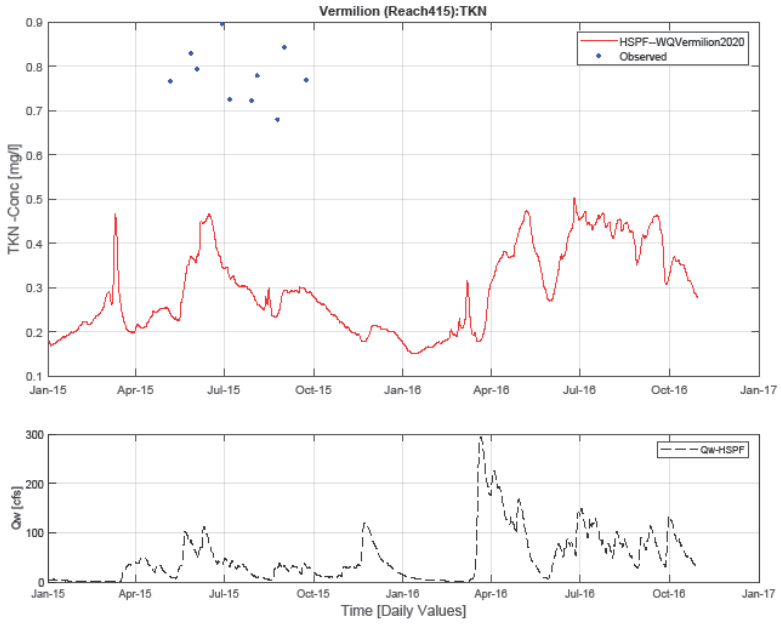
Vermilion (Reach415):TKN
HSPF--WQVermilion2020
Observed
TKN -Conc [mg/l]
Qw-HSPF
Qw [cfs]
Jan-15
Apr-15
Jul-15
Oct-15
Jan-16
Apr-16
Jul-16
Oct-16
Jan-17
Time [Daily Values]

6.2.2.7 Chl-*a*

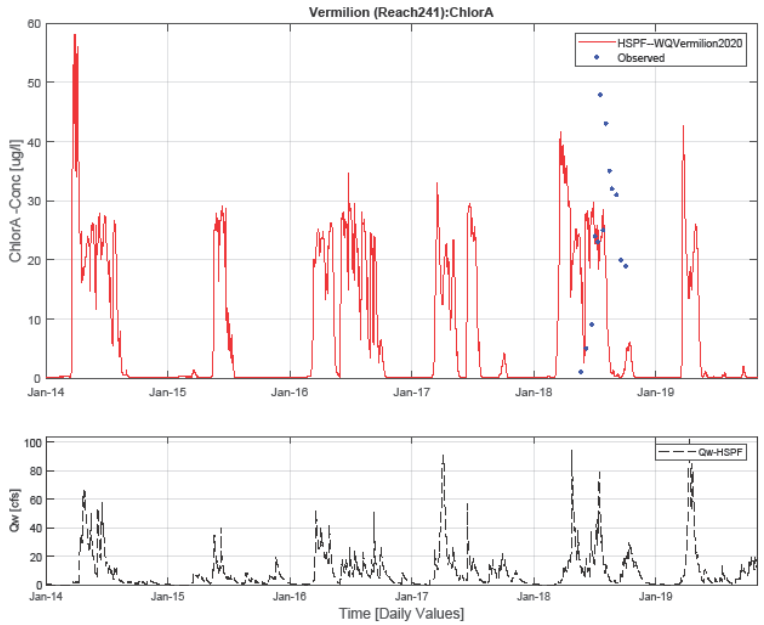
Vermilion (Reach241):ChlorA
HSPF--WQVermilion2020
Observed
ChlorA -Conc [ug/l]
Qw-HSPF
Qw [cfs]
Jan-14
Jan-15
Jan-16
Jan-17
Jan-18
Jan-19
Time [Daily Values]

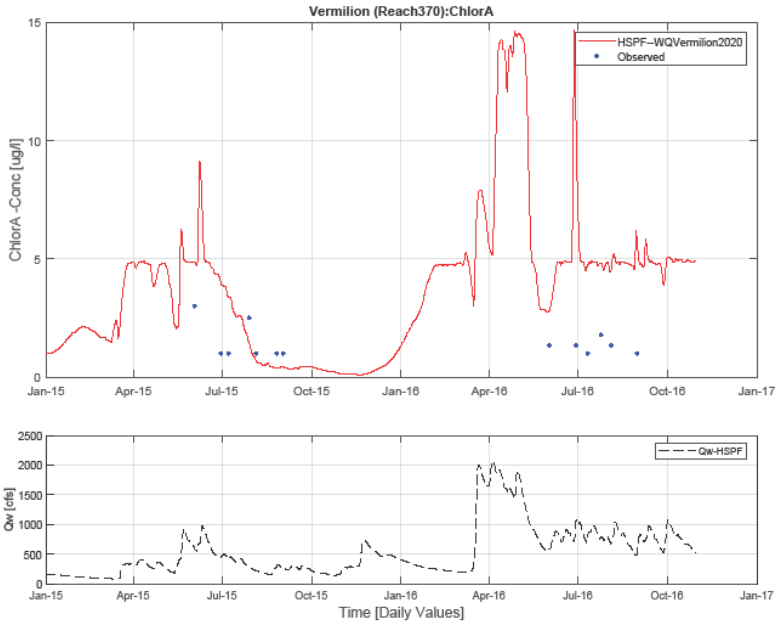
Vermilion (Reach370):ChlorA
HSPF--WQVermilion2020
Observed
ChlorA -Conc [ug/l]
Qw-HSPF
Qw [cfs]
Jan-15
Apr-15
Jul-15
Oct-15
Jan-16
Apr-16
Jul-16
Oct-16
Jan-17
Time [Daily Values]

6.2.3 Rainy Lake model

6.2.3.1 TSS

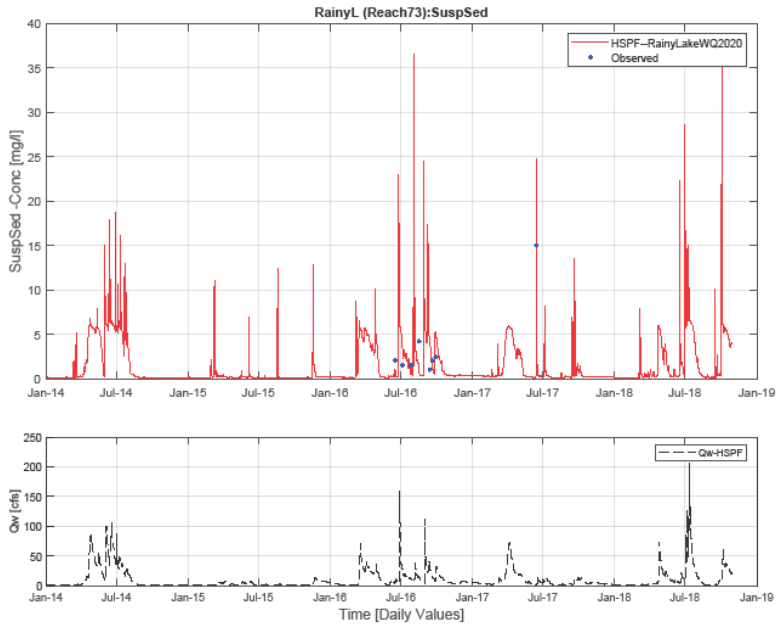

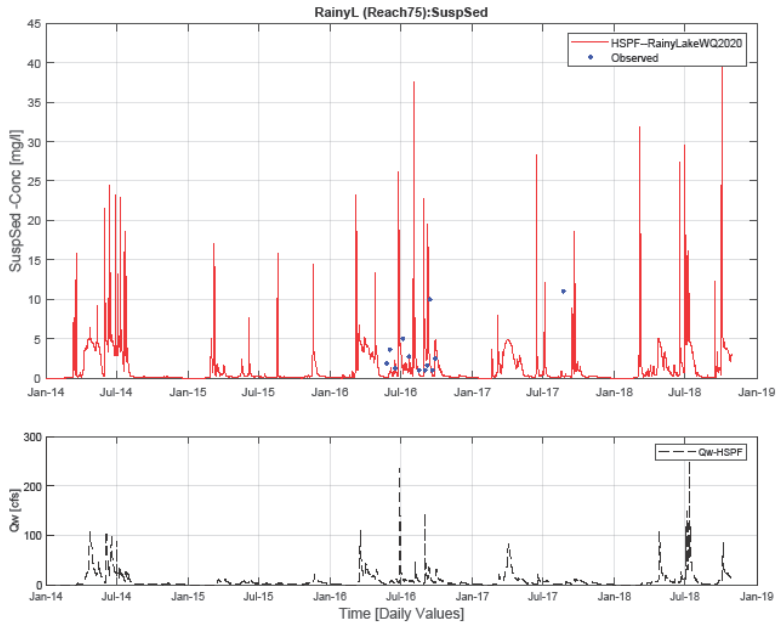

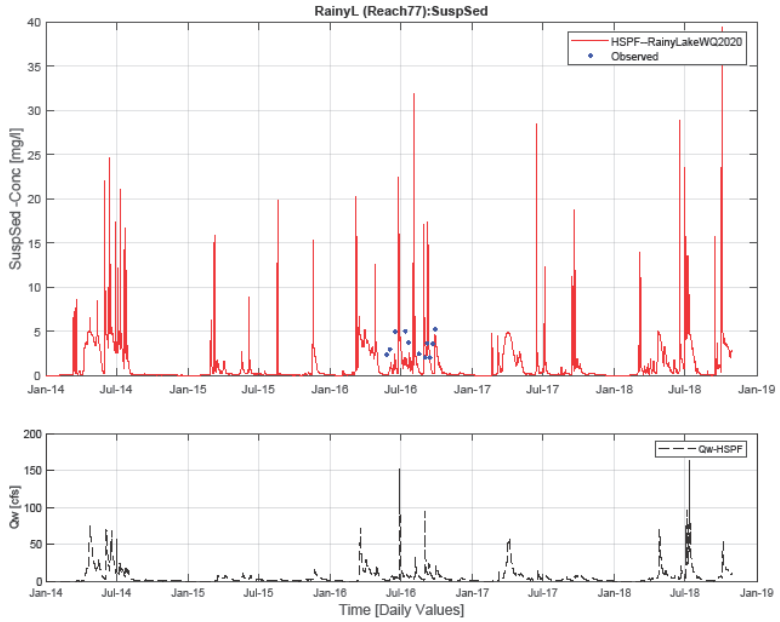
RainyL (Reach77):SuspSed
HSPF--RainyLakeWQ2020
Observed
SuspSed -Conc [mg/l]
Qw-HSPF
Qw [cfs]
Jan-14
Jul-14
Jan-15
Jul-15
Jan-16
Jul-16
Jan-17
Jul-17
Jan-18
Jul-18
Jan-19
Time [Daily Values]

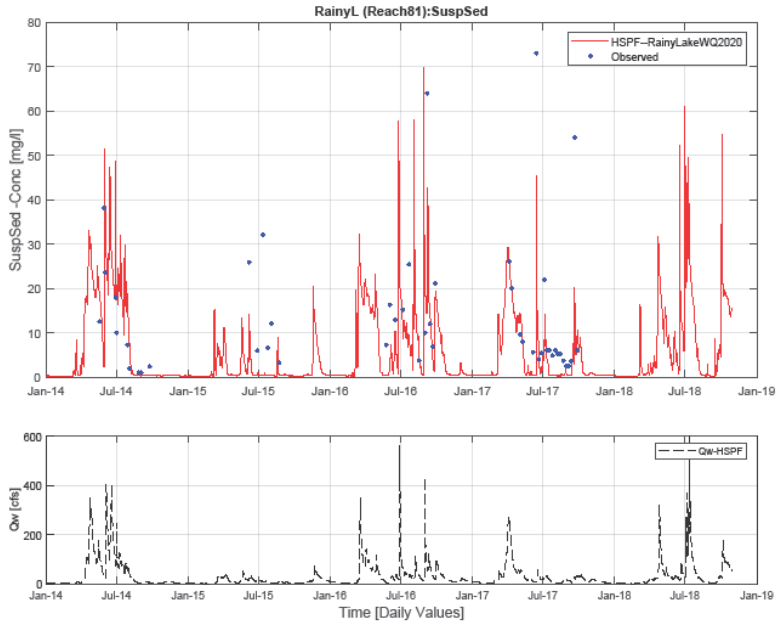
RainyL (Reach81):SuspSed
HSPF--RainyLakeWQ2020
Observed
SuspSed -Conc [mg/l]
Qw-HSPF
Qw [cfs]
Jan-14
Jul-14
Jan-15
Jul-15
Jan-16
Jul-16
Jan-17
Jul-17
Jan-18
Jul-18
Jan-19
Time [Daily Values]

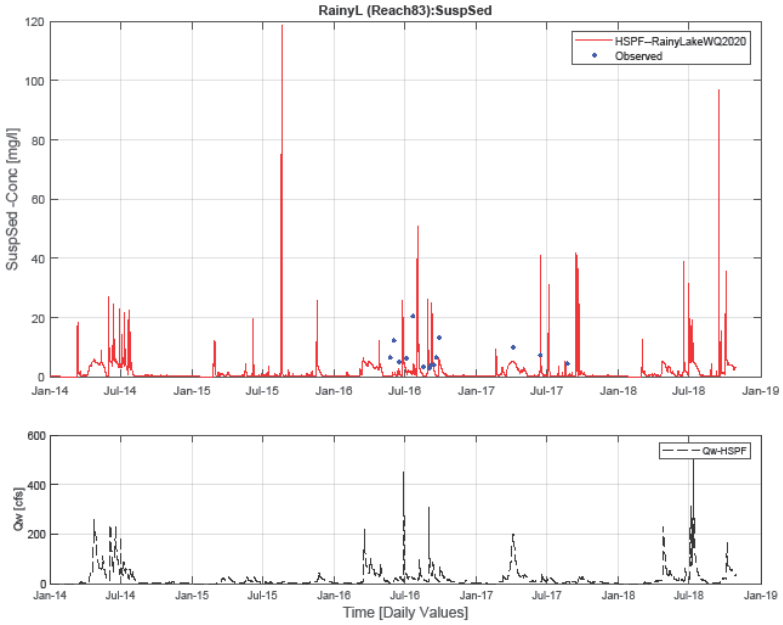
RainyL (Reach83):SuspSed
HSPF--RainyLakeWQ2020
Observed
SuspSed -Conc [mg/l]
Qw-HSPF
Qw [cfs]
Jan-14
Jul-14
Jan-15
Jul-15
Jan-16
Jul-16
Jan-17
Jul-17
Jan-18
Jul-18
Jan-19
Time [Daily Values]

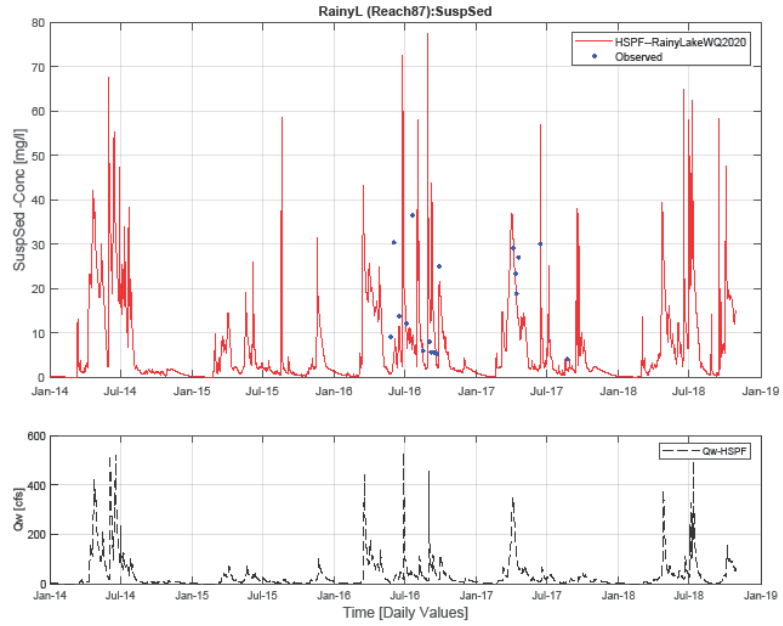
RainyL (Reach87):SuspSed
HSPF--RainyLakeWQ2020
Observed
SuspSed -Conc [mg/l]
Qw-HSPF
Qw [cfs]
Jan-14
Jul-14
Jan-15
Jul-15
Jan-16
Jul-16
Jan-17
Jul-17
Jan-18
Jul-18
Jan-19
Time [Daily Values]

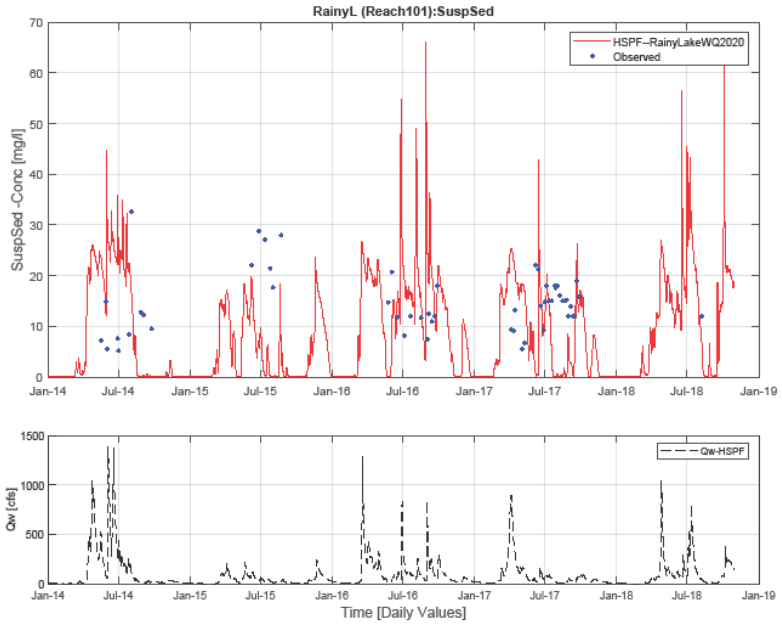
RainyL (Reach101):SuspSed
HSPF--RainyLakeWQ2020
Observed
SuspSed -Conc [mg/l]
Qw-HSPF
Qw [cfs]
Time [Daily Values]

6.2.3.2 PO_4

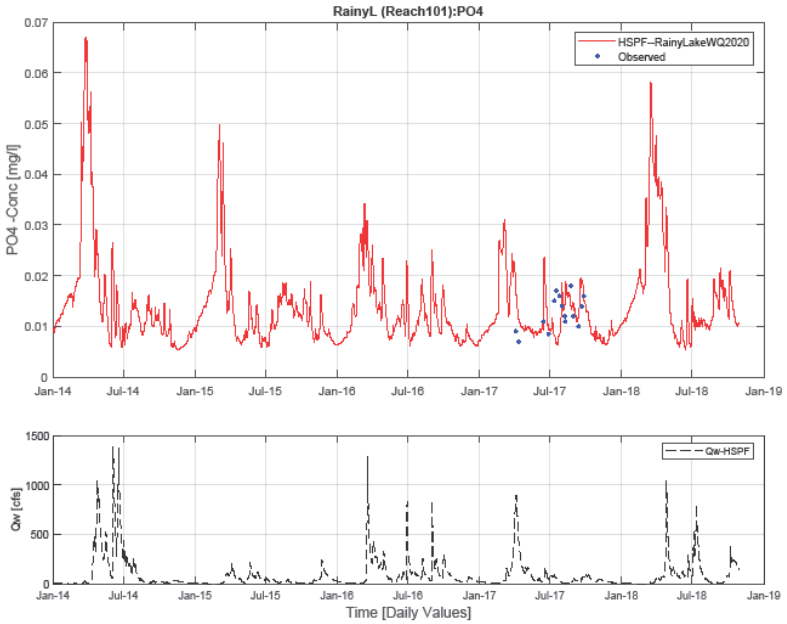
RainyL (Reach101):PO4
HSPF--RainyLakeWQ2020
Observed
PO4 -Conc [mg/l]
Qw-HSPF
Qw [cfs]
Time [Daily Values]

6.2.3.3 TP

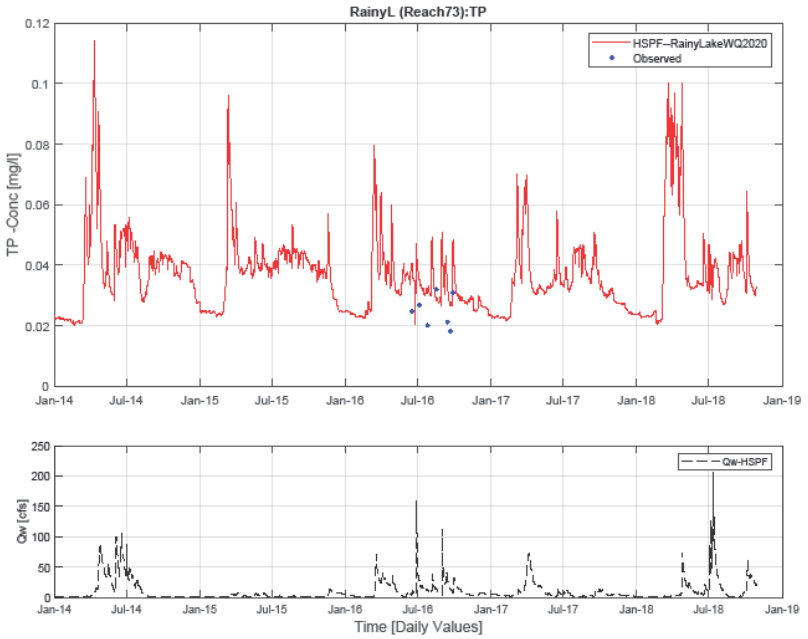
RainyL (Reach73):TP
HSPF--RainyLakeWQ2020
Observed
TP -Conc [mg/l]
Qw-HSPF
Qw [cfs]
Time [Daily Values]

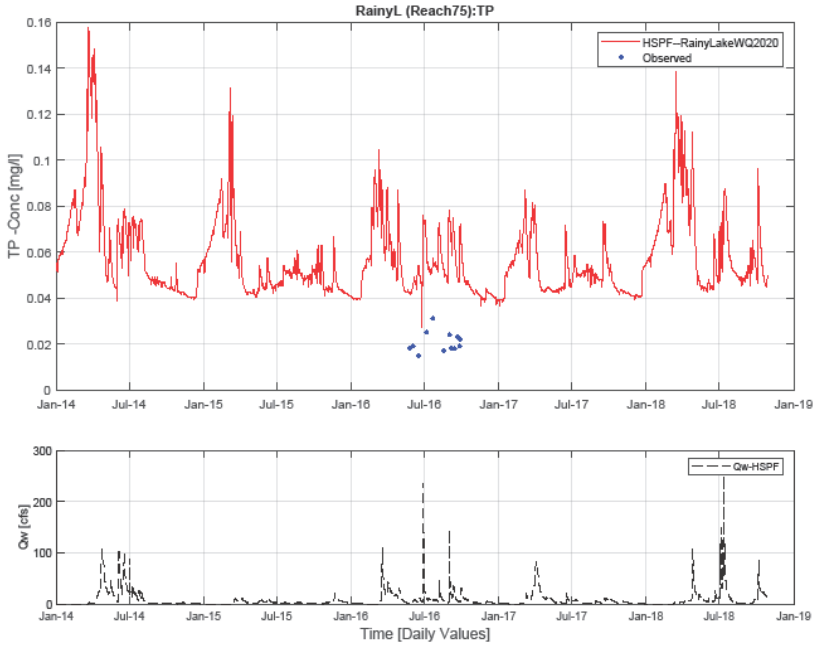
RainyL (Reach75):TP
HSPF--RainyLakeWQ2020
Observed
TP -Conc [mg/l]
Qw-HSPF
Qw [cfs]
Time [Daily Values]

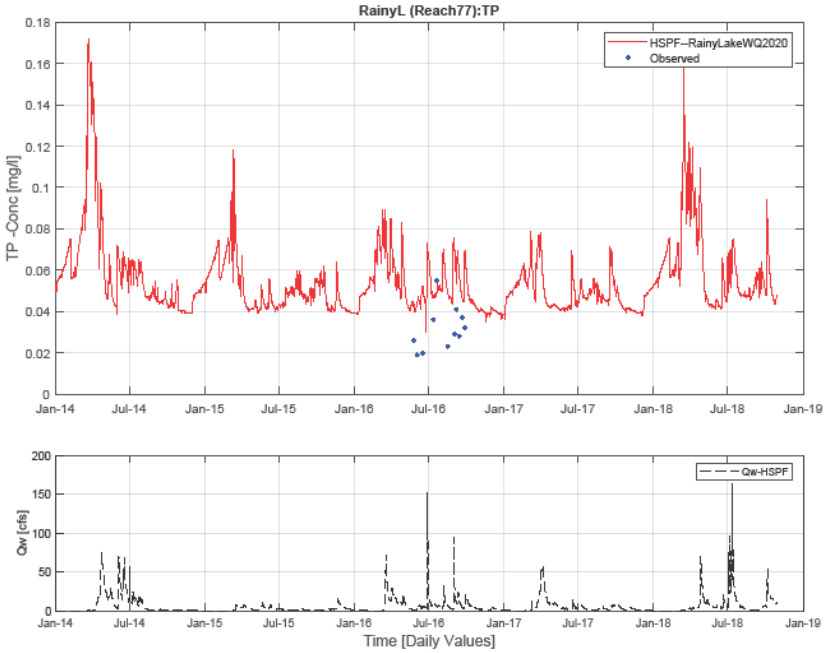
RainyL (Reach77):TP
HSPF--RainyLakeWQ2020
Observed
TP -Conc [mg/l]
Qw-HSPF
Qw [cfs]
Time [Daily Values]

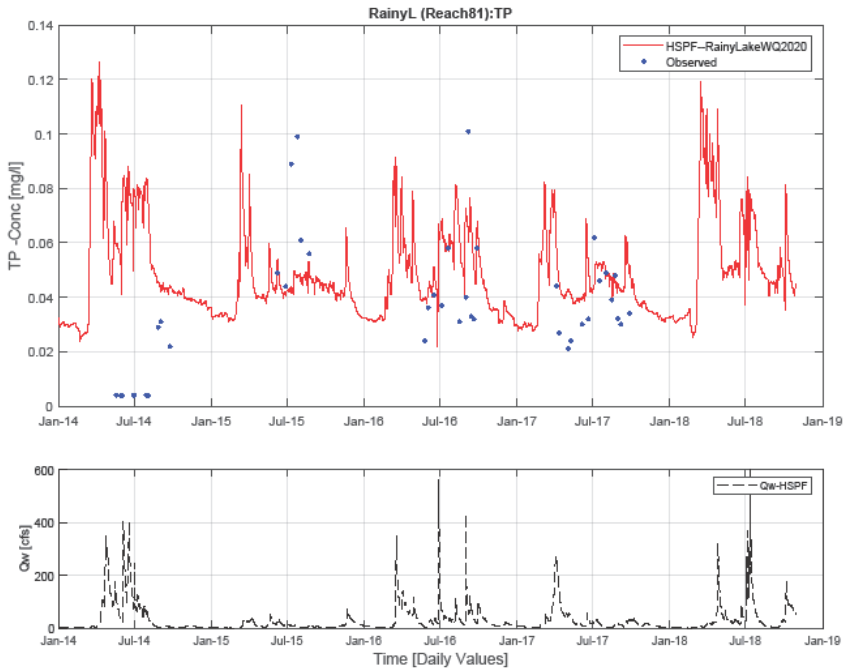
RainyL (Reach81):TP
HSPF--RainyLakeWQ2020
Observed
TP -Conc [mg/l]
Qw-HSPF
Qw [cfs]
Time [Daily Values]

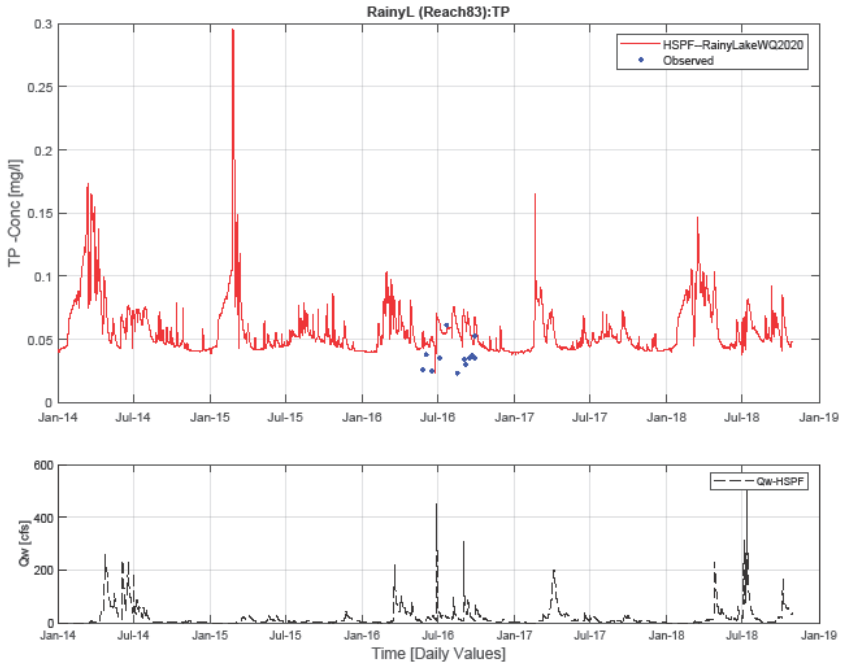
RainyL (Reach83):TP
HSPF--RainyLakeWQ2020
Observed
TP -Conc [mg/l]
Qw-HSPF
Qw [cfs]
Time [Daily Values]

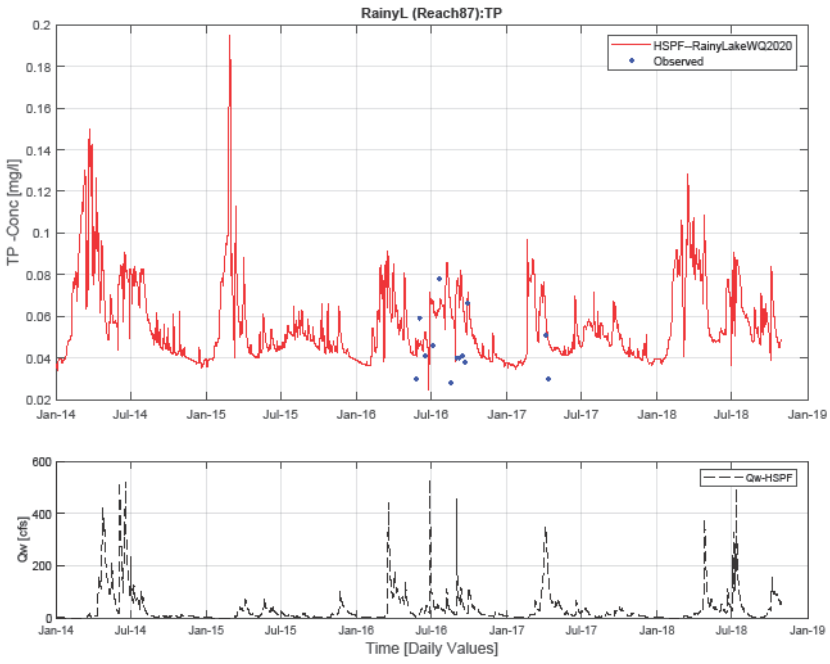
RainyL (Reach87):TP
HSPF--RainyLakeWQ2020
Observed
TP -Conc [mg/l]
Qw-HSPF
Qw [cfs]
Time [Daily Values]

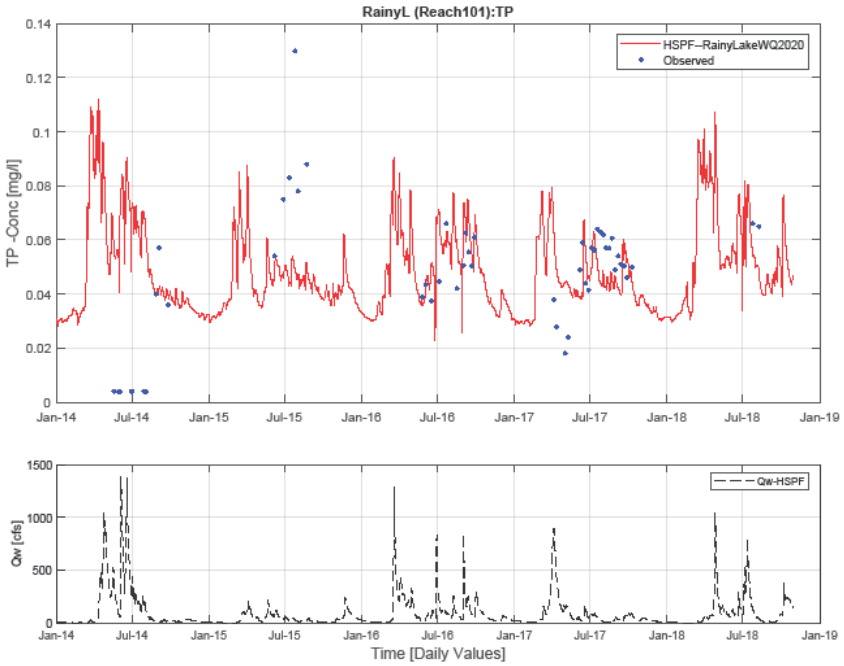
RainyL (Reach101):TP
HSPF--RainyLakeWQ2020
Observed
TP -Conc [mg/l]
0.14
0.12
0.1
0.08
0.06
0.04
0.02
0
Jan-14
Jul-14
Jan-15
Jul-15
Jan-16
Jul-16
Jan-17
Jul-17
Jan-18
Jul-18
Jan-19
Qw-HSPF
Qw [cfs]
1500
1000
500
0
Time [Daily Values]

6.2.3.4 TAM

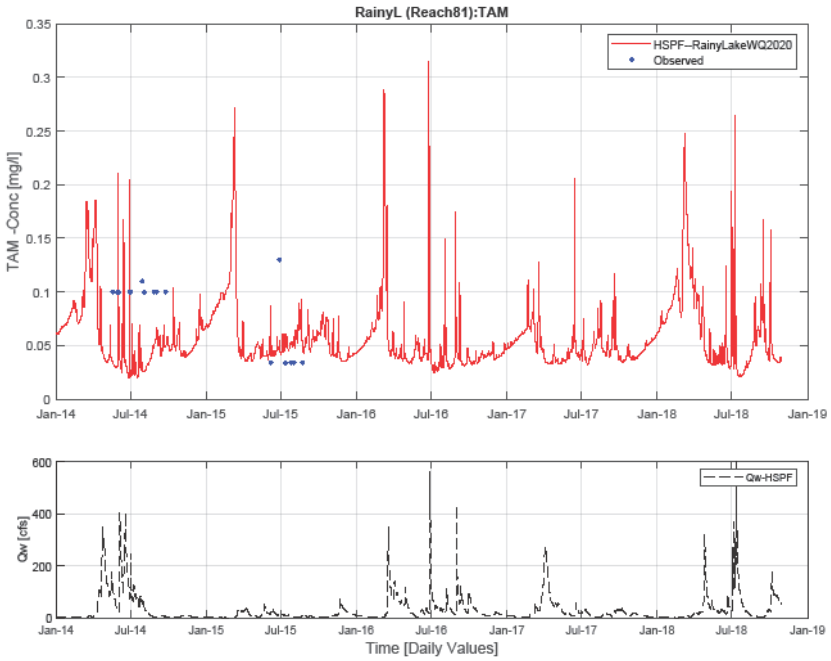
RainyL (Reach81):TAM
HSPF--RainyLakeWQ2020
Observed
TAM -Conc [mg/l]
Qw-HSPF
Qw [cfs]
Time [Daily Values]

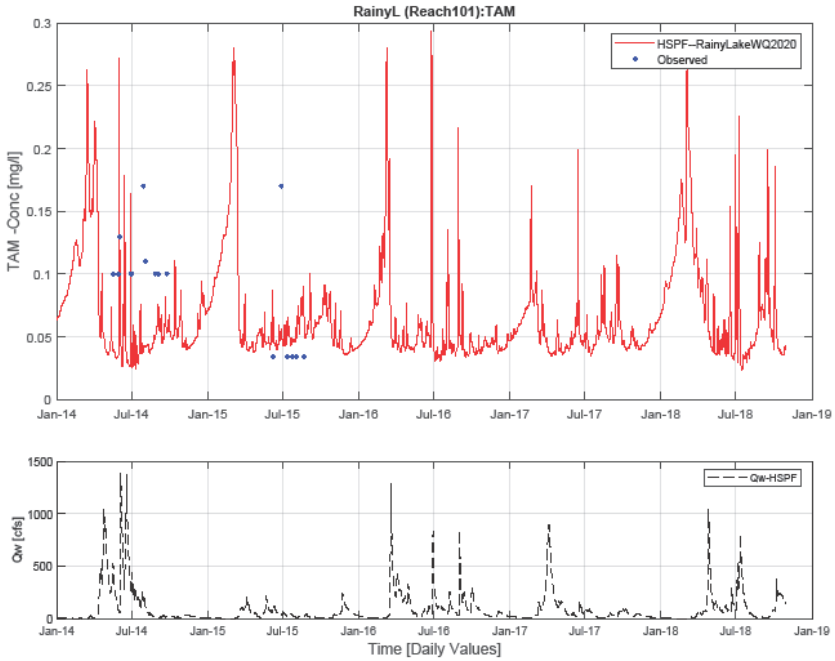
RainyL (Reach101):TAM
HSPF--RainyLakeWQ2020
Observed
TAM -Conc [mg/l]
Qw-HSPF
Qw [cfs]
Time [Daily Values]

6.2.3.5 TKN

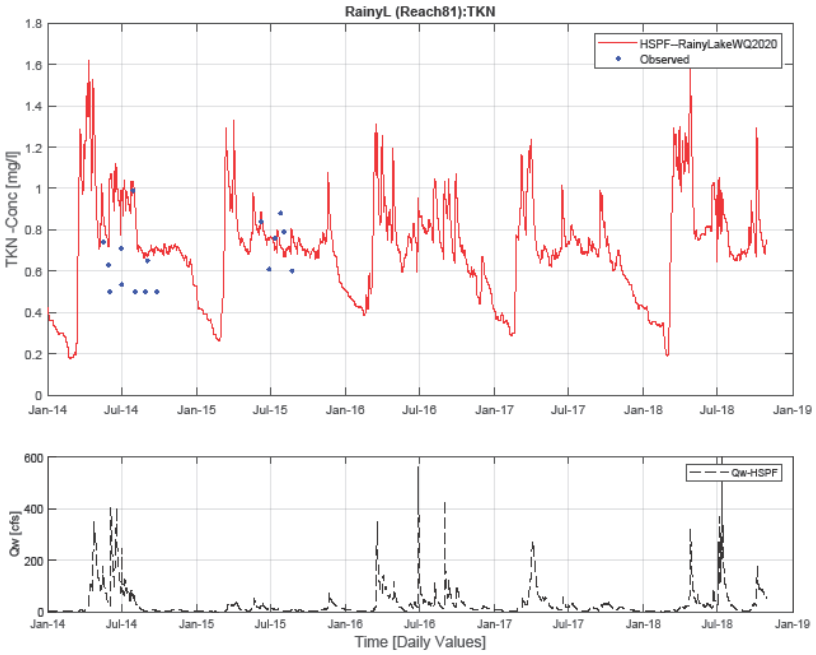
RainyL (Reach81):TKN
HSPF--RainyLakeWQ2020
Observed
TKN -Conc [mg/l]
Qw-HSPF
Qw [cfs]
Time [Daily Values]

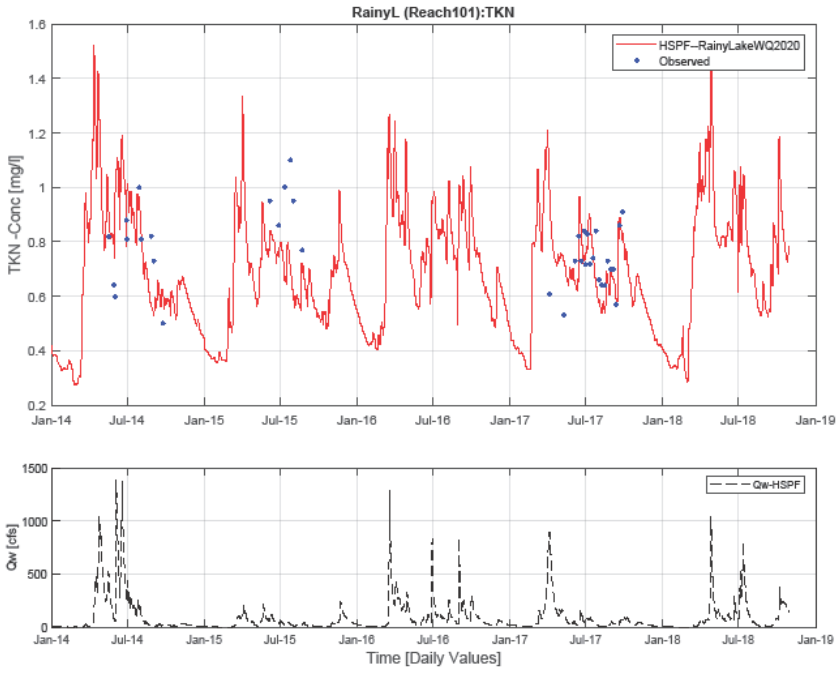
RainyL (Reach101):TKN
HSPF--RainyLakeWQ2020
Observed
TKN -Conc [mg/l]
Qw-HSPF
Qw [cfs]
Time [Daily Values]

6.2.3.6 Chl-*a*

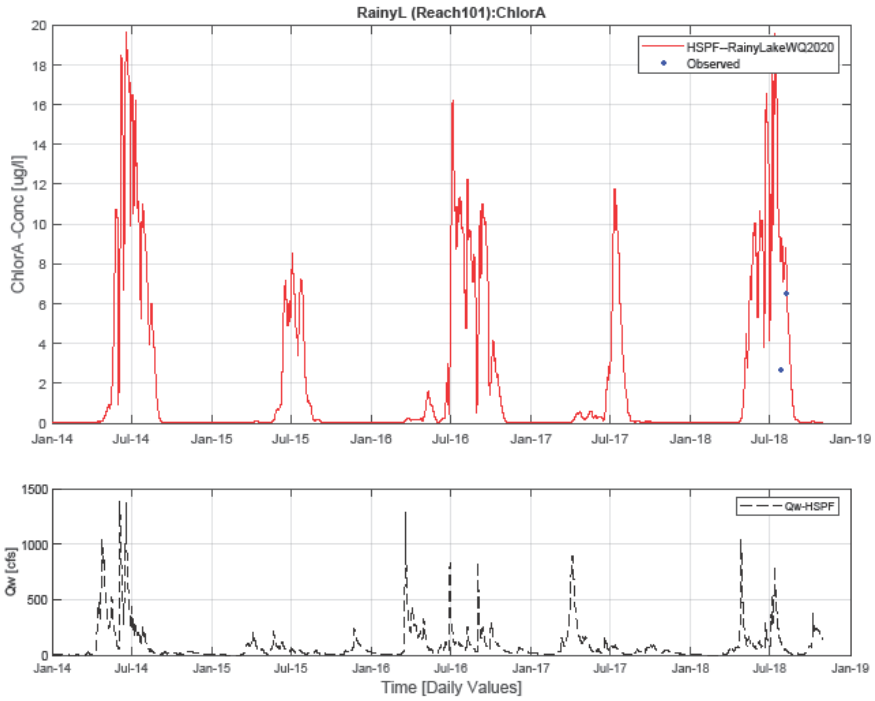
RainyL (Reach101):ChlorA
HSPF--RainyLakeWQ2020
Observed
ChlorA -Conc [ug/l]
Qw-HSPF
Qw [cfs]
Time [Daily Values]
Jan-14
Jul-14
Jan-15
Jul-15
Jan-16
Jul-16
Jan-17
Jul-17
Jan-18
Jul-18
Jan-19